We greatly value the careful reading and the detailed comments provided by the referees. The responses to the comments of the two referees in our direct reply (shown below) and within the revised manuscript (see marked copy) are provided below. The pages and lines indicated below correspond to those in the marked copy.

Response to Referee 1 (Referees' comments are italicized)

1. Referee comment: "*The authors assume in their analysis that coagulation between particles is negligible. I am worried that this assumption may not be appropriate and may be biasing the results, and I hence request that they justify this assumption by simulating coagulation of a typical particle size distribution (with or without simultaneous wall losses) and comment on the results. The assumption of "no coagulation" is made explicitly or implicitly in different places in the manuscript, for example:*

lines 228-229: The smallest diameter bin is initialized by the total number of particles measured at the end of the experiment to account for the fact that the model does not simulate nucleation. I am especially worried about the assumption in this instance since the smaller particles formed during nucleation are especially likely to coagulate.

lines 251-253: The authors state they are using a model without coagulation because including coagulation showed no change in the predicted SOA mass concentrations. It is not clear to me what is meant by this statement. The model contains several fitting parameters – were the best values for the fitting parameters the same if coagulation was included in the model? Further, even if there is no (large) change in predicted SOA when including coagulation, if a model with coagulation is available, why did the authors not use that model as it is expected to be more accurate?

There is some indication that ignoring coagulation may be biasing results. For example: lines 355-358: In their analysis of the appropriateness of the wall deposition number correction the authors note that the loss-corrected particle number concentrations are 9-17% less than the initial number concentrations for seeded experiments, and that it is unclear why this might be the case. Could this not be due to coagulation which is not accounted for in the calculations?"

Author response: We agree with the reviewer that coagulation may potentially be important and in fact are currently performing experiments to analyze the relationship between coagulation and particle wall loss. We expect to publish these results soon. In the meantime, we have added a brief analysis of coagulation to the current paper. As requested, we reanalyzed the AS seed-only particle wall loss data and α-pinene ozonolysis SOA growth data, this time accounting for coagulation. We applied the Aerosol Parameter Estimation (APE) model (detailed by Pierce et al. (2008)) to the AS seed-only particle wall loss experimental datasets to derive particle wall loss coefficients that correct for particle coagulation. This procedure was performed for both the low and high AS seed-only experiments. As described in Pierce et al. (2008), the coagulation-corrected particle wall loss coefficients were determined by simulating the decay of the

initial size distribution due to coagulation and then attributing the difference in this decay and the observed decay to particle wall loss. All nucleation and low AS data were then reanalyzed using modeled particle wall loss coefficients that correct for coagulation derived from the low AS seed-only experiments Similarly, all high AS data were reanalyzed using modeled particle wall loss coefficients that correct for coagulation derived from the high AS seed-only experiments.

Based on our reanalyzed α-pinene ozonolysis SOA growth data, the SOA mass yields stay roughly constant despite the increase in AS seed surface area for both O_3 concentrations. Higher SOA mass yields are observed in the 500 ppb O_3 experiments. These trends are similar to those presented in the original manuscript where we assumed that coagulation is negligible (and therefore not corrected for) in all our experiments. In addition, these newly obtained SOA mass yields obtained at peak SOA growth (where coagulation is corrected for) are generally consistent with those of previous studies.

These newly obtained absolute SOA mass concentrations and mass yields (where coagulation is corrected for) are higher than those reported in the original manuscript (where coagulation is not corrected for) by < 2 % (absolute values). Therefore, we do not anticipate these results will affect our main conclusions that (1) SOA formation in the α-pinene ozonolysis system is governed by quasi-equilibrium growth since the SOA mass yields stay roughly constant despite the increase in AS seed surface area for both O_3 concentrations, and (2) there is an "oxidation rate effect" since higher SOA mass yields are observed in the 500 ppb O_3 experiments.

We have added a discussion on the potential effect of coagulation on the SOA mass yields measured in this study to the revised manuscript:

Page 14 line 377: "Red and blue solid lines in Fig. 1 shows the size-dependent particle wall deposition coefficients measured in the low AS seed-only and high AS-seed only deposition experiments. In these measurements, we assume that the number concentration is low enough such that the effect of coagulation is small and only particle wall deposition affects the particle size distribution, thus allowing for the direct measurement of size-dependent particle wall deposition coefficients. The initial total AS seed surface area concentration in the low AS-seed only and high AS-seed only experiments (which are conducted using 0.015 M AS and 0.05 M AS solutions, respectively) are similar to those used in the α-pinene ozonolysis experiments (i.e., ~1000 and ~3000 μm^2 cm^{-3}, respectively). As shown in Fig. 1, the measured particle wall deposition coefficients from the low AS-seed only and high AS-seed only experiments generally fall within the range of those measured in routine monthly AS-seed only experiments conducted in the chamber. Figure 1 also shows the size-dependent particle wall deposition coefficients corrected for coagulation, shown using dashed lines, which are obtained as described in Pierce et al., 2008 using the data from the low AS-seed only and high AS-seed only experiments. A comprehensive description of the relationship between coagulation and particle wall deposition will be provided in a forthcoming publication. Briefly, as described in Pierce et al. (2008), the coagulation-corrected particle wall loss coefficients are determined by simulating the decay of the initial size distribution due to coagulation and then attributing the difference in this decay and the observed

decay to particle wall loss. For both the measured and coagulation-corrected particle wall deposition coefficients, the minimum coefficient for the low AS-seed only experiment is different from that of the high AS-seed only experiments. The cause of this difference is currently under investigation but may be due in part to uncertainties arising from the low particle number concentrations for the larger particles in the low AS-seed only experiment. To study how coagulation can potentially affect SOA mass yields in this study, both the measured and coagulation-corrected size-dependent particle wall deposition coefficients are used to correct for particle wall deposition in the α-pinene ozonolysis experiments.

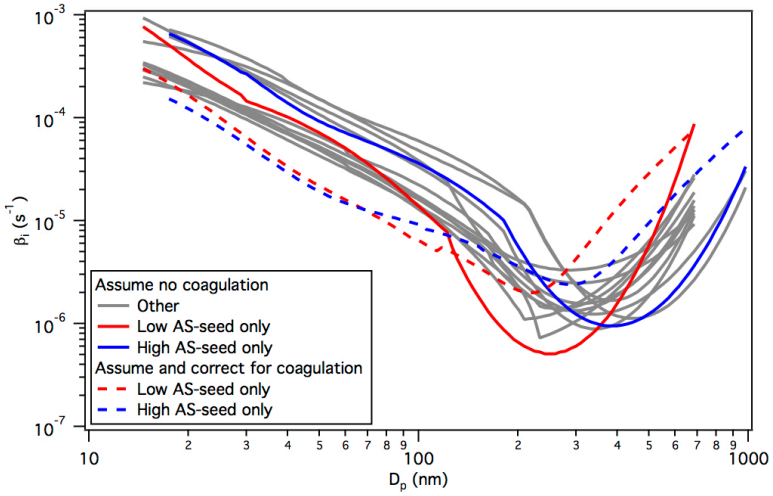

Figure 1: Particle wall deposition coefficients (β_i) measured during the low AS-seed only and high AS-seed only experiments in GTEC. Also shown are the particle wall deposition coefficients (labeled "Other") measured in previous routine monthly AS-seed only experiments in the chamber. These previous routine monthly AS-seed only experiments were performed using either a 0.008 M AS or a 0.1 M AS solution. Coagulation-corrected particle wall deposition coefficients (see Pierce et al. (2008) and main text for details) are also shown, using dashed lines.

Assuming that the effect of coagulation is small, the particle wall deposition corrected number concentration data provide a test of the appropriateness of the particle wall deposition correction. The corrected number concentration should level off at a constant value (i.e., the initial particle number concentration), assuming no significant coagulation, when particle wall deposition is properly accounted for since the wall-deposited particle number distribution is added to the suspended particle number distribution during particle wall loss correction. Neglecting coagulation, we account for particle wall deposition in nucleation and low AS experiments using deposition coefficients measured from the low AS-seed only experiments, while particle deposition in high AS experiments are accounted for using coefficients measured from the high AS-seed only experiments. Figures S1 and S2 show the particle wall deposition-corrected aerosol number and volume concentrations. Over all experiments, the particle wall deposition-corrected final particle number concentration (i.e., at the end of the reaction) is 9 to 17 % less than the initial particle number concentration for the low AS and high AS experiments

(Table S1), respectively, indicating that the particle wall deposition-corrected volume concentrations are slightly underestimated. The fact that the particle wall deposition-corrected final particle number concentrations are somewhat smaller than the initial particle number concentrations may be due to variations in particle wall deposition rates in the AS-seed only and α-pinene ozonolysis experiments or to coagulation. To first examine variations in particle wall deposition rates, we used the average of the measured low AS-seed only and high AS-seed only particle wall deposition coefficients to account for particle wall deposition in all the experiments (Figs. S3 and S4). While there is a negligible difference in the particle wall deposition corrected volume concentrations (Figs. S3 and S4 vs. Figs. S1 and S2), a larger spread (1 to 22 %) exists in the difference between the initial and final particle number concentrations when the average measured particle wall deposition coefficients are used (Table S1). Therefore, all subsequent nucleation and low AS data presented here are particle wall deposition-corrected using coefficients measured from the low AS-seed only experiments, and all high AS data are corrected using particle wall deposition coefficients measured from the high AS-seed only experiments. We furthermore conclude that variations in particle wall deposition rates do not cause the decrease in the particle wall deposition-corrected final number concentration and is most likely due to coagulation. Thus, the SOA data are also corrected using the coagulation-corrected particle wall deposition coefficients (discussed below). We show subsequently the relatively minor difference that correcting for coagulation has on overall SOA mass yields. Therefore, we use SOA concentrations corrected using the measured particle wall deposition coefficients for the bulk of the analysis in this study."

Page 18 line 493: "To investigate the influence of coagulation on the SOA mass yields, the coagulation-corrected size-dependent particle wall deposition coefficients are also used to correct for particle wall deposition in the α-pinene ozonolysis experiments. Specifically, all nucleation and low AS data are particle wall deposition-corrected using coagulation-corrected coefficients derived from the low AS-seed only experiments, and all high AS data are corrected using coagulation-corrected particle wall deposition coefficients derived from the high AS-seed only experiments. Figure S7 shows the time-dependent SOA mass yields (obtained using the coagulation-corrected and measured particle wall deposition coefficients) as a function of initial total AS seed surface area. SOA mass yields obtained using the coagulation-corrected particle wall deposition coefficients are < 2 % (absolute values) higher than those using the measured particle wall deposition coefficients. Similar to the SOA mass yields obtained using the measured particle wall deposition coefficients (Figs. 4, S7c and S7d), SOA mass yields obtained using the coagulation-corrected particle wall deposition coefficients stay roughly constant despite the increase in AS seed surface area for both O_3 concentrations, and the SOA mass yields are higher in the 500 ppb O_3 experiments (Figs. S7a and S7b). The mass yields obtained at peak SOA growth are also generally consistent with those of previous studies (Fig. S8). Taken together, this suggests that the effect of coagulation on the SOA mass yields is likely minor for the aerosol concentrations used in this study. Therefore, only data that have been particle wall deposition-corrected using coefficients measured in the low AS-seed only and high AS-seed only experiments

are fitted to determine model parameters for the vapor-particle dynamics model described in Section 3."

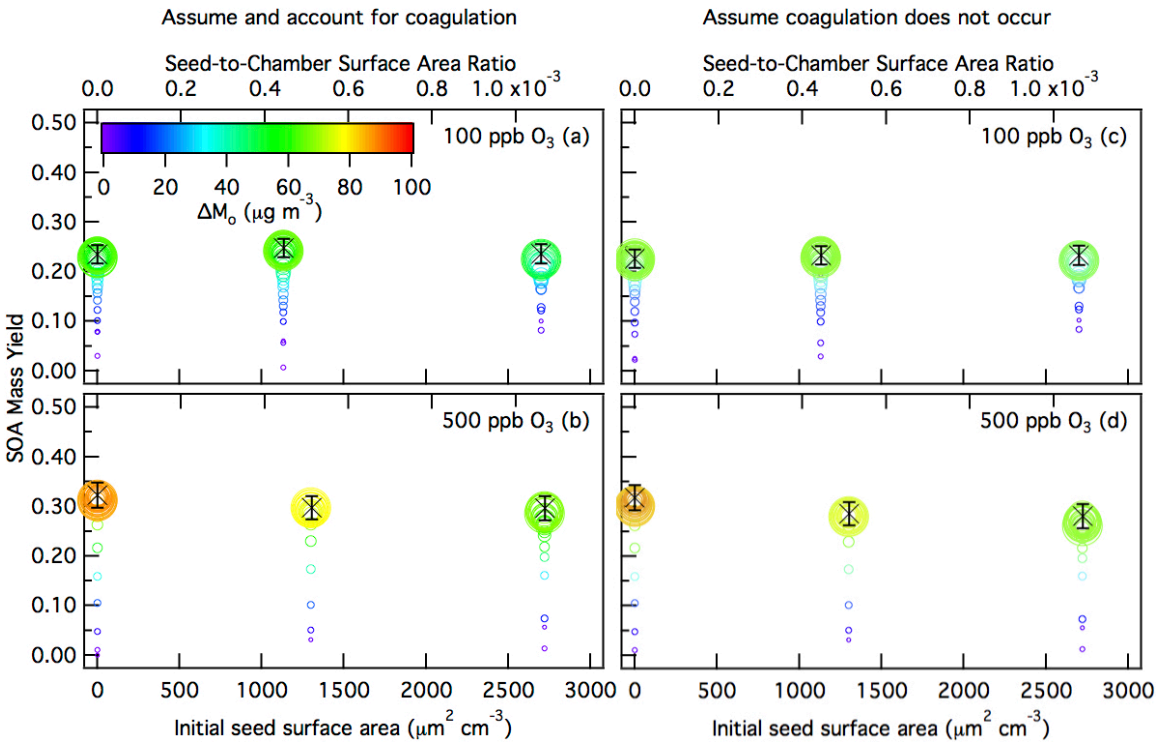

Figure S7: 10 min-averaged SOA mass yields over the course of an α-pinene ozonolysis experiment as a function of initial total AS seed surface area concentration. Panels (a) and (b) show the SOA mass yields obtained using the coagulation-corrected size-dependent particle wall deposition coefficients for the 100 and 500 ppb O_3 experiments, respectively. Panels (c) and (d) show the SOA mass yields obtained using the measured size-dependent particle wall deposition coefficients (that account for coagulation) for the 100 and 500 ppb O_3 experiments, respectively (also shown in Fig. 4 of the main text). Symbol color indicates the SOA mass concentration and symbol size indicates the time after O_3 is injected into the chamber. The × symbols are the SOA mass yields at peak SOA growth. The y-axis error bars represent the uncertainty in the peak SOA mass yield, which originates from the α-pinene injection and the aerosol volume concentration measured by the SMPS at peak SOA growth (one standard deviation). As discussed in the main text, the use of coagulation-corrected particle wall deposition coefficients for particle wall loss correction does not change the conclusions of this work: 1) SOA mass yields are enhanced at higher O_3 concentrations, and 2) there is a lack of a SOA mass yield dependence on the seed surface area within the range of AS seed surface area concentration used in this study.

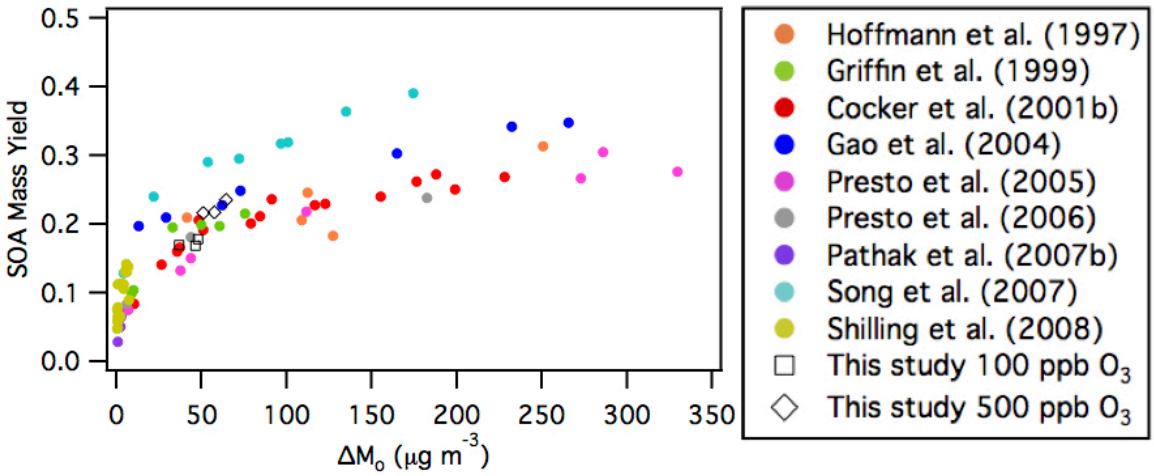

Figure S8: Comparison of SOA mass yields obtained using the coagulation-corrected size-dependent particle wall deposition coefficients to those of previous dark α-pinene ozonolysis studies (Table S2). The SOA mass yields and concentrations of majority of these previous studies (Hoffmann et al., 1997; Griffin et al., 1999; Cocker et al., 2001b; Gao et al., 2004; Presto et al., 2005; Presto et al. 2006; Pathak et al., 2007b; Song et al., 2007) were previously compiled by Shilling et al. (2008). Similar to Shilling et al. (2008), all the data shown here (including those reported in this study) have been adjusted using an organic density of 1.0 g cm^{-3}, and to 298 K using a temperature correction of 1.6 % per K, as recommended by Pathak et al. (2007b) to facilitate easier comparison among the different studies.

2. Referee comment: "*lines 405-407: The authors note that "Higher SOA mass yields are observed in the 500 ppb O3 experiments, which indicates that the a-pinene oxidation rate controls the absolute amount of SOA formed." It seems appropriate in this context to comment on why this may be the case – is it due to reduced wall losses when the oxidation rate is higher? This seems inconsistent with the observation that the SOA formation is not kinetically limited.*"

Author response: We believe that the higher SOA mass yields measured in the 500 ppb O_3 experiments is due to reduced vapor-wall deposition, even though SOA formation in the α-pinene ozonolysis system is governed by quasi-equilibrium growth. We direct the referee to sections 5.2 and 5.3 for a detailed discussion on why that is the case.

3. Referee comment: "*lines 477-479: I am unconvinced based on the data shown that the vapor-particle mass accommodation coefficient (alpha_p) equals 1 for two main reasons: 1) as the authors recognized, different combinations of fitting parameters could give similarly good fits (not explored in this manuscript – in the sensitivity analyses shown only one parameter is changed at a time) and 2) based on the data shown in Figure S8, alpha_p = 0.1 seems to yield similar agreement with data as alpha_p = 1. Thus, in my opinion the authors should not base conclusions on the result that alpha_p =1.*

Overall it is not clear how the fitting parameters were chosen. Figures are shown comparing modeled and measured results for different parameter choices. Was the choice of model parameter based on a visual comparison of modeled and measured

data? This reminds me of modeling of thermodenuder data (which also includes several fitting parameters), where Karnezi et al. (2014) have updated an evaporation model to explore the parameter space more fully. A similar approach seems appropriate for the model used in this manuscript.

Karnezi, E.; Riipinen, I.; Pandis, S. N. Measuring the atmospheric organic aerosol volatility distribution: a theoretical analysis. Atmos. Meas. Tech. 2014, 7, 2953–2965."

Author response: We thank the reviewer for the helpful reference. We have followed the methodology of Karnezi et al. (2014) and conducted a wide parameter sweep. We report both the parameters determined as optimal using the Karnezi et al. inverse error-weighting approach, as well as the combination of parameters with the lowest percentage error. We find that the lowest-error parameters give the best fit to the data, so we use these parameters for our analysis. The Karnezi et al. parameters and the lowest-error parameters are similar to each other, and to the parameters originally chosen in the manuscript, validating that these parameters are relatively robust. The following discussion was added to the paper:

Page 12, line 337: "In order to determine the parameters for α_w, α_p, τ_{olig} and the branching ratios between the oxidation products that provide the best fit to measured SOA data, the parameter space was discretized and all possible combinations of parameters were simulated, following Karnezi et al. (2014). In order to restrict the number of combinations required, only parameter values judged to be physically realistic were chosen. Because the branching ratios in this model are mole-based, they must sum to one; therefore only combinations of parameters summing to one were allowed. The discretization is shown in Table S1 and results in roughly 10,000 different combinations of parameters. All six experiments were simulated with each parameter combination, and simulations were run using GNU Parallel (Tange 2011). For each combination of parameters, the percentage error was calculated from equation 10 of Karnezi et al. (2014):

$$E_i = \frac{100}{n}\sqrt{\sum_i^n (Moa_{i,guess} - Moa_{i,meas})^2} \quad (13)$$

where $Moa_{i,guess}$ is the model-predicted SOA mass concentration at a particular timestep i for one of the experiments, $Moa_{i,meas}$ is the measured SOA mass concentration at a particular timestep i for one of the experiments, and n is the number of timesteps summed over all experiments. The best-fit combination of parameters is defined as the combination of parameters with the lowest percentage error. This lowest-error combination of parameters was compared to the "best estimate" parameters determined from the inverse error weighting factor of Karnezi et al. (2014):

$$\overline{x} = \frac{\sum_j^N \left[x_j \frac{1}{E_j}\right]}{\sum_j^N \frac{1}{E_j}} \quad (14)$$

where x_j is a value of one of the parameters (α_w, α_p, τ_{olig} or a branching ratio

between the oxidation products), with N different possible combinations of parameters, and E_j is the percent error for that particular combination of parameters. The lowest-error combination of parameters and the Karnezi et al. (2014) best estimate parameters are both reported, but the lowest-error combination of parameters resulted in a lower percentage error than the Karnezi et al. (2014) best estimate parameters. The lowest-error combination of parameters is used for the modeling analysis."

Table S2: Discretization of parameters

Parameter	Discretization
α_p	1, 0.1, 0.01, 0.001
α_w	10^{-7}, 10^{-6}, 10^{-5}
τ_{olig}	4, 6, 8
$>10^3$ branching ratio[a]	0.5, 0.6, 0.7, 0.8, 0.9, 1
10^2 branching ratio[a]	0, 0.1, 0.2, 0.3, 0.4, 0.5
10 branching ratio[a]	0, 0.01, 0.02, 0.03, 0.04, 0.05, 0.1, 0.15, 0.2
1 branching ratio[a]	0, 0.01, 0.02, 0.03, 0.04, 0.05, 0.1, 0.15, 0.2
0.1 branching ratio[a]	0, 0.01, 0.02, 0.03, 0.04, 0.05, 0.1, 0.15, 0.2

[a]Only combinations of parameters summing to one were allowed.

Page 19, line 519: "As noted earlier, optimal model values for α_p, α_w, τ_{olig} and the branching ratios between the oxidation products were determined by calculating the error between the observed and modeled time-dependent SOA concentrations for all possible combinations of model parameters. The combination of parameters with the lowest percent error is $\alpha_w = 10^{-6}$, $\alpha_p = 0.1$, $\tau_{olig} = 4$ h, branching ratios = 0.6, 0.3, 0.05, 0.05 and 0 for oxidation products with vapor pressures $>10^3$, 10^2, 10, 1 and 0.1 μg m^{-3}, respectively. This combination of parameters results in a percent error of 21% (Table S4). It is important to note that predictions using $\alpha_p = 0.1$ or 1 resulted in very similar errors; with the same combination of parameters and $\alpha_p = 1$, the percent error only increased to 22%. The "best estimate" parameters determined following the Karnezi et al. (2014) method are as follows: $\alpha_w = 3.6\times10^{-6}$, $\alpha_p = 0.35$, $\tau_{olig} = 6$ h, and branching ratios = 0.66, 0.16, 0.06, 0.06, and 0.06 for oxidation products with vapor pressures $>10^3$, 10^2, 10, 1 and 0.1 μg m^{-3}, respectively. This combination of parameters results in an error of 37% (Table S4). Model predictions using both sets of parameters are compared to measured SOA concentrations in Fig. S9. The lowest-error parameters are used for the analysis in the remainder of this study."

Table S4: Best-fit parameters, using lowest percentage error and Karnezi et al. (2014) method

Parameter	Lowest percentage error	Karnezi et al. (2014) method
α_p	0.1	0.35
α_w	10^{-6}	$3.6\text{x}10^{-6}$
τ_{olig} (h)	4	6
$>10^3$ branching ratio	0.6	0.66

10^2 branching ratio	**0.3**	**0.16**
10 branching ratio	**0.05**	**0.06**
1 branching ratio	**0.05**	**0.06**
0.1 branching ratio	**0**	**0.06**
Percentage error for combination	**21%**	**37%**

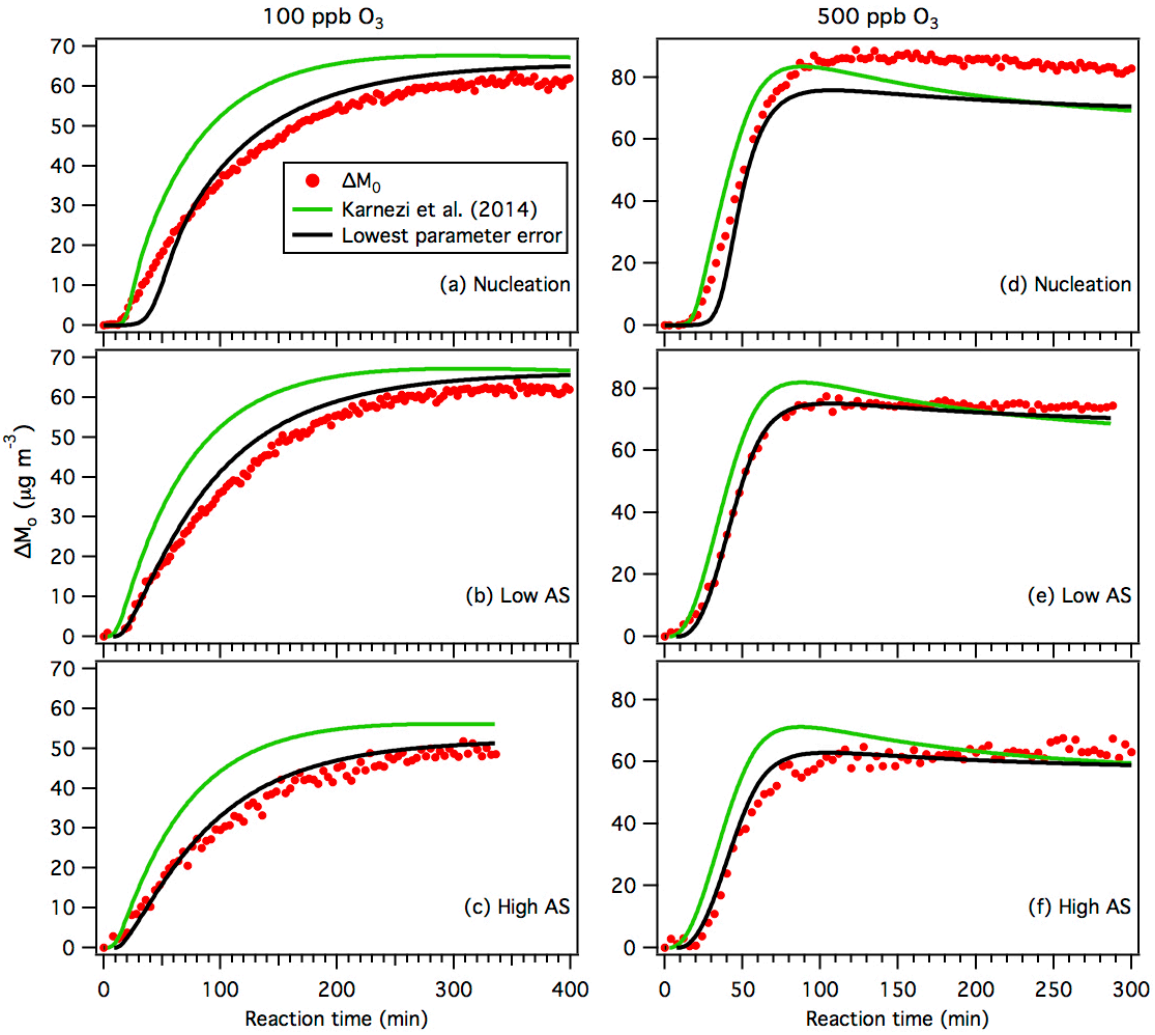

Figure S9: Reaction profiles for measured and modeled SOA concentration, using both the Karnezi et al. (2014) parameters and the lowest-error combination of parameters (see Table S4). Panels (a), (b) and (c) show results from the nucleation, low AS and high AS 100 ppb O_3 experiments, respectively. Panels (d), (e) and (f) show results from the nucleation, low AS and high AS 500 ppb O_3 experiments, respectively.

Page 21 line 588: "The best-fit $\alpha_p = 0.1$ (or $\alpha_p = 1$, with almost the same percentage error) suggests the absence of significant limitations to vapor-particle mass transfer in the present α-pinene ozonolysis study, and that SOA formation is governed by

quasi-equilibrium growth (Saleh et al., 2013; McVay et al., 2014), which occurs when SOA-forming vapors are produced at a rate that is significantly slower than that required to establish gas-particle equilibrium (Shiraiwa and Seinfeld, 2012; Zhang et al., 2012)."

Page 21 line 598: "The best-fit α_p = 0.1 is within the range of α_p coefficients determined from α-pinene ozonolysis SOA thermodenuder studies (α_p = 0.1) (Saleh et al., 2013; Saha et al., 2016) and α-pinene photooxidation chamber studies (α_p = 0.1 or 1) (McVay et al., 2016)."

Page 24 line 690: "A key aspect of vapor wall deposition is the potential interplay between the seed aerosol surface area effect and the oxidation rate effect. To examine this interplay in the α-pinene ozonolysis system, simulations were carried out by varying the seed aerosol surface area and the O_3 concentration simultaneously, while using the branching ratios, oligomerization rate, and vapor wall deposition rate parameters obtained in the present study. The initial α-pinene concentration was set to 50 ppb, and a fixed O_3 concentration was used in place of a linear injection. α_p was varied at 0.001, 0.01, 0.1, and 1 in these simulations. Figure 6 shows the SOA mass yield at peak SOA growth as a function of both the seed aerosol surface area and O_3 concentration for α_p = 1, 0.1, 0.01, and 0.001. For α_p = 1 or 0.1, the oxidation rate dominates: SOA mass yield increases significantly as O_3 concentration increases while the seed aerosol surface area has a negligible effect. For α_p = 0.01, both effects can be observed in different regions: at low O_3 concentrations and high seed aerosol surface areas, the oxidation rate effect dominates; at low seed aerosol surface areas and high O_3 concentrations, the seed surface area dominates. At low seed aerosol surface areas and low O_3 concentrations, both effects are present. For α_p = 0.001, the seed aerosol surface area effect dominates except at very high seed aerosol surface areas. These observations show that the presence of an oxidation rate effect and/or seed aerosol surface area effect depends on a complex interplay of factors, such as α_p, the rate of hydrocarbon oxidation, and the amount of seed surface area present."

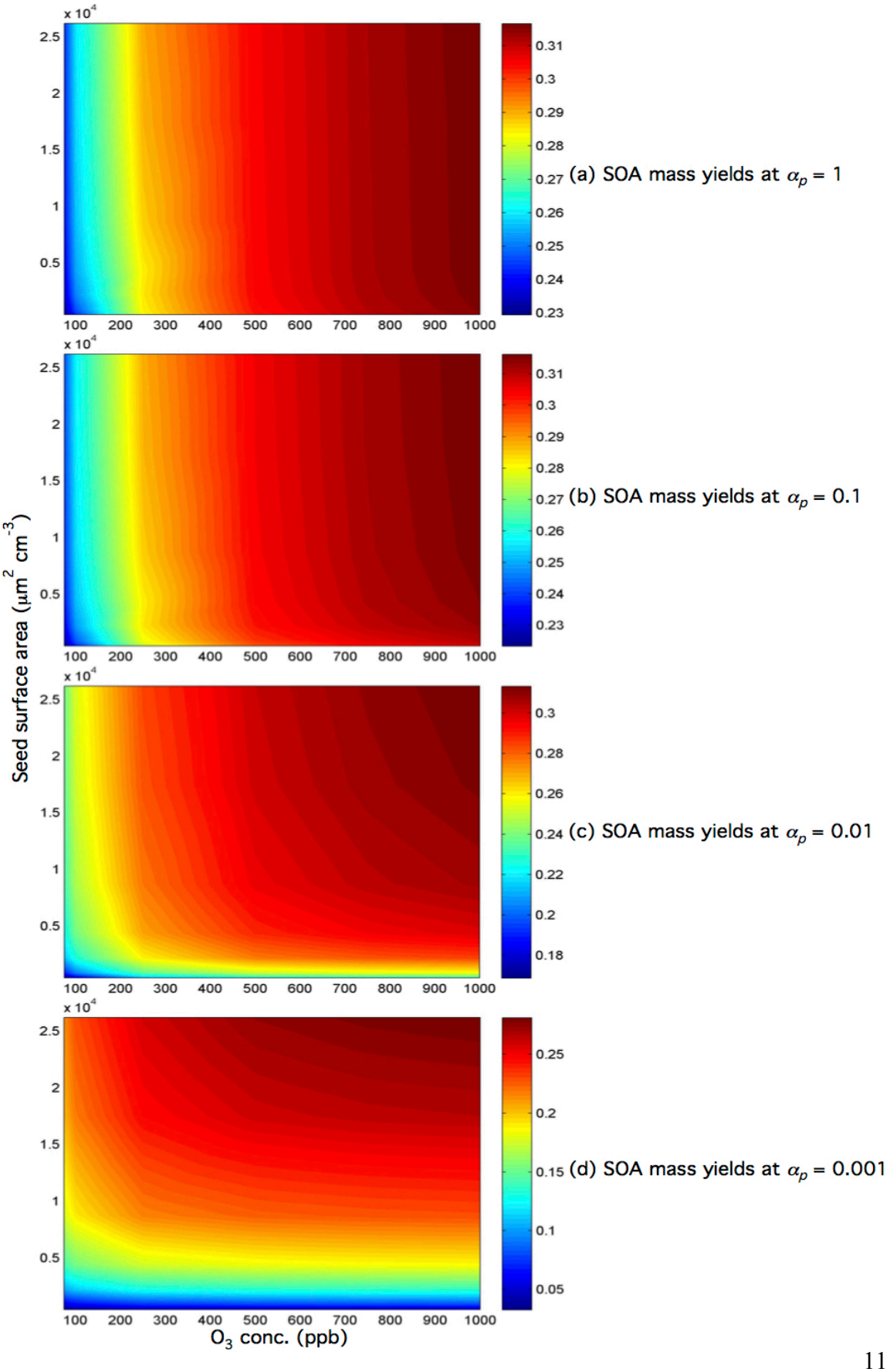
x 10^4
2.5
2
1.5
1
0.5
100 200 300 400 500 600 700 800 900 1000
0.31
0.3
0.29
0.28
0.27
0.26
0.25
0.24
0.23
(a) SOA mass yields at α_p = 1
(b) SOA mass yields at α_p = 0.1
0.22
0.2
0.18
(c) SOA mass yields at α_p = 0.01
0.15
0.1
0.05
(d) SOA mass yields at α_p = 0.001
Seed surface area (μm^2 cm^{-3})
O_3 conc. (ppb)

Figure 6: SOA mass yields at peak SOA growth as a function of both the seed surface area and O_3 concentration for α_p = 1, 0.1, 0.01, and 0.001. The SOA mass yields at peak SOA growth are indicated by colors and contours. Note that the color bars for panels (a), (b) and (c) have different SOA mass yield ranges. Simulations were carried out using the optimal branching ratios, oligomerization rate, and vapor wall deposition rate parameters obtained in this study. The initial α-pinene concentration was set to 50 ppb, and a fixed O_3 concentration was used in place of a linear injection.

4. Referee comment: "*The overall take-away message from this manuscript is unclear. The authors discuss the effect of seed surface area on vapor-wall deposition and resulting SOA yields, how this effect can be mitigated through the use of additional oxidant.,, but also that high oxidant levels may not be atmospherically relevant. This emphasizes the complexity of these experiments and their evaluation but does not provide guidance on how future chamber experiments should be conducted. It would be useful if the authors could add such recommendations in their discussion.*"

Author response: As requested, we have expanded our discussion to include recommendations on how future chamber experiments should be conducted:

Page 30 line 850: "More importantly, the impact of vapor-wall deposition on SOA formation and evolution in various VOC systems conducted under different reaction conditions (regardless of atmospheric relevance) needs to be quantified through a combination of experimental and modeling efforts. Similar to this study, experiments should be performed using different seed aerosol surface area and oxidant concentrations to study their influence on vapor-wall deposition and SOA mass yields. If the effects of vapor-wall loss are found to be strongly dependent on seed aerosol surface area and/or oxidant concentrations (e.g. toluene photooxidation, where SOA formation may be underestimated by factors as much as four (Zhang et al., 2014)), further experiments aimed at measuring the wall deposition rates of the oxidation products should be performed. These wall deposition rates can then be used in predictive models to determine the vapor-wall and vapor-particle mass accommodation coefficients of these oxidation products. Consequently, this will allow us to determine the fraction of SOA-forming vapors partitioning to the particle phase vs. lost to the chamber walls (Zhang et al., 2015; Krechmer et al., 2016)."

5. Referee comment: "*lines 133-134: Please add a comparison of the reactions rates (cyclohexane + OH vs. a-pinene +OH) since that (not the ratio of cyclohexane and a-pinene) determines the effectiveness of the OH scavenger.*"

Author response: Based on the concentrations of cyclohexane and α-pinene injected into the chamber, we expect the reaction rate of OH with cyclohexane to be ~60 times greater than α-pinene. This information is added to the revised manuscript:

Page 5 line 137: "Based on the concentrations of cyclohexane and α-pinene injected into the chamber, the reaction rate of OH with cyclohexane is ~60 times greater than that with α-pinene"

6. Referee comment: "*lines 149-150: I wonder whether it is appropriate to call this an "initial ratio" since the a-pinene is reacting away while the ozone is injected. Please address how much a-pinene has reacted when ozone injection is completed and to what extent the ratio of VOC/oxidant can truly be controlled in these experiments. Please also discuss the mixing time scale in the chamber and potential effects of a-pinene initially reacting with ozone "hot spots".*"

Author response: We agree with the reviewer that it is not appropriate to call this an "initial ratio" since α-pinene was reacting away while O_3 was being injected. Based on our GC measurements, we estimate that ~11 % and ~98 % of the α-pinene had reacted when O_3 injection was completed in the 100 and 500 ppb O_3 experiments, respectively. This information is added to the revised manuscript. Since α-pinene was reacting away while O_3 was being injected and the chamber was operated in batch mode in this study, the α-pinene:O_3 ratio cannot be controlled exactly in these experiments. Therefore, to remove any confusion, we have made the following changes in the revised manuscript:

Page 5 line 154: "The injected α-pinene:O_3 molar ratio were approximately 1:2 and 1:10 in the 100 and 500 ppb O_3 experiments, respectively."

Page 6 line 158: "Approximately 11 % and 98 % of the initial α-pinene had reacted when O_3 injection was completed in the 100 and 500 ppb O_3 experiments, respectively."

Page 16 line 445: "At either O_3 concentration, the molar ratio of O_3 reacted to α-pinene reacted is approximately 1:1 (i.e., 50 ppb α-pinene reacted with 50 ppb O_3), which indicates that O_3 reacts only with α-pinene and not its oxidation products."

Page 21 line 581: "Figure 4 shows that for both O_3 mixing ratios used, the time-dependent SOA mass yield is similar at any given AS seed surface area (see also Table 1)."

We estimate the O_3 mixing timescale for all experiments to be ~12 min based on the O_3 time series traces in the O_3-only experiments. This information is added to the revised manuscript. Due to the design of the GTEC facility, α-pinene closest to the O_3 injection port of the chamber likely reacted first in the α-pinene ozonolysis experiments. However, we do not anticipate this experimental limitation to affect our conclusions (which are derived from SOA mass yields at peak SOA growth) since the O_3 mixing timescale is significantly shorter than the times at which SOA peak growth is achieved. As noted in the manuscript, SOA peak growth is achieved at reaction times ~300 to 350 min and ~100 min for the 100 and 500 ppb O_3 experiments, respectively (the start of O_3 injection into the chamber is reaction time 0 min).

We have made the following changes in the revised manuscript:

Page 6 line 159: "In the GTEC chamber, α-pinene closest to the O_3 injection port likely reacted first in the α-pinene ozonolysis experiments. The O_3 injection times were established in separate experiments in which only O_3 was injected into the chamber. Based on the O_3 time series traces in the O_3-only experiments, the O_3 mixing timescale was estimated to be ~12 min for all experiments."

7. Referee comment: "*Table S1: units should be specified for the particle number concentrations (e.g. particles per cubic centimeter)*"

Author response: The units for the particle number concentration are added in the revised manuscript.

Response to Referee 2 (Referees' comments are italicized)

1. Referee comment: "*Lines 674-677. This sentence does not include any mention of vapor loss to Teflon walls, only to organic matter deposited on the walls. Studies indicate that the loss to Teflon is more important.*"

Author response: The referee is correct in pointing out that the loss of SOA-forming vapors to Teflon walls is more important. Therefore, we have made the following changes to the revised manuscript to better reflect this point:

Page 28 line 806: "One possible explanation for the higher SOA mass yields in the continuous-flow, steady state, mode is that the SOA-forming vapors are in equilibrium with the chamber walls and seed aerosol, hence minimizing the irreversible loss of SOA-forming vapors to the chamber walls (Shilling et al., 2008)."

2. Referee comment: "*The discussion about kinetically-limited vs. quasi-equilibrium controlled SOA formation does not mention the effect of the time constant for oligomer formation. I would think that this has a significant effect on the growth regime, and so should be discussed.*"

Author response: The referee is correct in pointing out that the timescale of oligomerization may play an important role in the SOA growth regime (i.e., kinetically-limited vs. quasi-equilibrium). Our model results suggest that the timescale of oligomerization for the α-pinene ozonolysis system (where SOA formation is governed by quasi-equilibrium) is ~4 hours based on best-fit model predictions with the experimental data (Fig. S9). Similar modeling work (in addition to experimental work) will need to be performed on a VOC system where the SOA formation is governed by kinetically-limited growth (e.g. toluene photooxidation (Zhang et al., 2014)), in order to determine how the timescale of oligomerization may differ between the two SOA growth regimes. This is currently outside the scope of this paper, which is focused primarily on the analysis of SOA formation from the α-pinene ozonolysis system. However, we have made the following changes to the revised manuscript to raise the possibility that the timescale of oligomerization may play an important role in the different SOA growth regimes and needs to be investigated in future studies:

Page 27 line 784: "While not investigated in detail in this study, the timescale of oligomerization may play an important role depending on the SOA growth regime (i.e., kinetically-limited vs. quasi-equilibrium). Currently, it is unclear how the timescale of oligomerization in a VOC system where SOA formation is dominated by quasi-equilibrium growth (e.g. α-pinene ozonolysis) may differ from one that is dominated by kinetically-limited growth (e.g. toluene photooxidation (Zhang et al.,

2014)). This requires further investigation through a combination of experimental and modeling efforts to improve our understanding of how particle-phase processes (e.g. oligomerization) affect gas-particle partitioning, and consequently influence the magnitude by which vapor-wall deposition affects SOA mass yields."

3. Referee comment: "*It appears that the time constant for wall loss is much smaller that the values inferred from previous measurements of wall loss for products of a-pinene photooxidation by Zhang et al. in the Caltech chamber. Do the authors have any comments on why?*"

Author response: A wide range of vapor wall loss rates have been reported in different studies, and the reason for this wide range has not yet been determined. We address this briefly as follows:

Page 19, line 539: "The best-fit $\alpha_w = 10^{-6}$ corresponds to a first-order vapor-wall deposition rate constant ($k_{wall,on}$) of 10^{-4} s^{-1}. A wide range of vapor wall loss rates has been reported (Figure 3 of Krechmer et al. (2016)). This $k_{wall,on}$ value is comparable to that reported by Matsunaga and Ziemann (2010) for a 8.2 m^3 chamber but significantly faster than wall loss rates that have been measured in the Caltech chamber (Zhang et al., 2015). The reason for this wide range of reported vapor wall loss rates is currently uncertain and outside the scope of this study."

4. Referee comment: "*For reactions conducted under low NOx conditions the oxidation rate will affect the chemistry of RO2 radicals. In the O3 reaction, where it has been previously observed that products of both RO2 + RO2 (such as pinic acid) and RO2 + HO2 (organic peroxides) are formed, it is to be expected that at higher oxidation rates the system will shift more towards RO2 + RO2 reactions. This can have a significant effect on SOA yields. This is also true for the referenced studies on monoterpene + NO3 reactions. The authors should discuss this effect and how it might alter the interpretation of their results.*"

Author response: We acknowledge that it is possible that the RO_2 radical chemistry may be different at low (100 ppb O_3) and high (500 ppb O_3) oxidation rates, which in turn, may affect the SOA mass yields. We also agree with the referee that differing RO_2 radical chemistry may also play a role in the different SOA mass yields measured in the reference NO_3+monoterpene studies. Therefore, we have made the following changes in the revised manuscript:

Page 24 line 677: "It should be noted that while we showed that the observed oxidation rate effect (i.e., higher SOA mass yields as a result of faster hydrocarbon oxidation rates) is a consequence of vapor-wall deposition, the possibility that differing peroxy radical (RO_2) chemistry in the 100 and 500 ppb O_3 experiments may play some role in influencing the SOA mass yields cannot be discounted. RO_2 radicals, which are formed from the decomposition of excited Criegee intermediates (Docherty et al., 2005), may be produced at faster rates in the 500 ppb O_3 experiments. This may lead to the higher production of condensable oxidation products from the RO_2+RO_2 reaction pathway in the 500 ppb O_3 experiments

(relative to those formed in the 100 ppb O_3 experiments), which may result in higher SOA mass yields."

Page 29 line 825: "In addition to differences in the experimental conditions of the two studies (which may lead to differing RO_2 chemistry), Boyd et al. (2015) hypothesized that the higher SOA mass yields could also be a result of the higher NO_3 concentrations used in their study (which led to faster β-pinene oxidation rates) compared to those used by Fry et al. (2009, 2014)."

5. Referee comment: "*Similar to the comments made in #4, when comparing studies the authors should consider the fact that oxidation rate is unlikely to affect RO2 chemistry under high NOx conditions, such as in aromatic VOC experiments.*"

Author response: We thank the referee for the comment. We have made the following changes to the revised manuscript:

Page 29 line 829: "The oxidation rate effect was also observed in the *m*-xylene photooxidation system, where Ng et al. (2007) showed that the SOA mass yields were dependent on the *m*-xylene oxidation rate, with higher OH concentrations (and hence faster oxidation rates) resulting in higher SOA mass yields. The authors dismissed the possibility of the different SOA mass yields being a result of different RO_2 chemistry since all their *m*-xylene photooxidation experiments were performed under high-NO_x conditions and the RO_2 reacted virtually entirely with NO."

6. Referee comment: "*Line 592: Should add "of" after "regardless".*"

Author response: This is corrected in the revised manuscript.

<u>The following are additional minor changes the authors have made to the manuscript:</u>

1. This sentence was added into the revised manuscript:

Page 3 line 68: "Determination of particle wall loss coefficients may be complicated if coagulation is significant. Particle dynamics models can be used to correct particle wall loss coefficients for coagulation."

2. We corrected the grammatical errors in the sentence:

Page 5 line 128: "Before each experiment, the chamber was flushed with dried, purified air for at least 36 h until the aerosol number concentration was < 30 cm^{-3}. All experiments were conducted under dry conditions (< 5 % RH) at room temperature (25 °C). All experiments were conducted under dry conditions (< 5 % RH) at room temperature (25 °C). NO_x mixing ratios in these experiments were < 1 ppb. Experimental conditions are summarized in Table 1."

3. This sentence was added into the revised manuscript:

Page 7 line 212: "As we describe subsequently, β_i may be measured directly during seed-only experiments or may be corrected for the influence of coagulation using a particle dynamics model."

4. This sentence was added into the revised manuscript:

Page 9 line 248: "Modeled O_3 and α-pinene concentrations are compared with observed concentrations in Fig. S5. The good fit of modeled and observed O_3 and α-pinene concentrations indicates that our representation of O_3 is appropriate."

5. This sentence was added into the revised manuscript:

Page 9 line 266: "Coagulation is not considered in the present model; we address the potential impact of coagulation later in the paper."

6.We added the word "measured" to the sentence:

Page 17 line 479: "It is important to note that these conclusions are robust even when the average of the measured low AS-seed only and high AS-seed only particle wall loss coefficients are used to account for particle wall loss in all the experiments (Fig. S6)."

7. Figures S6, S11, S12 and S13 in the original manuscript are changed to Figures S5, S10, S11 and S12, respectively, in the revised manuscript. Table S2 in the original manuscript is changed to Table S3 in the revised manuscript. Equations 13 and 14 in original manuscript are changed to equations 15 and 16, respectively in the revised manuscript.

8. We changed "ΔM_0" to "ΔM_o" in Table 1 headers.

9. We added a period after Shilling et al in Figure 5 caption:

"Figure 5: Comparison of SOA mass yields obtained in this study to those of previous dark α-pinene ozonolysis studies (Table S2). The SOA mass yields and concentrations of majority of these previous studies (Hoffmann et al., 1997; Griffin et al., 1999; Cocker et al., 2001b; Gao et al., 2004; Presto et al., 2005; Presto et al. 2006; Pathak et al., 2007b; Song et al., 2007) were previously compiled by Shilling et al. (2008). Similar to Shilling et al. (2008), all the data shown here (including those reported in this study) have been adjusted using an organic density of 1.0 g cm^{-3}, and to 298 K using a temperature correction of 1.6 % per K, as recommended by Pathak et al. (2007b) to facilitate easier comparison among the different studies."

10. We corrected Figure S4 caption:

"Figure S4: Raw and particle wall loss (PWL) corrected number and volume concentration data for the 500 ppb O_3 experiments. All the raw data are particle wall loss corrected using the average particle wall loss rates (i.e. average of the particle wall loss rates obtained from low AS-seed only and high-AS seed only experiments)."

11. We revised Figure S6 caption:

Figure S6: 10 min-averaged SOA mass yields over the course of an α-pinene ozonolysis experiment as a function of initial total AS seed surface area concentration for the (a) 100 ppb O_3 experiments, and (b) 500 ppb O_3 experiments. Here, all the data have been particle wall loss corrected using the average particle wall loss rates (i.e. average of the particle wall loss rates measured from low AS-seed only and high-AS seed only experiments). Symbol color indicates the SOA mass concentration and symbol size indicates the time after O_3 is injected into the chamber. The × symbols are the SOA mass yields at peak SOA growth. The y-axis error bars represent the uncertainty in the peak SOA mass yield, which originates from the α-pinene injection and the aerosol volume concentration measured by the SMPS at peak SOA growth (one standard deviation). As discussed in the main text, the use of average measured particle wall loss rates for particle wall loss correction does not change the conclusions of this work: 1) SOA mass yields are enhanced at higher O_3 concentrations, and 2) there is a lack of a SOA mass yield dependence on the seed surface area within the range of AS seed surface area concentration used in this study.

12. We corrected the grammatical errors in Figure S12 caption:

"Figure S12: Results from the coupled vapor-particle dynamics model showing how SOA mass concentration (ΔM_o) changes as a function of reacted α-pinene at different O_3 concentrations. In these model simulation runs, the initial α-pinene concentration is fixed at 48 ppb, while the O_3 concentration is varied from 75 to 1000 ppb. Here, the O_3 injection rate is 5 times faster than the base rate used in the model. The base rate is 500/54.25 ppb min^{-1}, the same rate used to analyze results from the 500 ppb O_3 experiments. As discussed in the main text, the oxidation rate effect persists at a higher O_3 concentration when a faster O_3 injection rate is used. It is important to note that SOA evaporation is predicted at high O_3 concentrations in the coupled vapor-particle dynamics model, but not observed in chamber experiments."

13. We corrected Table S3 caption:

"Table S3: Comparison of experimental conditions used in this work with those of previous dark α-pinene ozonolysis studies. The SOA mass yields and concentrations of these studies are shown Fig. 5."

14. In the original manuscript, the citation for Zaveri et al. (2014) was left out in the Reference section. This citation is added to the revised manuscript:

Zaveri, R. A., Easter, R. C., Shilling, J. E., and Seinfeld, J. H.: Modeling kinetic partitioning of secondary organic aerosol and size distribution dynamics: representing effects of volatility, phase state, and particle-phase reaction, Atmospheric Chemistry and Physics, 14, 5153-5181, 10.5194/acp-14-5153-2014, 2014.

15. The following references have also been added to the revised manuscript:

Docherty, K. S., Wu, W., Lim, Y. B., and Ziemann, P. J.: Contributions of organic peroxides to secondary aerosol formed from reactions of monoterpenes with O-3, Environmental Science & Technology, 39, 4049-4059, 10.1021/es050228s, 2005.

Krechmer, J. E., Pagonis, D., Ziemann, P. J., and Jimenez, J. L.: Quantification of Gas-Wall Partitioning in Teflon Environmental Chambers Using Rapid Bursts of Low-Volatility Oxidized Species Generated in Situ, Environmental Science & Technology, 50, 5757-5765, 10.1021/acs.est.6b00606, 2016.

Saha, P. K., and Grieshop, A. P.: Exploring Divergent Volatility Properties from Yield and Thermodenuder Measurements of Secondary Organic Aerosol from α-Pinene Ozonolysis, Environmental Science & Technology, 50, 5740-5749, 10.1021/acs.est.6b00303, 2016.

Ye, P., Ding, X., Hakala, J., Hofbauer, V., Robinson, E. S., and Donahue, N. M.: Vapor wall loss of semi-volatile organic compounds in a Teflon chamber, Aerosol Sci. Technol., 50, 822-834, 10.1080/02786826.2016.1195905, 2016.

Influence of Seed Aerosol Surface Area and Oxidation Rate on Vapor-Wall Deposition and SOA Mass Yields: A case study with α-pinene Ozonolysis

T. Nah,[1] R. C. McVay,[2] X. Zhang,[3,#] C. M. Boyd,[1] J. H. Seinfeld[2,3] and N. L. Ng[1,4*]

[1]*School of Chemical and Biomolecular Engineering, Georgia Institute of Technology, Atlanta, GA, USA*
[2]*Division of Chemistry and Chemical Engineering, California Institute of Technology, Pasadena, CA, USA*
[3]*Division of Engineering and Applied Science, California Institute of Technology, Pasadena, CA, USA*
[4]*School of Earth and Atmospheric Sciences, Georgia Institute of Technology, Atlanta, GA, USA*
[#]*Now at: Center for Aerosol and Cloud Chemistry, Aerodyne Research, Billerica, MA, USA*

** To whom correspondence should be addressed: ng@chbe.gatech.edu*

Abstract

Laboratory chambers, invaluable in atmospheric chemistry and aerosol formation studies, are subject to particle and vapor wall deposition, processes that need to be accounted for in order to accurately determine secondary organic aerosol (SOA) mass yields. Although particle wall deposition is reasonably well understood and usually accounted for, vapor wall deposition is less so. The effects of vapor wall deposition on SOA mass yields in chamber experiments can be constrained experimentally by increasing the seed aerosol surface area to promote the preferential condensation of SOA-forming vapors onto seed aerosol. Here, we study the influence of seed aerosol surface area and oxidation rate on SOA formation in α-pinene ozonolysis. The observations are analyzed using a coupled vapor-particle dynamics model to interpret the roles of gas-particle partitioning (quasi-equilibrium vs. kinetically-limited SOA growth) and α-pinene oxidation rate in influencing vapor wall deposition. We find that the SOA growth rate and mass yields are independent of seed surface area within the range of seed surface area concentrations used in this study. This behavior arises when the condensation of SOA-forming vapors is dominated by quasi-equilibrium growth. Faster α-pinene oxidation rates and higher SOA mass yields are observed at increasing O_3 concentrations for the same initial α-pinene concentration. When the α-pinene oxidation rate increases relative to vapor wall deposition, rapidly produced SOA-forming oxidation products condense more readily onto seed aerosol particles, resulting in higher SOA mass yields. Our results indicate that the extent to which vapor wall deposition affects SOA mass yields depends on the

particular VOC system, and can be mitigated through the use of excess oxidant concentrations.

1. Introduction

Secondary organic aerosol (SOA), formed from the oxidation of volatile and intermediate volatility organic compounds (VOCs and IVOCs), contributes a significant fraction of the global organic aerosol burden (Kanakidou et al., 2005; Hallquist et al., 2009; Tsigaridis et al., 2014). SOA formation studies, which are typically conducted in laboratory chambers in the presence of seed aerosol particles, provide fundamental data that can be used to predict the rate of atmospheric SOA formation. An essential parameter of interest in laboratory chamber studies is the SOA mass yield (Y), which is defined as the ratio of mass concentration of SOA formed to mass concentration of parent hydrocarbon reacted ((ΔHC), $Y = \Delta M_o/\Delta HC$ (Odum et al., 1996; Odum et al., 1997a; Odum et al., 1997b)). The measured SOA mass yields can subsequently be applied in atmospheric models to predict regional and global organic aerosol burdens. In order to obtain accurate SOA mass yields from the evolving aerosol size distribution in chamber experiments, the loss of both particles and vapors to the chamber walls needs to be accurately accounted for (Crump and Seinfeld, 1981; McMurry and Grosjean, 1985; McMurry and Rader, 1985; Cocker et al., 2001a; Weitkamp et al., 2007; Pierce et al., 2008; Hildebrandt et al., 2009; Loza et al., 2010; Matsunaga and Ziemann, 2010; Loza et al., 2012; Kokkola et al., 2014; McVay et al., 2014; Yeh and Ziemann, 2014; Zhang et al., 2014; Yeh and Ziemann, 2015; Zhang et al., 2015a; La et al., 2016; Ye et al., 2016).

The mechanisms by which particles in chambers deposit on chamber walls are reasonably well understood. Particles are transported to the boundary layer on the chamber walls via diffusion, gravitational settling, and electrostatic forces (Crump and Seinfeld, 1981; McMurry and Grosjean, 1985; McMurry and Rader, 1985; Pierce et al., 2008). The rate at which particles are transported to the edge of the boundary layer is dictated primarily by mixing conditions in the chamber. An effective approach for characterizing particle wall loss involves measuring the size-dependent wall loss rates of polydisperse inert seed aerosol (e.g. ammonium sulfate particles) injected into the chamber during seed-only experiments (Keywood et al., 2004; Pierce et al., 2008). The

observed particle number concentration decay in each size bin is then fitted to a first-order exponential decay from which the first-order wall loss coefficients are determined as a function of particle size. These wall loss coefficients are subsequently used to correct for size-dependent particle wall loss in actual SOA formation experiments. Determination of particle wall loss coefficients may be complicated if coagulation is significant. Particle dynamics models can be used to correct particle wall loss coefficients for coagulation.

Vapor-wall deposition mechanisms in chambers are not as well understood or accounted for as those for particles. The degree to which SOA-forming vapors deposit onto chamber walls is governed by the rate at which these gas-phase organic molecules are transported to the walls, the strength of adherence of the organic molecule to the wall, and the extent of reversible vapor-wall partitioning (Loza et al., 2010; Matsunaga and Ziemann, 2010; Zhang et al., 2015a). For example, Loza et al. (2010) showed that the loss of 2,3-epoxy-1,4-butanediol, an isoprene oxidation product analogue, to walls in the Caltech chamber was essentially irreversible on short time scales but became reversible on longer time scales. In contrast, glyoxal, a common isoprene oxidation product, exhibited reversible vapor-wall partitioning over all time scales. Recent studies show that SOA mass yields measured in chamber experiments can be significantly underestimated due to wall deposition of SOA-forming vapors that would otherwise contribute to SOA growth (McVay et al., 2014; Zhang et al., 2014; La et al., 2016). Zhang et al. (2014) found that chamber-derived SOA mass yields from toluene photooxidation may be underestimated by as much as a factor of four as a result of vapor wall loss. Consequently, the use of underestimated chamber-derived SOA mass yields in atmospheric models will lead to the underprediction of ambient SOA mass concentrations (Cappa et al., 2016).

For the toluene photooxidation system, Zhang et al. (2014) showed that the measured SOA mass yields increased with increasing seed aerosol surface area, demonstrating that increasing the seed-to-chamber surface area ratio promoted the condensation of SOA-forming vapors onto seed aerosol particles. However, increasing the seed aerosol surface area to promote condensation of SOA-forming vapors onto seed aerosol particles may not be effective in all VOC oxidation systems. A modeling study by

McVay et al. (2014) showed that the SOA mass yield depends on seed aerosol surface area only in cases where the condensation of SOA-forming vapors onto seed aerosol particles is kinetically limited (i.e., the timescale for gas-particle equilibrium is competitive with or greater than the timescale for reaction and vapor-wall deposition). In addition to the seed aerosol surface area, VOC oxidation rate may also play an important role in the effect of vapor wall loss on SOA formation. Ng et al. (2007) showed that the SOA mass yields from *m*-xylene photooxidation are dependent on the oxidation rate, with higher OH concentrations (hence faster oxidation rates) resulting in higher SOA mass yields. It was suggested that the "oxidation rate effect" could arise as a result of competition between growing particles and chamber walls for condensable VOC oxidation products (Ng et al., 2007). However, McVay et al. (2016) reported similar SOA growth at low and high OH concentrations in α-pinene photooxidation. Taken together, these studies show the importance of understanding how gas-particle partitioning and VOC oxidation rate impact vapor-wall deposition and SOA mass yields in laboratory chamber experiments.

In this study, we examine the influence of seed aerosol surface area and oxidation rate on SOA formation in α-pinene ozonolysis chamber experiments. α-pinene is the most abundant monoterpene, with global emissions estimated to be ~66 Tg yr^{-1} (Guenther et al., 2012). Ozonolysis is the major atmospheric oxidation pathway of α-pinene, and is estimated to account for reaction of ~46 % of emitted α-pinene (Griffin et al., 1999; Capouet et al., 2008). α-pinene ozonolysis, a major source of atmospheric SOA on both regional and global scales (Kanakidou et al., 2005; Hallquist et al., 2009; Carlton et al., 2010; Pye et al., 2010), has been the subject of numerous studies (Hoffmann et al., 1997; Griffin et al., 1999; Cocker et al., 2001b; Gao et al., 2004; Presto et al., 2005; Presto and Donahue, 2006; Pathak et al., 2007a; Pathak et al., 2007b; Song et al., 2007; Shilling et al., 2008; Henry et al., 2012; Ehn et al., 2014; Kristensen et al., 2014; Zhang et al., 2015b). Here, we measure the α-pinene SOA mass yield as a function of seed aerosol surface area concentration (0 to 3000 μm^2 cm^{-3}) and O_3 mixing ratio (100 vs. 500 ppb). These results are analyzed using a coupled vapor-particle dynamics model to evaluate the roles of gas-particle partitioning and VOC oxidation rate in influencing vapor-wall deposition effects on the measured SOA mass yields.

2. Experimental

2.1. Dark α-pinene ozonolysis experiments

Experiments were conducted in the Georgia Tech Environmental Chamber (GTEC) facility. Details of the dual chamber facility are provided elsewhere (Boyd et al., 2015). Only one FEP Teflon chamber (volume 13 m^3) was used for the entirety of this study. Before each experiment, the chamber ~~is~~ was flushed with dried, purified air for at least 36 h until the aerosol number concentration ~~is~~ was < 30 cm^{-3}. All experiments were conducted under dry conditions (< 5 % RH) at room temperature (25 °C). NO_x mixing ratios in these experiments ~~are~~were < 1 ppb. Experimental conditions are summarized in Table 1.

22 ppm of cyclohexane (Sigma Aldrich, ≥ 99.9 %) was first injected into the chamber to act as an OH scavenger (~440 times the initial α-pinene concentration). Based on the concentrations of cyclohexane and α-pinene injected into the chamber, the reaction rate of OH with cyclohexane is ~60 times greater than that with α-pinene. After the cyclohexane concentration had stabilized in the chamber for 30 min, a known concentration (~50 ppb in all experiments) of α-pinene (Sigma Aldrich, > 99 %) was injected into the chamber, followed by inorganic seed aerosol via atomization of an aqueous ammonium sulfate (AS) solution (in seeded experiments). To vary the seed aerosol surface area, different concentrations of AS solutions were used to generate seed aerosol particles in the seeded experiments. In the "low AS" experiments, a 0.015 M AS solution was used to generate seed particles, and the resulting initial total AS seed surface area concentration was ~1000 μm^2 cm^{-3}. In the "high AS" experiments, a 0.05 M AS solution was used to generate seed aerosol particles, and the resulting initial total AS seed surface area concentration was ~3000 μm^2 cm^{-3}. In selected experiments, no seed aerosol particles were introduced into the chamber and SOA was formed via nucleation. After the seed aerosol concentration in the chamber stabilized, O_3 (100 or 500 ppb), which was generated by passing purified air into a photochemical cell (Jelight 610), was introduced into the chamber. The start of O_3 injection into the chamber marked the beginning of the reaction (i.e., reaction time = 0 min). The ~~initial~~ injected α-pinene:O_3 molar ratio ~~was fixed at~~were~~was~~ approximately 1:2 and 1:10 in the 100 and 500 ppb O_3 experiments,

respectively. O_3 was injected into the chamber for 13.5 and 54.25 min in the 100 and 500 ppb O_3 experiments, respectively, to achieve the desired O_3 concentrations. Approximately 11 % and 98 % of the initial α-pinene had reacted when O_3 injection was completed in the 100 and 500 ppb O_3 experiments, respectively. ~~Due to the design of~~In the GTEC ~~facility~~chamber, α-pinene closest to the O_3 injection port ~~of the chamber~~ likely reacted first in the α-pinene ozonolysis experiments. The O_3 injection times were established in separate experiments in which only O_3 was injected into the chamber. Based on the O_3 time series traces in the O_3-only experiments, the O_3 mixing timescale was estimated to be ~12 min for all experiments.

The α-pinene and O_3 concentrations were measured by a Gas Chromatograph-Flame Ionization Detector (GC-FID, Agilent 7890A) and O_3 monitor (Teledyne T400), respectively. GC-FID measurements were taken 12 min apart. A High Resolution Time-of-Flight Aerosol Mass Spectrometer (HR-ToF-AMS, Aerodyne Research Inc.) was used to measure the aerosol elemental composition (DeCarlo et al., 2006; Canagaratna et al., 2015). Details on the operation of the HR-ToF-AMS and its data analysis are described elsewhere (Canagaratna et al., 2015). Aerosol size distributions, number and volume concentrations were measured by a Scanning Mobility Particle Sizer (SMPS, TSI), which consists of a Differential Mobility Analyzer (DMA, TSI 3081) and a Condensation Particle Counter (CPC, TSI 3775). For nucleation and low AS experiments, the measured aerosol size range was set to 14 to 686 nm diameter. For high AS experiments, the measured aerosol size range was set to 17 to 983 nm. Prior checks were made to confirm that no particles larger than 686 nm were detected in the nucleation and low AS experiments. The SOA mass concentrations reported in this study were measured using the SMPS. The SOA density was calculated from the ratio of the aerosol size distributions measured by the HR-ToF-AMS and the SMPS during nucleation experiments (DeCarlo et al., 2004; Bahreini et al., 2005).

2.2. Particle wall deposition correction

Particle wall deposition needs to be accounted for to determine the SOA mass concentration in the chamber. Two limiting assumptions have traditionally been made regarding interactions between particles deposited on the chamber walls and suspended

vapors when accounting for particle wall loss in the computation of SOA mass yields (Weitkamp et al., 2007; Hildebrandt et al., 2009; Loza et al., 2012; Zhang et al., 2014). The first case assumes that particles deposited on the walls cease to interact with suspended vapors, and therefore the SOA mass present on these deposited particles does not change after deposition (Loza et al., 2012; Zhang et al., 2014). Adding the SOA mass present on these deposited particles to that present on the suspended particles provides a lower bound of the total SOA mass concentration. In the second case, it is assumed that particles deposited on the walls continue to interact with suspended vapors as if these particles had remained suspended, and therefore the SOA mass present on these deposited particles increases at the same rate as those suspended (Hildebrandt et al., 2009; Weitkamp et al., 2007). Thus, this case provides an upper bound of the total SOA mass concentration due to the additional uptake of suspended vapors to wall-deposited particles. However, it must be kept in mind that the calculated SOA mass concentration can be underestimated even in the upper bound case since the calculation accounts neither for differences in the vapor-particle and vapor-wall interaction and transport timescales nor for the significantly larger amount of absorbing mass of the chamber walls (relative to the deposited particles) for suspended vapors (McVay et al., 2014; Zhang et al., 2014; McVay et al., 2016).

In this study, we calculate SOA mass yields using the lower bound of the total SOA mass concentration obtained from SMPS measurements, which has been described in detail previously (Loza et al., 2012), and will be reviewed briefly here. For each particle size bin i at each time increment Δt, the particle number distribution deposited on the wall ($n_{w,i,j}$) is:

$$n_{w,i,j} = n_{s,i,j} \times (1 - \exp(-\beta_i \Delta t)) \quad (1)$$

where $n_{s,i,j}$ is the suspended particle number distribution in particle size bin i at time step j, Δt is the difference between time step j and time step $j+1$, and β_i is the size-dependent first-order exponential wall loss rate obtained from seed-only experiments. As we describe subsequently, β_i may be measured directly during seed-only experiments or may be corrected for the influence of coagulation using a particle dynamics model. The

particle wall loss corrected number distribution ($n_{total,i,j}$) is obtained from the sum of the particle number distribution of deposited particles ($n_{w,i,j}$) and suspended particles ($n_{s,i,j}$):

$$n_{total,i,j} = n_{s,i,j} + n_{w,i,j} \quad (2)$$

Assuming spherical particles, the particle wall loss corrected volume concentration ($V_{total,j}$) is:

$$V_{total,j} = \sum_{i=1}^{m} \frac{n_{total,i,j}}{D_{p,i} \ln 10} \times (D_{p,i+} - D_{p,i-}) \times \frac{\pi}{6} D_{p,i}^3 \quad (3)$$

where m is the number of particle size bins, $D_{p,i+}$ and $D_{p,i-}$ are the upper and lower limits for size bin i, respectively, and $D_{p,i}$ is the median particle diameter for size bin i. The term $D_{p,i}$ln10 is needed to convert from a lognormal distribution. Figures S1-S4 and Table S1 show results from the particle wall loss correction. To calculate the SOA mass concentration ($\Delta M_{o,j}$), the SOA density (ρ_{org}) is multiplied by the difference of the particle wall loss corrected volume concentration ($V_{total,j}$) and the initial seed volume concentration (V_{seed}):

$$\Delta M_{o,j} = \rho_{org} \times (V_{total,j} - V_{seed}) \quad (4)$$

The measured densities of the α-pinene SOA are 1.39 and 1.37 g cm^{-3} for the 100 and 500 ppb O_3 experiments, respectively, and are within the range (i.e., 1.19 to 1.52 g cm^{-3}) reported in previous α-pinene ozonolysis studies (Bahreini et al., 2005; Kostenidou et al., 2007; Song et al., 2007; Shilling et al., 2009).

3. Vapor-particle dynamics model

A coupled vapor-particle dynamics model is used to evaluate the influence of seed aerosol surface area and oxidation rate on SOA formation in the α-pinene ozonolysis chamber experiments. This model is similar to that used in McVay et al. (2014), and will be briefly described here. Parameters from the experimental data (temperature, pressure, initial α-pinene concentration) are used as model inputs. The initial size distribution is set to that measured by the SMPS, with the exception of the two nucleation experiments. Because nucleation is not explicitly simulated, an approximation is used in which the

smallest diameter bin is initialized with the total number of particles measured at the end of the experiment (see Table S1). In each simulation, the decay of α-pinene, the consumption of O_3, the SOA mass concentration, and the SOA mass yield are calculated throughout the duration of the experiment. We assume a linear injection rate of O_3 based on the time required to inject the desired O_3 concentration. For example, O_3 is injected at a rate of 500/54.25 ppb min^{-1} for the first 54.25 min during the 500 ppb O_3 experiments. O_3 simultaneously decays by reaction with α-pinene at a rate constant of 9.4×10^{-17} cm^3 $molec.^{-1}$ s^{-1} (Saunders et al., 2003). Modeled O_3 and α-pinene concentrations are compared with observed concentrations in Fig. S5. The good fit of modeled and observed O_3 and α-pinene concentrations indicates that our representation of O_3 is appropriate. The O_3+α-pinene reaction is assumed to occur in a well-mixed chamber and produces 5 classes of first-generation products, which are grouped according to mass saturation concentrations, similar to the volatility basis set (Donahue et al., 2006): $>10^3$ (assumed to be completely volatile), 10^2, 10, 1 and 0.1 μg m^{-3}. Branching ratios between these products are optimized to fit the experimental data. These branching ratios cannot be compared directly to previously reported VBS parameters for α-pinene ozonolysis (e.g. Henry et al. (2012)) since VBS parameters are typically mass-based, while the branching ratios in the model are mole-based. Furthermore, the branching ratios here account for the influence of vapor wall deposition, while typical VBS parameters do not. We assume that these 5 classes of products have molecular weights 168, 184, 192, 200 and 216 g $mole^{-1}$ based on the group contribution method (Donahue et al., 2011). The first-generation products are assumed not to undergo further reaction with O_3 upon formation.

The aerosol dynamics in the chamber obey the aerosol general dynamic equation (Seinfeld and Pandis, 2006):

$$\left(\frac{\partial n(D_p,t)}{\partial t}\right) = \left(\frac{\partial n(D_p,t)}{\partial t}\right)_{\text{coag}} + \left(\frac{\partial n(D_p,t)}{\partial t}\right)_{\text{cond/evap}} + \left(\frac{\partial n(D_p,t)}{\partial t}\right)_{\text{wall loss}} \quad (5)$$

Coagulation is not considered in the present model; we address the potential impact of coagulation later in the paper~~, since an alternative version of the model including coagulation showed no change in the predicted α-pinene ozonolysis SOA mass~~

~~concentrations in simulations with and without coagulation~~. The change in particle number distribution due to particle wall loss is:

$$\left(\frac{\partial n(D_p,t)}{\partial t}\right)_{\text{wall loss}} = -\beta_j(D_p)n(D_p,t) \quad (6)$$

where, as noted in section 2.2, $\beta_j(D_p)$ is the size-dependent first-order wall loss rate coefficient obtained from fitting seed-only experiments. The rate at which vapor condenses onto a spherical aerosol particle is:

$$J_i = 2\pi D_p D_i (G_i - G_i^{eq}) F_{FS} \quad (7)$$

where G_i is the concentration of gas-phase species i, G_i^{eq} is the saturation concentration of gas-phase species i, D_i is the gas-phase molecular diffusivity (assumed to be 3×10^{-6} m^2 s^{-1} (McVay et al., 2014)), and F_{FS} is the Fuchs-Sutugin correction for non-continuum gas-phase diffusion:

$$F_{FS} = \frac{0.75\alpha_p(1+\text{Kn})}{\text{Kn}^2 + \text{Kn} + 0.283\text{Kn}\alpha_p + 0.75\alpha_p} \quad (8)$$

where α_p is the vapor-particle mass accommodation coefficient, and Kn is the Knudsen number, $\text{Kn} = 2\lambda_{AB}/D_p$. The vapor-particle mass accommodation coefficient accounts for any resistance to vapor molecule uptake at the particle surface (e.g. surface accommodation and particle-phase diffusion limitations). λ_{AB} is the mean free path of the gas-phase species, which is:

$$\lambda_{AB} = 3D_i \times \sqrt{\frac{\pi M_i}{8RT}} \quad (9)$$

where R is the ideal gas constant, T is the temperature, and M_i is the molecular weight of diffusing gas-phase molecule i. For each particle size bin, Eqs. 7-9 are used to compute the flux of each gas-phase species to and from an aerosol particle, scaled by the particle number concentration in the size bin. The net rate of change for each gas-phase species

due to evaporation or condensation is obtained from the total flux summed over all the particle size bins.

G_i^{eq} varies for each particle size bin because it depends on the mass concentration of species *i* and the total organic mass concentration in the size bin:

$$G_i^{eq} = \frac{A_i C_i^*}{\sum_k A_k + M_{init}} \quad (10)$$

where A_i is the concentration of species *i* in the particle phase, C_i^* is the saturation concentration of species *i*, $\sum_k A_k$ is the sum of all the species concentration in the particle phase, and M_{init} is the mass concentration of any absorbing organic material initially present in the seed aerosol. To avoid numerical errors in Eq. 10 at the first time step, M_{init} is set to 0.01 μg m^{-3}.

The oxidation products of α-pinene ozonolysis are assumed to be subject to vapor-wall deposition, which is simulated using a first-order wall-loss coefficient (McMurry and Grosjean, 1985):

$$k_{wall,on} = (\frac{A}{V}) \frac{\frac{\alpha_{wall}\bar{c}}{4}}{1 + \frac{\pi}{2}(\frac{\alpha_{wall}\bar{c}}{4\sqrt{k_e D_i}})} \quad (11)$$

where *A/V* is the surface area-to-volume ratio of the chamber (estimated to be 2.5 m^{-1}), α_{wall} is the vapor-wall mass accommodation coefficient, and k_e is the eddy diffusion coefficient that describes mixing conditions in the chamber. Based on the measured size-dependent particle wall loss rates (method is described in Zhang et al. (2014)), k_e is estimated to be 0.03 s^{-1} for the GTEC chamber. Vapor-wall deposition is assumed to be reversible, and the rate constant of vapor desorption from the chamber walls is:

$$k_{wall,off} = \frac{k_{wall,on}}{K_W C_W} = k_{wall,on}(\frac{C_i^* M_w \gamma_w}{C_W M_p \gamma_p}) \quad (12)$$

where C_w is the equivalent organic mass concentration in the wall (designated to treat gas-wall partitioning in terms of gas-particle partitioning theory and not necessarily representative of a physical layer of organic concentration on the wall (Matsunaga and Ziemann, 2010)), K_w is the gas-wall partitioning coefficient, M_w is the effective molecular weight of the wall material, γ_w is the activity coefficient of the species in the wall layer, M_p is the average molecular weight of organic species in the particle, and γ_p is the activity coefficient of the species in the particle. For simplicity, we assume that $M_w = M_p$ and $\gamma_w = \gamma_p$. C_w is set to 10 mg m^{-3} based on previous inferences by Matsunaga and Ziemann (2010). Sensitivity studies (not shown) show no change in model predictions when varying C_w above $C_w = 0.1$ mg m^{-3}.

In the initial version of the model, after all the α-pinene is consumed, vapor wall deposition was assumed to continue to deplete the gas-phase oxidation products and aerosol mass evaporates to maintain gas-particle equilibrium. SOA evaporation was not observed experimentally (i.e., the SOA mass concentration does not decrease significantly over time after peak SOA growth has been achieved in these chamber experiments (Fig. 2)). In order to represent these observations in the model, a first-order, particle-phase reaction is introduced by which aerosol species are converted into non-volatile absorbing organic mass with a timescale of τ_{olig}. This mechanism (which is not included in the model used in McVay et al. (2014)) is similar to that used by the sequential equilibrium partitioning model, in which aerosol is converted from an absorbing to non-absorbing, non-volatile phase in order to explain the inhibited diffusion and evaporation observed in α-pinene ozonolysis SOA (Cappa and Wilson, 2011). Although we assume here that the converted non-volatile aerosol mass still participates in partitioning, either mechanism invokes a particle-phase process to retard SOA evaporation.

In order to determine the parameters for α_w, α_p, τ_{olig} and the branching ratios between the oxidation products that provide the best fit to measured SOA data, the parameter space was discretized and all possible combinations of parameters were simulated, following Karnezi et al. (2014). In order to restrict the number of combinations required, only parameter values judged to be physically realistic were

chosen. Because the branching ratios in this model are mole-based, they must sum to one; therefore only combinations of parameters summing to one were allowed. The discretization is shown in Table S2 and results in roughly 10,000 different combinations of parameters. All six experiments were simulated with each parameter combination, and simulations were run using GNU Parallel (Tange 2011). For each combination of parameters, the percentage error was calculated from equation 10 of Karnezi et al. (2014):

$$E_i = \frac{100}{n}\sqrt{\sum_i^n (Moa_{i,guess} - Moa_{i,meas})^2} \quad (13)$$

where $Moa_{i,guess}$ is the model-predicted SOA mass concentration at a particular timestep i for one of the experiments, $Moa_{i,meas}$ is the measured SOA mass concentration at a particular timestep i for one of the experiments, and n is the number of timesteps summed over all experiments. The best-fit combination of parameters is defined as the combination of parameters with the lowest percentage error. This lowest-error combination of parameters was compared to the "best estimate" parameters determined from the inverse error weighting factor of Karnezi et al. (2014):

$$\bar{x} = \frac{\sum_j^N \left[x_j \frac{1}{E_j}\right]}{\sum_j^N \frac{1}{E_j}} \quad (14)$$

where x_j is a value of one of the parameters (α_w, α_p, τ_{olig} or a branching ratio between the oxidation products), with N different possible combinations of parameters, and E_j is the percent error for that particular combination of parameters. The lowest-error combination of parameters and the Karnezi et al. (2014) best estimate parameters are both reported, but the lowest-error combination of parameters resulted in a lower percentage error than the Karnezi et al. (2014) best estimate parameters. The lowest-error combination of parameters is used for the modeling analysis.

~~Model parameters α_w, α_p, τ_{olig} and the branching ratios between the oxidation products are optimized to best fit the predictions with the experimental observations. Specifically, model predictions are compared to experimental data: SOA mass concentration vs. reaction time, α-pinene concentration vs. reaction time, and O_3~~

~~concentration vs. reaction time. Figure S8 compares reaction profiles of measured and modeled O_3 and α-pinene concentrations for the base model case. Sensitivity tests were also performed on each model parameter, shown in Figs. S7S9-S10S12. Table 2 summarizes the parameters used. While the optimized parameters provide a good fit to the data, we caution that the parameters are interconnected, and other fits may also be possible. We are confident that our conclusions derived using these parameters are robust.~~

4. Results

Red and blue solid lines in Fig~~ure~~ 1 shows the size-dependent particle wall deposition coefficients ~~inferred~~ measured ~~from~~ in the low AS-seed only and high AS-seed-only deposition experiments. In these measurements, we assume that the number concentration is low enough such that the effect of coagulation is small and only particle wall deposition affects the particle size distribution, thus allowing for the direct measurement of size-dependent particle wall deposition coefficients. The initial total AS seed surface area concentration in the low AS-seed only and high AS-seed only experiments (which are conducted using 0.015 M AS and 0.05 M AS solutions, respectively) are similar to those used in the α-pinene ozonolysis experiments (i.e., ~1000 and ~3000 μm^2 cm^{-3}, respectively). As shown in Fig. 1, the measured particle wall deposition coefficients from the low AS-seed only and high AS-seed only experiments generally fall within the range of those measured in routine monthly AS-seed only experiments conducted in the chamber. Figure 1 also shows the size-dependent particle wall deposition coefficients corrected for coagulation, shown using dashed lines, which are obtained as described in Pierce et al., 2008 using the data from the low AS-seed only and high AS-seed only experiments. A comprehensive description of the relationship between coagulation and particle wall deposition will be provided in a forthcoming publication. Briefly, as described in Pierce et al. (2008), the coagulation-corrected particle wall loss coefficients ~~we~~are determined by simulating the decay of the initial size distribution due to coagulation and then attributing the difference in this decay and the observed decay to particle wall loss. For both the measured and coagulation-corrected particle wall deposition coefficients, the minimum coefficient for the low AS-seed only

experiment is different from that of the high AS-seed only experiments. ~~-~~The cause of this difference is currently under investigation but may be due in part to ~~-~~uncertainties arising from the low particle number concentrations for the larger particles in the low AS-seed only experiment. To study how coagulation can potentially affect SOA mass yields in this study, both the measured and coagulation-corrected size-dependent particle wall deposition coefficients are used to correct for particle wall deposition in the α-pinene ozonolysis experiments.

Assuming that the effect of coagulation is small, t~~T~~he particle wall deposition corrected number concentration data provide a test of the appropriateness of the particle wall deposition correction. ~~This is because t~~The corrected number concentration should level off at a constant value (i.e., the initial particle number concentration), assuming no significant coagulation, when particle wall deposition is properly accounted for since the wall-deposited particle number distribution is added to the suspended particle number distribution during particle wall loss correction. Neglecting coagulation, ~~W~~we account for particle wall deposition in nucleation and low AS experiments using deposition coefficients ~~determined~~ measured from the low AS-seed only experiments, while particle deposition in high AS experiments are accounted for using coefficients ~~determined~~ measured from the high AS-seed only experiments. Figures S1 and S2 show the particle wall deposition-corrected aerosol number and volume concentrations. Over all experiments, the particle wall deposition-corrected final particle number concentration (i.e., at the end of the reaction) is 9 to 17 % less than the initial particle number concentration for the low AS and high AS experiments (Table S1), respectively, indicating that the particle wall deposition-corrected volume concentrations are slightly underestimated. ~~It is currently unclear why~~ The fact that the particle wall deposition-corrected final particle number concentrations are somewhat smaller than the initial particle number concentrations~~, though this could~~ may be due to variations in particle wall deposition rates in the AS-seed only and α-pinene ozonolysis experiments or to coagulation. ~~As a sensitivity test~~To first examine variations in particle wall deposition rates, we used the average of the measured low AS-seed only and high AS-seed only particle wall deposition coefficients to account for particle wall deposition in all the experiments (Figs. S3 and S4). While there is a negligible difference in the particle wall

deposition corrected volume concentrations (Figs. S3 and S4 vs. Figs. S1 and S2), a larger spread (1 to 22 %) exists in the difference between the initial and final particle number concentrations when the average measured particle wall deposition coefficients are used (Table S1). Therefore, all subsequent nucleation and low AS data presented here are particle wall deposition-corrected using coefficients ~~determined~~ measured from the low AS-seed only experiments, and all high AS data are corrected using particle wall deposition coefficients measured~~determined~~ from the high AS-seed only experiments. We furthermore conclude that variations in particle wall deposition rates do not cause the decrease in the particle wall deposition-corrected final number concentration and is most likely due to coagulation. Thus, the SOA data are~~is~~ also corrected using the coagulation-corrected particle wall deposition coefficients (discussed below). We show subsequently the relatively minor difference that correcting for coagulation has on overall SOA mass yields. Therefore, we use SOA concentrations corrected using the measured particle wall deposition coefficients for the bulk of the analysis in this study.

Figure 2 shows the reaction profiles of the α-pinene ozonolysis experiments. SOA growth typically starts within 10 to 20 min of the start of the reaction. At either ~~initial~~ O_3 concentration, the molar ratio of O_3 reacted to α-pinene reacted is approximately 1:1 (i.e., 50 ppb α-pinene reacted with 50 ppb O_3), which indicates that O_3 reacts only with α-pinene and not its oxidation products. As anticipated, the α-pinene oxidation rates in the 100 ppb O_3 experiments are significantly slower than those in the 500 ppb O_3 experiments. Figures 2a-c show that peak SOA levels are typically reached at reaction time ~300 to 350 min in the 100 ppb O_3 experiments, during which ≥ 95 % of the injected α-pinene has reacted. In contrast, all the α-pinene reacts within 80 to 90 min of the start of reaction in the 500 ppb O_3 experiments, and peak SOA levels are achieved at reaction time ~100 min (Figs. 2d-f). These results indicate that the O_3 concentration dictates both the rate of α-pinene oxidation and the time it takes to achieve peak SOA growth.

Figure 3 shows the time-dependent growth curves (SOA mass concentration vs. α-pinene reacted (Ng et al., 2006)) for the 100 and 500 ppb O_3 experiments. Only SOA growth data up to SOA peak concentrations are shown. SOA growth essentially stops

once all the α-pinene has reacted. This is expected, as α-pinene has only one double bond; the first step of α-pinene ozonolysis is rate-limiting and the first-generation products are condensable (Ng et al., 2006; Chan et al., 2007). The time-dependent SOA growth curves for experiments corresponding to different seed aerosol concentrations overlap for both low and high O_3 concentrations. This indicates that the initial AS seed surface area does not influence the SOA growth rate within the range of AS seed surface area concentration used. It is important to note that while it appears that the SOA growth rate is faster in the 100 ppb O_3 relative to the 500 ppb O_3 experiments based on the time-dependent growth curves shown in Fig. 3, this is not the case. Instead, the observed time-dependent growth curves can be explained by the higher concentration of α-pinene having reacted during the 10 to 20 min delay of SOA formation in the 500 ppb O_3 experiments compared to the 100 ppb O_3 experiments (Fig. 2).

Figure 4 shows the time-dependent SOA mass yields as a function of initial total AS seed surface area for the 100 and 500 ppb O_3 experiments. Regardless of the O_3 concentration, the SOA mass yields stay roughly constant despite the increase in AS seed surface area. This indicates that the surface area concentration of AS seed aerosol does not noticeably influence the partitioning of gas-phase α-pinene ozonolysis products to the particle phase within the range of AS seed surface area concentration used. Higher SOA mass yields are observed in the 500 ppb O_3 experiments, which indicates that the α-pinene oxidation rate controls the absolute amount of SOA formed. It is important to note that these conclusions are robust even when the average of the measured low AS-seed only and high AS-seed only particle wall loss coefficients are used to account for particle wall loss in all the experiments (Fig. ~~S5~~S6). The enhancement of SOA mass yields at higher O_3 concentrations and the lack of a SOA mass yield dependence on AS seed surface area (within the range of AS seed surface area concentration used in this study) will be discussed further in Section 5.

The α-pinene ozonolysis SOA mass yields obtained in this study are compared to those reported in previous studies in Fig. 5. ~~Table S2~~Table S3 lists the experimental conditions employed in these studies. To facilitate comparison between the different studies, all the SOA mass yield and concentration data (including this study) are adjusted

to an organic density of 1.0 g cm^{-3}. As shown in Fig. 5, the SOA mass yields obtained at peak SOA growth in this study are generally consistent with those of previous studies where the chamber was operated in batch mode (that in this study).

To investigate the influence of coagulation on the SOA mass yields, the ~~modeled~~ coagulation-corrected size-dependent particle wall deposition coefficients ~~(that account for coagulation)~~ are also used to correct for particle wall deposition in the α-pinene ozonolysis experiments. Specifically, all nucleation and low AS data are particle wall deposition-corrected using coagulation-corrected~~modeled~~ coefficients derived from the low AS-seed only experiments, and all high AS data are corrected using coagulation-corrected~~modeled~~ particle wall deposition coefficients derived from the high AS-seed only experiments. Figure S7 shows the time-dependent SOA mass yields (obtained using the ~~modeled~~coagulation-corrected and measured particle wall deposition coefficients) as a function of initial total AS seed surface area. SOA mass yields obtained using the ~~modeled~~coagulation-corrected particle wall deposition coefficients are < 2 % (absolute values) higher than those using the measured particle wall deposition coefficients. Similar to the SOA mass yields obtained using the measured particle wall deposition coefficients (Figs. 4, S7c and S7d), SOA mass yields obtained using the coagulation-corrected~~modeled~~ particle wall deposition coefficients stay roughly constant despite the increase in AS seed surface area for both O_3 concentrations, and the SOA mass yields are higher in the 500 ppb O_3 experiments (Figs. S7a and S7b). The mass yields obtained at peak SOA growth are also generally consistent with those of previous studies (Fig. S8). Taken together, this suggests that the effect of coagulation on the SOA mass yields is likely minor for the aerosol concentrations used in this study. Therefore, only data that have been particle wall deposition-corrected using coefficients measured in the low AS-seed only and high AS-seed only experiments are fitted ~~with model predictions~~to determine model parameters for the vapor-particle dynamics model described in Section 3.

~~The competition between the condensation of SOA-forming vapor to aerosol particles vs. to chamber walls is investigated using the coupled vapor-particle dynamics model described in Section 3.~~ As noted earlier, optimal model values for α_p, α_w, τ_{olig} and

the branching ratios between the oxidation products were determined ~~for the 100 and 500 ppb O_3 experiments~~ by ~~comparing~~ calculating the error between the observed and ~~best-fit~~modeled time-dependent SOA~~, α-pinene, and O_3 concentrations profiles~~ concentrations for all possible combinations of model parameters ~~(Figs. S8–S10~~S12~~)~~. ~~Sensitivity tests were performed for each parameter to establish that the set of optimal model values provide the best overall agreement with time-dependent SOA formation profiles observed for all experiments (Figs. S7~~S9 S10S12~~). Predictions from the coupled vapor-particle dynamics model show that the optimal parameters are~~ The combination of parameters with the lowest percent error is~~:~~ $\alpha_w = 10^{-6}$, $\alpha_p = 0.1$, $\tau_{olig} = 4$ h, branching ratios = 0.~~57~~6, 0.3~~5~~, 0.0~~5~~4, 0.0~~1~~5 and 0~~.025~~ for oxidation products with vapor pressures $>10^3$, 10^2, 10, 1 and 0.1 μg m^{-3}, respectively. This combination of parameters results in a percent error of 21% (Table S4). It is important to note that predictions using $\alpha_p = 0.1$ or 1 resulted in very similar errors; with the same combination of parameters and $\alpha_p = 1$, the percent error only increased to 22%. The "best estimate" parameters determined following the Karnezi et al. (2014) method are as follows: $\alpha_w = 3.6\times10^{-6}$, $\alpha_p = 0.35$, $\tau_{olig} = 6$ h, and branching ratios = 0.66, 0.16, 0.06, 0.06, and 0.06 for oxidation products with vapor pressures $>10^3$, 10^2, 10, 1 and 0.1 μg m^{-3}, respectively. This combination of parameters results in an error of 37% (Table S4). Model predictions using both sets of parameters are compared to measured SOA concentrations in Fig~~.~~. S9. The lowest-error parameters are used for the analysis in the remainder of this study. The best-fit $\alpha_w = 10^{-6}$ ~~(Fig. S7S9)~~ corresponds to a first-order vapor-wall deposition rate constant ($k_{wall,on}$) of 10^{-4} s^{-1}. A wide range of vapor wall loss rates has been reported (Figure 3 of Krechmer et al. (2016)). This $k_{wall,on}$ value is comparable to that reported by Matsunaga and Ziemann (2010) for a 8.2 m^3 chamber but significantly faster than wall loss rates that have been measured in the Caltech chamber (Zhang et al., 2015). The reason for this wide range of reported vapor wall loss rates is currently uncertain and outside the scope of this study.

5. Discussion

α-pinene ozonolysis has been carried out at two O_3 mixing ratios (100 and 500 ppb) under varying AS seed aerosol surface area concentrations (0, ~1000 and ~3000 μm^2 cm^{-3}).

550 **5.1 Seed aerosol surface area effect**

551 Figure 3 shows that the time-dependent SOA growth curves for experiments with
552 different seed area concentrations overlap at both O_3 concentrations, which indicates the
553 AS seed surface area does not affect the rate of SOA growth within the range of AS seed
554 surface area concentration used in this study. This observation differs from findings by
555 Pathak et al. (2007b) for the O_3+α-pinene system, who showed that even though the final
556 SOA mass yields measured in the reaction of 7.3 ppb α-pinene with 1500 ppb O_3 were
557 similar in their seeded and unseeded experiments, SOA growth was considerably slower
558 in unseeded experiments compared to seeded experiments. The authors suggested that the
559 slow SOA formation rate in their unseeded experiment was the result of SOA formation
560 being limited by the mass transfer of semi-volatile oxidation products to newly formed
561 particles (via nucleation) during the early stages of the experiment. These newly formed
562 particles have a significantly smaller aerosol surface area for gas-particle partitioning as
563 compared to that of seed aerosol particles in the seeded experiments. Consequently, the
564 semi-volatile oxidation products accumulated in the gas phase during the early stages of
565 the unseeded experiments, resulting in slower SOA growth compared to the seeded
566 experiments. The observation that the presence of seed aerosol does not influence the
567 SOA growth rate in the present study may be explained by the relatively high
568 concentrations of α-pinene reacted and SOA mass loadings obtained. Previous studies
569 have shown that the delay between the onset of VOC oxidation and SOA formation in
570 unseeded experiments is most pronounced at low aerosol loadings (Kroll et al., 2007).
571 We note that the concentrations of α-pinene reacted and SOA mass loadings obtained in
572 this study are significantly larger than those reported by Pathak et al. (2007b). Therefore,
573 it is possible that due to the relatively large concentrations of α-pinene reacted in this
574 study, substantial concentrations of gas-phase oxidation products are generated, which
575 results in rapid partitioning into the particle phase even in the absence of seed aerosol.
576 This is evident from the large increase in the particle number concentration during the
577 early stages of the unseeded 100 and 500 ppb O_3 experiments, where the particle number
578 concentration increased to ~8000 and ~10000 particles/cm^3 during the first 45 min of the
579 100 and 500 ppb O_3 experiments, respectively (Fig. S1a and S2a). Thus, the SOA growth
580 rates are not controlled by the presence of AS seed in this study.

Figure 4 shows that for both ~~initial~~ O_3 mixing ratios used, the time-dependent SOA mass yield is similar at any given AS seed surface area (see also Table 1). The absence of a SOA growth dependence on the AS seed surface area is similar to observations reported by McVay et al. (2016) for the α-pinene photooxidation (OH-driven chemistry) system, but differ from those reported by Zhang et al. (2014) for the toluene photooxidation system in which the SOA mass yield increased with the surface area concentration of seed aerosol.

The best-fit $\alpha_p = 0.1$ (or $\alpha_p = 1$, with almost the same percentage error) ~~(Fig. S108)~~ suggests the absence of significant limitations to vapor-particle mass transfer in the present α-pinene ozonolysis study, and that SOA formation is governed by quasi-equilibrium growth (Saleh et al., 2013; McVay et al., 2014), which occurs when SOA-forming vapors are produced at a rate that is significantly slower than that required to establish gas-particle equilibrium (Shiraiwa and Seinfeld, 2012; Zhang et al., 2012). Moreover, the characteristic timescale to establish gas-particle equilibrium is less than those for reaction and vapor-wall deposition. When the vapor and particle phases maintain equilibrium, gas-particle equilibrium is controlled by the amount of organic matter in the VOC system. As a result, the rate of condensation of SOA-forming vapors is independent of the seed aerosol surface area (McVay et al., 2014). The best-fit $\alpha_p = 0.1$ is within the ~~approximate~~ range of α_p coefficients determined from α-pinene ozonolysis SOA thermodenuder studies ($\alpha_p = 0.1$) (Saleh et al., 2013; Saha et al., 2016) and α-pinene photooxidation chamber studies ($\alpha_p = 0.1$ or 1) (McVay et al., 2016). Notably, this result differs markedly from that for toluene photooxidation (Zhang et al., 2014), where α_p was determined to be 0.001, and for which, since the SOA mass yield was strongly dependent on the seed aerosol surface area, the condensation of SOA-forming vapors onto seed aerosol particles was kinetically limited (McVay et al., 2014). Kinetically-limited SOA growth occurs when the timescale for gas-particle equilibrium is competitive with or exceeds the timescale for reaction and vapor wall deposition, and may reflect imperfect accommodation of gas-phase organics to the particle phase. The markedly different behavior of the α-pinene and toluene SOA systems could be due to differences in SOA volatility and aerosol physical phase state (McVay et al., 2016).

5.2 Oxidation rate effect

At higher O_3 concentrations, the α-pinene oxidation rate increases, leading to higher SOA mass yields (the "oxidation rate effect"). This behavior was previously observed by Ng et al. (2007) for the *m*-xylene photooxidation system, for which the oxidation rate effect was attributed to the loss of semi-volatile condensable products to chamber walls in competition with condensation onto seed particles to form SOA.

SOA formation from α-pinene ozonolysis is presumed to be driven by a range of semi- and low-volatility first-generation products arising from reaction of O_3 with the single C=C double bond (Ng et al., 2006). These products are subject to two competing routes: condensation to particles to form SOA or deposition on the chamber walls. Each process can be represented in terms of a first-order rate constant: $k_{wall,on}$ and $k_{particle,on}$ (s^{-1}). The rate of vapor-wall deposition of condensable species A is then $k_{wall,on}$ × [A] (molec cm^{-3} s^{-1}) and the rate of condensation onto particles is $k_{particle,on}$ × [A] (molec cm^{-3} s^{-1}). Increasing the rate of reaction increases the concentration of [A], but the relative rates of vapor-wall deposition and condensation onto particles will remain the same. In general, however, both vapor-wall deposition and vapor-particle condensation are reversible processes (McVay et al., 2014; Zhang et al., 2014). The first-order rate constant for evaporation from the wall can be represented as (Matsunaga and Ziemann, 2010):

$$k_{wall,off} = k_{wall,on}\left(\frac{C_i^*}{C_w}\right) \qquad (15\text{~~13~~})$$

where C_i^* is the saturation concentration and C_w is the assumed equivalent wall organic concentration. The rate of evaporation from particles is:

$$k_{particle,off} = k_{particle,on}\left(\frac{C_i^*}{C_{aer}}\right) \qquad (16\text{~~14~~})$$

where C_{aer} is the organic aerosol concentration ($C_{aer}=\sum A_k+M_{init}$).

The difference between C_{aer} and C_w is the key to explaining the oxidation rate effect. At the beginning of the experiment, C_{aer} is very small because the inorganic seeds

are essentially non-absorbing. Therefore, $k_{particle,off}$ is large, and the net SOA growth is small. In contrast, C_w is considered to be substantial (on the order of 10 mg m^{-3}) and to be essentially constant throughout the experiment (Matsunaga and Ziemann, 2010; McVay et al., 2014; Zhang et al., 2014). Model predictions are insensitive to the value of C_w since, in any event, C_w is significantly larger than C_{aer} (Zhang et al., 2014). Therefore, $k_{wall,off}$ is small at the beginning of the experiment and the net vapor wall loss rate is fast. As C_{aer} increases, the net SOA condensation rate increases relative to the net vapor wall loss rate. When the reaction rate increases corresponding to higher O_3 concentrations, C_{aer} grows more quickly because more condensable species are available to form SOA, and the net condensation rate increases more rapidly. Therefore, the observed oxidation rate effect is due to vapor wall deposition, and arises because vapor-particle and vapor-wall condensation are essentially reversible processes. This explanation is consistent with simulations varying the O_3 concentration in which all species are non-volatile (i.e., do not evaporate from the particles or the wall). In this case, no oxidation rate effect is observed as the O_3 concentration increases. The growth curves for different O_3 concentrations overlap, and the same yield is obtained regardless of O_3 concentration (Fig. ~~S11~~S10).

Sensitivity tests were performed to determine the point at which SOA formation is no longer influenced by the O_3 concentration. In these simulations, the initial α-pinene concentration is fixed at 48 ppb, while the O_3 concentration is varied from 75 to 1000 ppb. The rate of O_3 injection is assumed to remain constant as the O_3 concentration is increased to mimic the experimental protocol (i.e., O_3 injection time is increased to achieve higher O_3 concentrations). The O_3 injection rate used in these simulations is fixed at 500/54.25 ppb min^{-1}, which is the same as that used to analyze results from the 500 ppb O_3 experiments. Model predictions in Fig. ~~S12~~ S11 show that the maximum SOA mass concentration increases with increasing O_3 concentration up to approximately 500 ppb O_3. Beyond this O_3 concentration, the SOA growth curves overlap and the maximum SOA mass concentration does not increase even when more O_3 is added. This plateau arises due to the lengthening time required to inject increasing amounts of O_3. More than 1 h is required to inject > 500 ppb of O_3, and by this time, virtually all of the α-pinene has reacted. Increasing the O_3 concentration after all of the α-pinene has reacted does not lead to any changes in the SOA mass concentration. However, if a faster injection rate of O_3 is

used, the oxidation rate effect will persist to higher O_3 concentrations (i.e., > 500 ppb O_3) (Fig ~~S13~~S12). With a faster injection rate, 500 ppb O_3 is injected before all of the α-pinene has reacted. Continuing to inject O_3 to a higher concentration (i.e., 750 ppb) will cause α-pinene to decay faster and SOA to grow faster than when the O_3 injection stops at 500 ppb. The oxidation rate effect is then apparent at higher O_3 concentrations. If, instead of using an injection rate of O_3, simulations are run using fixed initial O_3 (not possible experimentally), the rate effect persists to even higher O_3 concentrations. The relative increase in yield with increasing O_3 concentrations slows at very high O_3 concentrations because the rate of reaction becomes substantially faster than the vapor wall deposition rate, and there is less marginal effect to increasing the reaction rate.

It should be noted that while we showed that the observed oxidation rate effect (i.e., higher SOA mass yields as a result of faster hydrocarbon oxidation rates) is a consequence of vapor-wall deposition, the possibility that differing peroxy radical (RO_2) chemistry in the 100 and 500 ppb O_3 experiments may play some role in influencing the SOA mass yields cannot be discounted. RO_2 radicals, which are formed from the decomposition of excited Criegee intermediates (Docherty et al., 2005), may be produced at faster rates in the 500 ppb O_3 experiments. This may lead to the higher production of condensable oxidation products from the RO_2+RO_2 reaction pathway in the 500 ppb O_3 experiments (relative to those formed in the 100 ppb O_3 experiments), which may result in higher SOA mass yields.

5.3 Interplay of the seed aerosol surface area effect and the oxidation rate effect

In this study, we observe an oxidation rate effect but not a seed aerosol surface area effect. In Zhang et al. (2014), a seed aerosol surface area effect was observed, but the variation of the oxidation rate was not studied. A key aspect of vapor wall deposition is the potential interplay between the seed aerosol surface area effect and the oxidation rate effect. To examine this interplay in the α-pinene ozonolysis system, simulations were carried out by varying the seed aerosol surface area and the O_3 concentration simultaneously, while using the branching ratios, oligomerization rate, and vapor wall deposition rate parameters obtained in the present study. The initial α-pinene concentration was set to 50 ppb, and a fixed O_3 concentration was used in place of a

linear injection. α_p was varied at 0.001, 0.01, 0.1, and 1 in these simulations. Figure 6 shows the SOA mass yield at peak SOA growth as a function of both the seed aerosol surface area and O_3 concentration for α_p = 1, 0.1, 0.01, and 0.001. For α_p = 1 or 0.1, the oxidation rate dominates: SOA mass yield increases significantly as O_3 concentration increases while the seed aerosol surface area has a negligible effect. For α_p = 0.01, both effects can be observed in different regions: at low O_3 concentrations and high seed aerosol surface areas, the oxidation rate effect dominates; at low seed aerosol surface areas and high O_3 concentrations, the seed surface area dominates. At low seed aerosol surface areas and low O_3 concentrations, both effects are present. For α_p = 0.001, the seed aerosol surface area effect dominates except at very high seed aerosol surface areas. These observations show that the presence of an oxidation rate effect and/or seed aerosol surface area effect depends on a complex interplay of factors, such as α_p, the rate of hydrocarbon oxidation, and the amount of seed surface area present.

6. Implications

In this study, we systematically examine the roles of gas-particle partitioning and VOC oxidation rate in the presence of vapor-wall deposition in α-pinene ozonolysis. We show that despite the presence of vapor-wall deposition, SOA mass yields at peak SOA growth remain approximately constant regardless of the seed aerosol surface area (within the range of AS seed surface area concentration used in this study). This observation is consistent with SOA formation in the α-pinene ozonolysis system being governed by quasi-equilibrium growth, for which there are no substantial limitations to vapor-particle mass transfer. This result was demonstrated in a previous modeling study which showed that increasing the seed-to-chamber surface area ratio will lead to increased SOA growth only in cases in which the condensation of SOA-forming vapors onto seed aerosol particles is kinetically limited as a result of imperfect accommodation of gas-phase organics to the particle phase (McVay et al., 2014).

An important implication of this study is that diverting vapor-wall deposition in chamber studies via the addition of ever-increasing quantities of seed aerosol particles is not effective in VOC systems for which SOA formation is governed by quasi-equilibrium growth. This study also underscores the importance of accounting for particle wall

deposition appropriately in chamber studies, to avoid erroneous conclusions regarding the role of gas-particle partitioning (quasi-equilibrium vs. kinetically-limited SOA growth) in influencing vapor wall loss in the VOC system.

We note that the present study shows that the SOA mass yield is independent of seed aerosol surface area concentration for values ranging from 0 to ~3000 μm^2 cm^{-3}. This corresponds to a seed-to-chamber surface area ratio of 0 to ~1 × 10^{-3}, which is substantially smaller than the range used by Zhang et al. (2014) to study the influence of vapor-wall deposition on toluene photooxidation SOA formation in the Caltech chamber (i.e., 0 to ~5 × 10^{-3}). It is possible that a SOA mass yield dependence on the seed surface area may have become more apparent had a larger range of seed aerosol surface area (i.e., > 3000 μm^2 cm^{-3}), and hence a larger range of seed-to-chamber surface area ratio, been used here. One consideration is that coagulation may become increasingly important, and will need to be accounted for, when higher seed aerosol number concentrations (relative to those used in this study) are used (Seinfeld and Pandis, 2006; Pierce et al., 2008). A detailed analysis of the effect of seed aerosol surface area concentrations > 3000 μm^2 cm^{-3} on α-pinene ozonolysis SOA mass yields will be the subject of forthcoming work.

Higher SOA mass yields at peak SOA growth are observed in the present study when O_3 is increased from 100 to 500 ppb. This is because α-pinene is oxidized more quickly, which leads to gas-phase oxidation products being formed more rapidly, and consequently partitioning more quickly onto AS seed aerosol particles before they are lost to the chamber walls. Therefore, the oxidation rate effect (i.e., higher SOA mass yields as a result of faster hydrocarbon oxidation rates) is a consequence of vapor-wall deposition. An important implication of this study is that SOA mass yields can be affected by vapor-wall deposition in VOC systems that are not characterized by slow mass accommodation of gas-phase organics to the particle phase (Zhang et al., 2014). Thus, this work demonstrates that the effect of vapor-wall deposition on SOA mass yields can be mitigated through the use of excess oxidant concentrations. It should be noted that the α-pinene ozonolysis SOA mass yields (absolute values) increased by 5 to 9 % when O_3 is increased from 100 to 500 ppb (for an initial α-pinene concentration of ~50 ppb), where SOA formation is governed by quasi-equilibrium growth. In the absence of vapor-

wall deposition, SOA mass yields are predicted by the model used here to approximately double from those observed experimentally. In contrast, Zhang et al. (2014) showed that the presence of vapor-wall deposition led to underestimation of SOA formation by factors as much as four in the toluene photooxidation system, where the condensation of SOA-forming vapors onto seed aerosol is kinetically limited. Taken together, these results indicate that the magnitude by which vapor-wall deposition affects SOA mass yields depends on the extent to which the VOC system is governed by kinetically-limited SOA condensational growth.

Given these observations of how gas-particle partitioning can influence the magnitude by which vapor-wall deposition affects SOA mass yields, an overriding question is: what controls the gas-particle partitioning behavior of SOA formed in different VOC systems? α_p describes the overall mass transfer of vapor molecules into the particle phase (McVay et al., 2014; Zhang et al., 2014). Thus, α_p affects the vapor-particle equilibrium timescale, which, depending on the extent to which it is competitive with the timescales for reaction and vapor-wall deposition, determines whether SOA formation is governed by kinetically-limited or quasi-equilibrium growth. Markedly different α_p values could arise from the physical phase state of the SOA formed. As discussed by McVay et al. (2014, 2016), if the SOA formed exists in a semi-solid state (Vaden et al., 2010; Virtanen et al., 2010; Cappa and Wilson, 2011; Vaden et al., 2011; Virtanen et al., 2011; Kuwata and Martin, 2012; Perraud et al., 2012; Saukko et al., 2012; Abramson et al., 2013; Renbaum-Wolff et al., 2013), a low value of α_p might be expected owing to retarded surface accommodation and particle-phase diffusion (Zaveri et al., 2014). Quantification of α_p is challenging experimentally, and reported α_p values for the same system can vary by several orders of magnitude (Grieshop et al., 2007; Stanier et al., 2007; Vaden et al., 2011; Miles et al., 2012; Saleh et al., 2013 Saha et al., 2016). Therefore, α_p of SOA formed in different VOC systems need to be better constrained through a combination of experimental and modeling efforts.

While not investigated in detail in this study, the timescale of oligomerization may play an important role depending on the SOA growth regime (i.e., kinetically-limited vs. quasi-equilibrium). Currently, it is unclear how the timescale of

oligomerization in a VOC system where SOA formation is dominated by quasi-equilibrium growth (e.g. α-pinene ozonolysis) may differ from one that is dominated by kinetically-limited growth (e.g. toluene photooxidation (Zhang et al., 2014)). This requires further investigation through a combination of experimental and modeling efforts to improve our understanding of how particle-phase processes (e.g. oligomerization) affect gas-particle partitioning, and consequently influence the magnitude by which vapor-wall deposition affects SOA mass yields.

The SOA mass yield from the ozonolysis of monoterpenes in the GEOS-CHEM chemical transport model (19 % at 10 μg m^{-3}) is currently based on that measured in α-pinene ozonolysis studies by Shilling et al. (2008) (Pye et al., 2010). Shilling et al. (2008) measured these SOA mass yields in a teflon chamber operated in continuous-flow mode, as opposed to batch mode, which is how experiments in the present study and most of those shown in Fig. 5 and ~~Table S2~~Table S3 were conducted. While it is not possible to directly compare our results with those of Shilling et al. (2008) due to differences in SOA mass concentrations, the SOA mass concentrations and yields measured in the current study are generally consistent with those of previous batch chamber studies. The SOA mass yields at ~10 μg m^{-3} SOA mass concentration measured by Shilling et al. (2008) are generally higher than those measured in chambers operated in batch mode (Griffin et al., 1999; Cocker et al., 2001b; Presto et al., 2005; Presto and Donahue, 2006; Pathak et al., 2007b) (Fig. 5). One possible explanation for the higher SOA mass yields in the continuous-flow, steady state, mode is that the SOA-forming vapors are in equilibrium with the ~~organic mass present on the~~ chamber walls and seed aerosol, hence minimizing the irreversible loss of SOA-forming vapors to the chamber walls (Shilling et al., 2008). However, the extent to which SOA mass yields obtained in a continuous-flow reactor are influenced by vapor wall loss is unclear. Using a continuous-flow reactor, Ehn et al. (2014) observed α-pinene ozonolysis SOA mass yields to increase with increasing seed aerosol surface area but required $\alpha_p = 1$ to fit the observed SOA growth. The observed vapor-wall deposition rate constant in their continuous-flow reactor (0.011 s^{-1}) is two orders of magnitude larger than that of the GTEC chamber (10^{-4} s^{-1}). The estimated timescales for gas-particle and gas-wall partitioning are also approximately equal in their continuous-flow reactor. This indicates that SOA condensational growth is kinetically

limited in their continuous-flow reactor even at $\alpha_p = 1$ (Ehn et al., 2014; McVay et al., 2014), which suggests that SOA mass yields measured in their continuous-flow reactor may be significantly affected by vapor-wall deposition.

Previous studies on SOA formation from the OH and NO_3 oxidation of biogenic VOCs have similarly reported higher SOA mass yields in the presence of higher oxidant concentrations. For example, in the NO_3 oxidation of β-pinene, Boyd et al. (2015) reported SOA mass yields 10 to 30 % higher than those previously reported by Fry et al. (2009, 2014). In addition to differences in the experimental conditions of the two studies (which may lead to differing RO_2 chemistry), Boyd et al. (2015) hypothesized that the higher SOA mass yields could also be a result of the higher NO_3 concentrations used in their study (which led to faster β-pinene oxidation rates) compared to those used by Fry et al. (2009, 2014). The oxidation rate effect was also observed in the *m*-xylene photooxidation system, where Ng et al. (2007) showed that the SOA mass yields were dependent on the *m*-xylene oxidation rate, with higher OH concentrations (and hence faster oxidation rates) resulting in higher SOA mass yields. The authors dismissed the possibility of the different SOA mass yields being a result of different RO_2 chemistry since all their *m*-xylene photooxidation experiments were performed under high-NO_x conditions and the RO_2 reacted virtually entirely with NO. Together, these studies show that faster hydrocarbon oxidation rates can alleviate the effects of vapor-wall deposition on SOA mass yields in different VOC systems.

This gives rise to the question: should chamber SOA experiments on different VOC systems be performed under as rapid oxidation conditions as possible (i.e., large oxidant concentrations) to reduce the effects of vapor-wall deposition? A recent study by McVay et al. (2016) reported similar SOA growth under low and high OH levels for α-pinene photooxidation. The authors hypothesized that the autoxidation mechanism likely becomes a more important pathway at low OH levels (Crounse et al., 2013), and thus contributes substantially to SOA growth. Therefore, it is possible that certain reaction pathways and mechanisms (which are important in the atmosphere) are biased when unusually high levels of oxidants are used in chamber experiments (e.g. autoxidation). Thus, this underscores the need to design chamber experiments that simultaneously

mitigate the magnitude of vapor-wall deposition while ensuring that reaction conditions, and consequently reaction pathways and oxidation products, are atmospherically relevant. More importantly, the impact of vapor-wall deposition on SOA formation and evolution in various VOC systems conducted under different reaction conditions (regardless of atmospheric relevance) needs to be quantified through a combination of experimental and modeling efforts. Similar to this study, experiments should be performed using different seed aerosol surface area and oxidant concentrations to study their influence on vapor-wall deposition and SOA mass yields. If the effects of vapor-wall loss are found to be strongly dependent on seed aerosol surface area and/or oxidant concentrations (e.g. toluene photooxidation, where SOA formation may be underestimated by factors as much as four (Zhang et al., 2014)), further experiments aimed at measuring the wall deposition rates of the oxidation products should be performed. These wall deposition rates can then be used in predictive models to determine the vapor-wall and vapor-particle mass accommodation coefficients of these oxidation products. Consequently, this will allow us to determine the fraction of SOA-forming vapors partitioning to the particle phase vs. lost to the chamber walls (Zhang et al., 2015; Krechmer et al., 2016).

Acknowledgements

This research was funded by NSF Grants 1455588 and AGS-1523500, and US Environmental Protection Agency STAR grant (Early Career) RD-83540301. This publication's contents are solely the responsibility of the grantee and do not necessarily represent the official views of the US EPA. Further, US EPA does not endorse the purchase of any commercial products or services mentioned in the publication. R.C. McVay was supported by a National Science Foundation Graduate Research Fellowship under Grant No. DGE-1144469.

References

Abramson, E., Imre, D., Beranek, J., Wilson, J., and Zelenyuk, A.: Experimental determination of chemical diffusion within secondary organic aerosol particles, Phys. Chem. Chem. Phys., 15, 2983-2991, 10.1039/c2cp44013j, 2013.

876 Bahreini, R., Keywood, M. D., Ng, N. L., Varutbangkul, V., Gao, S., Flagan, R. C.,
877 Seinfeld, J. H., Worsnop, D. R., and Jimenez, J. L.: Measurements of Secondary Organic
878 Aerosol from Oxidation of Cycloalkenes, Terpenes, and m-Xylene Using an Aerodyne
879 Aerosol Mass Spectrometer, Environmental Science & Technology, 39, 5674-5688,
880 10.1021/es048061a, 2005.

881 Boyd, C. M., Sanchez, J., Xu, L., Eugene, A. J., Nah, T., Tuet, W. Y., Guzman, M. I., and
882 Ng, N. L.: Secondary organic aerosol formation from the β-pinene+NO3 system: effect of
883 humidity and peroxy radical fate, Atmos. Chem. Phys., 15, 7497-7522, 10.5194/acp-15-
884 7497-2015, 2015.

885 Canagaratna, M. R., Jimenez, J. L., Kroll, J. H., Chen, Q., Kessler, S. H., Massoli, P.,
886 Hildebrandt Ruiz, L., Fortner, E., Williams, L. R., Wilson, K. R., Surratt, J. D., Donahue,
887 N. M., Jayne, J. T., and Worsnop, D. R.: Elemental ratio measurements of organic
888 compounds using aerosol mass spectrometry: characterization, improved calibration, and
889 implications, Atmos. Chem. Phys., 15, 253-272, 10.5194/acp-15-253-2015, 2015.

890 Capouet, M., Müller, J. F., Ceulemans, K., Compernolle, S., Vereecken, L., and Peeters,
891 J.: Modeling aerosol formation in alpha-pinene photo-oxidation experiments, Journal of
892 Geophysical Research: Atmospheres, 113, n/a-n/a, 10.1029/2007JD008995, 2008.

893 Cappa, C. D., and Wilson, K. R.: Evolution of organic aerosol mass spectra upon heating:
894 implications for OA phase and partitioning behavior, Atmospheric Chemistry and
895 Physics, 11, 1895-1911, 10.5194/acp-11-1895-2011, 2011.

896 Cappa, C. D., Jathar, S. H., Kleeman, M. J., Docherty, K. S., Jimenez, J. L., Seinfeld, J.
897 H., and Wexler, A. S.: Simulating secondary organic aerosol in a regional air quality
898 model using the statistical oxidation model – Part 2: Assessing the influence of vapor
899 wall losses, Atmos. Chem. Phys., 16, 3041-3059, 10.5194/acp-16-3041-2016, 2016.

900 Carlton, A. G., Bhave, P. V., Napelenok, S. L., Edney, E. D., Sarwar, G., Pinder, R. W.,
901 Pouliot, G. A., and Houyoux, M.: Model Representation of Secondary Organic Aerosol in
902 CMAQv4.7, Environmental Science & Technology, 44, 8553-8560, 10.1021/es100636q,
903 2010.

Chan, A. W. H., Kroll, J. H., Ng, N. L., and Seinfeld, J. H.: Kinetic modeling of secondary organic aerosol formation: effects of particle- and gas-phase reactions of semivolatile products, Atmospheric Chemistry and Physics, 7, 4135-4147, 2007.

Cocker, D. R., Flagan, R. C., and Seinfeld, J. H.: State-of-the-art chamber facility for studying atmospheric aerosol chemistry, Environmental Science & Technology, 35, 2594-2601, 10.1021/es0019169, 2001a.

Cocker, D. R., Clegg, S. L., Flagan, R. C., and Seinfeld, J. H.: The effect of water on gas-particle partitioning of secondary organic aerosol. Part I: alpha-pinene/ozone system, Atmospheric Environment, 35, 6049-6072, 10.1016/s1352-2310(01)00404-6, 2001b.

Crounse, J. D., Nielsen, L. B., Jorgensen, S., Kjaergaard, H. G., and Wennberg, P. O.: Autoxidation of Organic Compounds in the Atmosphere, J. Phys. Chem. Lett., 4, 3513-3520, 10.1021/jz4019207, 2013.

Crump, J. G., and Seinfeld, J. H.: Turbulent Deposition and Gravitational Sedimentation of an Aerosol in a Vessel of Arbitrary Shape, Journal of Aerosol Science, 12, 405-415, 10.1016/0021-8502(81)90036-7, 1981.

DeCarlo, P. F., Slowik, J. G., Worsnop, D. R., Davidovits, P., and Jimenez, J. L.: Particle morphology and density characterization by combined mobility and aerodynamic diameter measurements. Part 1: Theory, Aerosol Sci. Technol., 38, 1185-1205, 10.1080/027868290903907, 2004.

DeCarlo, P. F., Kimmel, J. R., Trimborn, A., Northway, M. J., Jayne, J. T., Aiken, A. C., Gonin, M., Fuhrer, K., Horvath, T., Docherty, K. S., Worsnop, D. R., and Jimenez, J. L.: Field-deployable, high-resolution, time-of-flight aerosol mass spectrometer, Analytical Chemistry, 78, 8281-8289, 10.1021/ac061249n, 2006.

Docherty, K. S., Wu, W., Lim, Y. B., and Ziemann, P. J.: Contributions of organic peroxides to secondary aerosol formed from reactions of monoterpenes with O3, Environmental Science & Technology, 39, 4049-4059, 10.1021/es050228s, 2005.

930 Donahue, N. M., Robinson, A. L., Stanier, C. O., and Pandis, S. N.: Coupled partitioning,
931 dilution, and chemical aging of semivolatile organics, Environmental Science &
932 Technology, 40, 2635-2643, 10.1021/es052297c, 2006.

933 Donahue, N. M., Epstein, S. A., Pandis, S. N., and Robinson, A. L.: A two-dimensional
934 volatility basis set: 1. organic-aerosol mixing thermodynamics, Atmospheric Chemistry
935 and Physics, 11, 3303-3318, 10.5194/acp-11-3303-2011, 2011.

936 Ehn, M., Thornton, J. A., Kleist, E., Sipila, M., Junninen, H., Pullinen, I., Springer, M.,
937 Rubach, F., Tillmann, R., Lee, B., Lopez-Hilfiker, F., Andres, S., Acir, I. H., Rissanen,
938 M., Jokinen, T., Schobesberger, S., Kangasluoma, J., Kontkanen, J., Nieminen, T.,
939 Kurten, T., Nielsen, L. B., Jorgensen, S., Kjaergaard, H. G., Canagaratna, M., Dal Maso,
940 M., Berndt, T., Petaja, T., Wahner, A., Kerminen, V. M., Kulmala, M., Worsnop, D. R.,
941 Wildt, J., and Mentel, T. F.: A large source of low-volatility secondary organic aerosol,
942 Nature, 506, 476-479, 10.1038/nature13032, 2014.

943 Fry, J. L., Kiendler-Scharr, A., Rollins, A. W., Wooldridge, P. J., Brown, S. S., Fuchs,
944 H., Dube, W., Mensah, A., dal Maso, M., Tillmann, R., Dorn, H. P., Brauers, T., and
945 Cohen, R. C.: Organic nitrate and secondary organic aerosol yield from NO3 oxidation of
946 beta-pinene evaluated using a gas-phase kinetics/aerosol partitioning model, Atmospheric
947 Chemistry and Physics, 9, 1431-1449, 2009.

948 Fry, J. L., Draper, D. C., Barsanti, K. C., Smith, J. N., Ortega, J., Winkler, P. M., Lawler,
949 M. J., Brown, S. S., Edwards, P. M., Cohen, R. C., and Lee, L.: Secondary Organic
950 Aerosol Formation and Organic Nitrate Yield from NO3 Oxidation of Biogenic
951 Hydrocarbons, Environmental Science & Technology, 48, 11944-11953,
952 10.1021/es502204x, 2014.

953 Gao, S., Ng, N. L., Keywood, M., Varutbangkul, V., Bahreini, R., Nenes, A., He, J. W.,
954 Yoo, K. Y., Beauchamp, J. L., Hodyss, R. P., Flagan, R. C., and Seinfeld, J. H.: Particle
955 phase acidity and oligomer formation in secondary organic aerosol, Environmental
956 Science & Technology, 38, 6582-6589, 10.1021/es049125k, 2004.

957 Grieshop, A. P., Donahue, N. M., and Robinson, A. L.: Is the gas-particle partitioning in
958 alpha-pinene secondary organic aerosol reversible?, Geophys. Res. Lett., 34, n/a-n/a,
959 10.1029/2007GL029987, 2007.

960 Griffin, R. J., Cocker, D. R., Flagan, R. C., and Seinfeld, J. H.: Organic aerosol formation
961 from the oxidation of biogenic hydrocarbons, J. Geophys. Res.-Atmos., 104, 3555-3567,
962 10.1029/1998jd100049, 1999.

963 Guenther, A. B., Jiang, X., Heald, C. L., Sakulyanontvittaya, T., Duhl, T., Emmons, L.
964 K., and Wang, X.: The Model of Emissions of Gases and Aerosols from Nature version
965 2.1 (MEGAN2.1): an extended and updated framework for modeling biogenic emissions,
966 Geoscientific Model Development, 5, 1471-1492, 10.5194/gmd-5-1471-2012, 2012.

967 Hallquist, M., Wenger, J. C., Baltensperger, U., Rudich, Y., Simpson, D., Claeys, M.,
968 Dommen, J., Donahue, N. M., George, C., Goldstein, A. H., Hamilton, J. F., Herrmann,
969 H., Hoffmann, T., Iinuma, Y., Jang, M., Jenkin, M. E., Jimenez, J. L., Kiendler-Scharr,
970 A., Maenhaut, W., McFiggans, G., Mentel, T. F., Monod, A., Prevot, A. S. H., Seinfeld,
971 J. H., Surratt, J. D., Szmigielski, R., and Wildt, J.: The formation, properties and impact
972 of secondary organic aerosol: current and emerging issues, Atmospheric Chemistry and
973 Physics, 9, 5155-5236, 2009.

974 Henry, K. M., Lohaus, T., and Donahue, N. M.: Organic Aerosol Yields from alpha-
975 Pinene Oxidation: Bridging the Gap between First-Generation Yields and Aging
976 Chemistry, Environmental Science & Technology, 46, 12347-12354, 10.1021/es302060y,
977 2012.

978 Hildebrandt, L., Donahue, N. M., and Pandis, S. N.: High formation of secondary organic
979 aerosol from the photo-oxidation of toluene, Atmospheric Chemistry and Physics, 9,
980 2973-2986, 2009.

981 Hoffmann, T., Odum, J. R., Bowman, F., Collins, D., Klockow, D., Flagan, R. C., and
982 Seinfeld, J. H.: Formation of organic aerosols from the oxidation of biogenic
983 hydrocarbons, Journal of Atmospheric Chemistry, 26, 189-222,
984 10.1023/a:1005734301837, 1997.

985 Kanakidou, M., Seinfeld, J. H., Pandis, S. N., Barnes, I., Dentener, F. J., Facchini, M. C.,
986 Van Dingenen, R., Ervens, B., Nenes, A., Nielsen, C. J., Swietlicki, E., Putaud, J. P.,
987 Balkanski, Y., Fuzzi, S., Horth, J., Moortgat, G. K., Winterhalter, R., Myhre, C. E. L.,
988 Tsigaridis, K., Vignati, E., Stephanou, E. G., and Wilson, J.: Organic aerosol and global
989 climate modelling: a review, Atmospheric Chemistry and Physics, 5, 1053-1123, 2005.

990 Karnezi, E., Riipinen, I., and Pandis, S. N.: Measuring the atmospheric organic aerosol
991 volatility distribution: a theoretical analysis, Atmospheric Measurement Techniques, 7,
992 2953—2965, 2014.

993 Keywood, M. D., Varutbangkul, V., Bahreini, R., Flagan, R. C., and Seinfeld, J. H.:
994 Secondary organic aerosol formation from the ozonolysis of cycloalkenes and related
995 compounds, Environmental Science & Technology, 38, 4157-4164, 10.1021/es035363o,
996 2004.

997 Kokkola, H., Yli-Pirila, P., Vesterinen, M., Korhonen, H., Keskinen, H., Romakkaniemi,
998 S., Hao, L., Kortelainen, A., Joutsensaari, J., Worsnop, D. R., Virtanen, A., and Lehtinen,
999 K. E. J.: The role of low volatile organics on secondary organic aerosol formation,
1000 Atmospheric Chemistry and Physics, 14, 1689-1700, 10.5194/acp-14-1689-2014, 2014.

1001 Kostenidou, E., Pathak, R. K., and Pandis, S. N.: An algorithm for the calculation of
1002 secondary organic aerosol density combining AMS and SMPS data, Aerosol Sci.
1003 Technol., 41, 1002-1010, 10.1080/02786820701666270, 2007.

1004 Krechmer, J. E., Pagonis, D., Ziemann, P. J., and Jimenez, J. L.: Quantification of Gas-
1005 Wall Partitioning in Teflon Environmental Chambers Using Rapid Bursts of Low-
1006 Volatility Oxidized Species Generated in Situ, Environmental Science & Technology, 50,
1007 5757-5765, 10.1021/acs.est.6b00606, 2016.

1008 Kristensen, K., Cui, T., Zhang, H., Gold, A., Glasius, M., and Surratt, J. D.: Dimers in
1009 alpha-pinene secondary organic aerosol: effect of hydroxyl radical, ozone, relative
1010 humidity and aerosol acidity, Atmospheric Chemistry and Physics, 14, 4201-4218,
1011 10.5194/acp-14-4201-2014, 2014.

1012 Kroll, J. H., Chan, A. W. H., Ng, N. L., Flagan, R. C., and Seinfeld, J. H.: Reactions of
1013 semivolatile organics and their effects on secondary organic aerosol formation,
1014 Environmental Science & Technology, 41, 3545-3550, 10.1021/es062059x, 2007.

1015 Kuwata, M., and Martin, S. T.: Phase of atmospheric secondary organic material affects
1016 its reactivity, Proc. Natl. Acad. Sci. U. S. A., 109, 17354-17359,
1017 10.1073/pnas.1209071109, 2012.

1018 La, Y. S., Camredon, M., Ziemann, P. J., Valorso, R., Matsunaga, A., Lannuque, V., Lee-
1019 Taylor, J., Hodzic, A., Madronich, S., and Aumont, B.: Impact of chamber wall loss of
1020 gaseous organic compounds on secondary organic aerosol formation: explicit modeling
1021 of SOA formation from alkane and alkene oxidation, Atmos. Chem. Phys., 16, 1417-
1022 1431, 10.5194/acp-16-1417-2016, 2016.

1023 Loza, C. L., Chan, A. W. H., Galloway, M. M., Keutsch, F. N., Flagan, R. C., and
1024 Seinfeld, J. H.: Characterization of Vapor Wall Loss in Laboratory Chambers,
1025 Environmental Science & Technology, 44, 5074-5078, 10.1021/es100727v, 2010.

1026 Loza, C. L., Chhabra, P. S., Yee, L. D., Craven, J. S., Flagan, R. C., and Seinfeld, J. H.:
1027 Chemical aging of m-xylene secondary organic aerosol: laboratory chamber study,
1028 Atmospheric Chemistry and Physics, 12, 151-167, 10.5194/acp-12-151-2012, 2012.

1029 Matsunaga, A., and Ziemann, P. J.: Gas-Wall Partitioning of Organic Compounds in a
1030 Teflon Film Chamber and Potential Effects on Reaction Product and Aerosol Yield
1031 Measurements, Aerosol Sci. Technol., 44, 881-892, 10.1080/02786826.2010.501044,
1032 2010.

1033 McMurry, P. H., and Grosjean, D.: Gas and Aerosol Wall Losses in Teflon Film Smog
1034 Chambers, Environmental Science & Technology, 19, 1176-1182, 10.1021/es00142a006,
1035 1985.

1036 McMurry, P. H., and Rader, D. J.: Aerosol Wall Losses in Electrically Charged
1037 Chambers, Aerosol Sci. Technol., 4, 249-268, 10.1080/02786828508959054, 1985.

McVay, R. C., Cappa, C. D., and Seinfeld, J. H.: Vapor-Wall Deposition in Chambers: Theoretical Considerations, Environmental Science & Technology, 48, 10251-10258, 10.1021/es502170j, 2014.

McVay, R. C., Zhang, X., Aumont, B., Valorso, R., Camredon, M., La, Y. S., Wennberg, P. O., and Seinfeld, J. H.: SOA formation from the photooxidation of α-pinene: systematic exploration of the simulation of chamber data, Atmos. Chem. Phys., 16, 2785-2802, 10.5194/acp-16-2785-2016, 2016.

Miles, R. E. H., Reid, J. P., and Riipinen, I.: Comparison of Approaches for Measuring the Mass Accommodation Coefficient for the Condensation of Water and Sensitivities to Uncertainties in Thermophysical Properties, J. Phys. Chem. A, 116, 10810-10825, 10.1021/jp3083858, 2012.

Ng, N. L., Kroll, J. H., Keywood, M. D., Bahreini, R., Varutbangkul, V., Flagan, R. C., Seinfeld, J. H., Lee, A., and Goldstein, A. H.: Contribution of first- versus second-generation products to secondary organic aerosols formed in the oxidation of biogenic hydrocarbons, Environmental Science & Technology, 40, 2283-2297, 10.1021/es052269u, 2006.

Ng, N. L., Kroll, J. H., Chan, A. W. H., Chhabra, P. S., Flagan, R. C., and Seinfeld, J. H.: Secondary organic aerosol formation from m-xylene, toluene, and benzene, Atmospheric Chemistry and Physics, 7, 3909-3922, 2007.

Odum, J. R., Hoffmann, T., Bowman, F., Collins, D., Flagan, R. C., and Seinfeld, J. H.: Gas/Particle Partitioning and Secondary Organic Aerosol Yields, Environmental Science & Technology, 30, 2580-2585, 10.1021/es950943+, 1996.

Odum, J. R., Jungkamp, T. P. W., Griffin, R. J., Flagan, R. C., and Seinfeld, J. H.: The atmospheric aerosol-forming potential of whole gasoline vapor, Science, 276, 96-99, 10.1126/science.276.5309.96, 1997a.

Odum, J. R., Jungkamp, T. P. W., Griffin, R. J., Forstner, H. J. L., Flagan, R. C., and Seinfeld, J. H.: Aromatics, reformulated gasoline, and atmospheric organic aerosol

1065 formation, Environmental Science & Technology, 31, 1890-1897, 10.1021/es960535l,
1066 1997b.

1067 Pathak, R. K., Presto, A. A., Lane, T. E., Stanier, C. O., Donahue, N. M., and Pandis, S.
1068 N.: Ozonolysis of alpha-pinene: parameterization of secondary organic aerosol mass
1069 fraction, Atmospheric Chemistry and Physics, 7, 3811-3821, 2007a.

1070 Pathak, R. K., Stanier, C. O., Donahue, N. M., and Pandis, S. N.: Ozonolysis of alpha-
1071 pinene at atmospherically relevant concentrations: Temperature dependence of aerosol
1072 mass fractions (yields), J. Geophys. Res.-Atmos., 112, 8, 10.1029/2006jd007436, 2007b.

1073 Perraud, V., Bruns, E. A., Ezell, M. J., Johnson, S. N., Yu, Y., Alexander, M. L.,
1074 Zelenyuk, A., Imre, D., Chang, W. L., Dabdub, D., Pankow, J. F., and Finlayson-Pitts, B.
1075 J.: Nonequilibrium atmospheric secondary organic aerosol formation and growth, Proc.
1076 Natl. Acad. Sci. U. S. A., 109, 2836-2841, 10.1073/pnas.1119909109, 2012.

1077 Pierce, J. R., Engelhart, G. J., Hildebrandt, L., Weitkamp, E. A., Pathak, R. K., Donahue,
1078 N. M., Robinson, A. L., Adams, P. J., and Pandis, S. N.: Constraining particle evolution
1079 from wall losses, coagulation, and condensation-evaporation in smog-chamber
1080 experiments: Optimal estimation based on size distribution measurements, Aerosol Sci.
1081 Technol., 42, 1001-1015, 10.1080/02786820802389251, 2008.

1082 Presto, A. A., Hartz, K. E. H., and Donahue, N. M.: Secondary organic aerosol
1083 production from terpene ozonolysis. 2. Effect of NOx concentration, Environmental
1084 Science & Technology, 39, 7046-7054, 10.1021/es050400s, 2005.

1085 Presto, A. A., and Donahue, N. M.: Investigation of alpha-pinene plus ozone secondary
1086 organic aerosol formation at low total aerosol mass, Environmental Science &
1087 Technology, 40, 3536-3543, 10.1021/es052203z, 2006.

1088 Pye, H. O. T., Chan, A. W. H., Barkley, M. P., and Seinfeld, J. H.: Global modeling of
1089 organic aerosol: the importance of reactive nitrogen (NOx and NO3), Atmospheric
1090 Chemistry and Physics, 10, 11261-11276, 10.5194/acp-10-11261-2010, 2010.

Renbaum-Wolff, L., Grayson, J. W., Bateman, A. P., Kuwata, M., Sellier, M., Murray, B. J., Shilling, J. E., Martin, S. T., and Bertram, A. K.: Viscosity of alpha-pinene secondary organic material and implications for particle growth and reactivity, Proc. Natl. Acad. Sci. U. S. A., 110, 8014-8019, 10.1073/pnas.1219548110, 2013.

Saha, P. K., and Grieshop, A. P.: Exploring Divergent Volatility Properties from Yield and Thermodenuder Measurements of Secondary Organic Aerosol from α-Pinene Ozonolysis, Environmental Science & Technology, 50, 5740-5749, 10.1021/acs.est.6b00303, 2016.

Saleh, R., Donahue, N. M., and Robinson, A. L.: Time Scales for Gas-Particle Partitioning Equilibration of Secondary Organic Aerosol Formed from Alpha-Pinene Ozonolysis, Environmental Science & Technology, 47, 5588-5594, 10.1021/es400078d, 2013.

Saukko, E., Lambe, A. T., Massoli, P., Koop, T., Wright, J. P., Croasdale, D. R., Pedernera, D. A., Onasch, T. B., Laaksonen, A., Davidovits, P., Worsnop, D. R., and Virtanen, A.: Humidity-dependent phase state of SOA particles from biogenic and anthropogenic precursors, Atmospheric Chemistry and Physics, 12, 7517-7529, 10.5194/acp-12-7517-2012, 2012.

Saunders, S. M., Jenkin, M. E., Derwent, R. G., and Pilling, M. J.: Protocol for the development of the Master Chemical Mechanism, MCM v3 (Part A): tropospheric degradation of non-aromatic volatile organic compounds, Atmos. Chem. Phys., 3, 161-180, 10.5194/acp-3-161-2003, 2003.

Seinfeld, J. H., and Pandis, S. N.: Atmospheric chemistry and physics : from air pollution to climate change, 2nd ed., Wiley, Hoboken, N.J., xxviii, 1203 p. pp., 2006.

Shilling, J. E., Chen, Q., King, S. M., Rosenoern, T., Kroll, J. H., Worsnop, D. R., McKinney, K. A., and Martin, S. T.: Particle mass yield in secondary organic aerosol formed by the dark ozonolysis of alpha-pinene, Atmospheric Chemistry and Physics, 8, 2073-2088, 2008.

Shilling, J. E., Chen, Q., King, S. M., Rosenoern, T., Kroll, J. H., Worsnop, D. R., DeCarlo, P. F., Aiken, A. C., Sueper, D., Jimenez, J. L., and Martin, S. T.: Loading-dependent elemental composition of alpha-pinene SOA particles, Atmospheric Chemistry and Physics, 9, 771-782, 2009.

Shiraiwa, M., and Seinfeld, J. H.: Equilibration timescale of atmospheric secondary organic aerosol partitioning, Geophys. Res. Lett., 39, 6, 10.1029/2012gl054008, 2012.

Song, C., Zaveri, R. A., Alexander, M. L., Thornton, J. A., Madronich, S., Ortega, J. V., Zelenyuk, A., Yu, X. Y., Laskin, A., and Maughan, D. A.: Effect of hydrophobic primary organic aerosols on secondary organic aerosol formation from ozonolysis of alpha-pinene, Geophys. Res. Lett., 34, 5, 10.1029/2007gl030720, 2007.

Stanier, C. O., Pathak, R. K., and Pandis, S. N.: Measurements of the volatility of aerosols from alpha-piniene ozonolysis, Environmental Science & Technology, 41, 2756-2763, 10.1021/es0519280, 2007.

Tabge, O. GNU Parallel – The Command-Line Power Tool, :login: The USENIX Magazine, http://www.gnu.org/s/parallel, 2011.

Tsigaridis, K., Daskalakis, N., Kanakidou, M., Adams, P. J., Artaxo, P., Bahadur, R., Balkanski, Y., Bauer, S. E., Bellouin, N., Benedetti, A., Bergman, T., Berntsen, T. K., Beukes, J. P., Bian, H., Carslaw, K. S., Chin, M., Curci, G., Diehl, T., Easter, R. C., Ghan, S. J., Gong, S. L., Hodzic, A., Hoyle, C. R., Iversen, T., Jathar, S., Jimenez, J. L., Kaiser, J. W., Kirkevåg, A., Koch, D., Kokkola, H., Lee, Y. H., Lin, G., Liu, X., Luo, G., Ma, X., Mann, G. W., Mihalopoulos, N., Morcrette, J. J., Müller, J. F., Myhre, G., Myriokefalitakis, S., Ng, N. L., O'Donnell, D., Penner, J. E., Pozzoli, L., Pringle, K. J., Russell, L. M., Schulz, M., Sciare, J., Seland, Ø., Shindell, D. T., Sillman, S., Skeie, R. B., Spracklen, D., Stavrakou, T., Steenrod, S. D., Takemura, T., Tiitta, P., Tilmes, S., Tost, H., van Noije, T., van Zyl, P. G., von Salzen, K., Yu, F., Wang, Z., Wang, Z., Zaveri, R. A., Zhang, H., Zhang, K., Zhang, Q., and Zhang, X.: The AeroCom evaluation and intercomparison of organic aerosol in global models, Atmos. Chem. Phys., 14, 10845-10895, 10.5194/acp-14-10845-2014, 2014.

Vaden, T. D., Song, C., Zaveri, R. A., Imre, D., and Zelenyuk, A.: Morphology of mixed primary and secondary organic particles and the adsorption of spectator organic gases during aerosol formation, Proc. Natl. Acad. Sci. U. S. A., 107, 6658-6663, 10.1073/pnas.0911206107, 2010.

Vaden, T. D., Imre, D., Beranek, J., Shrivastava, M., and Zelenyuk, A.: Evaporation kinetics and phase of laboratory and ambient secondary organic aerosol, Proc. Natl. Acad. Sci. U. S. A., 108, 2190-2195, 10.1073/pnas.1013391108, 2011.

Virtanen, A., Joutsensaari, J., Koop, T., Kannosto, J., Yli-Pirila, P., Leskinen, J., Makela, J. M., Holopainen, J. K., Poschl, U., Kulmala, M., Worsnop, D. R., and Laaksonen, A.: An amorphous solid state of biogenic secondary organic aerosol particles, Nature, 467, 824-827, 10.1038/nature09455, 2010.

Virtanen, A., Kannosto, J., Kuuluvainen, H., Arffman, A., Joutsensaari, J., Saukko, E., Hao, L., Yli-Pirila, P., Tiitta, P., Holopainen, J. K., Keskinen, J., Worsnop, D. R., Smith, J. N., and Laaksonen, A.: Bounce behavior of freshly nucleated biogenic secondary organic aerosol particles, Atmospheric Chemistry and Physics, 11, 8759-8766, 10.5194/acp-11-8759-2011, 2011.

Weitkamp, E. A., Sage, A. M., Pierce, J. R., Donahue, N. M., and Robinson, A. L.: Organic aerosol formation from photochemical oxidation of diesel exhaust in a smog chamber, Environmental Science & Technology, 41, 6969-6975, 10.1021/es070193r, 2007.

Yeh, G. K., and Ziemann, P. J.: Alkyl Nitrate Formation from the Reactions of C-8-C-14 n-Alkanes with OH Radicals in the Presence of NOx: Measured Yields with Essential Corrections for Gas-Wall Partitioning, J. Phys. Chem. A, 118, 8147-8157, 10.1021/jp500631v, 2014.

Yeh, G. K., and Ziemann, P. J.: Gas-Wall Partitioning of Oxygenated Organic Compounds: Measurements, Structure-Activity Relationships, and Correlation with Gas Chromatographic Retention Factor, Aerosol Sci. Technol., 49, 726-737, 10.1080/02786826.2015.1068427, 2015.

Ye, P., Ding, X., Hakala, J., Hofbauer, V., Robinson, E. S., and Donahue, N. M.: Vapor wall loss of semi-volatile organic compounds in a Teflon chamber, Aerosol Sci. Technol., 50, 822-834, 10.1080/02786826.2016.1195905, 2016.

Zaveri, R. A., Easter, R. C., Shilling, J. E., and Seinfeld, J. H.: Modeling kinetic partitioning of secondary organic aerosol and size distribution dynamics: representing effects of volatility, phase state, and particle-phase reaction, Atmospheric Chemistry and Physics, 14, 5153-5181, 10.5194/acp-14-5153-2014, 2014.

Zhang, X., Pandis, S. N., and Seinfeld, J. H.: Diffusion-Limited Versus Quasi-Equilibrium Aerosol Growth, Aerosol Sci. Technol., 46, 874-885, 10.1080/02786826.2012.679344, 2012.

Zhang, X., Cappa, C. D., Jathar, S. H., McVay, R. C., Ensberg, J. J., Kleeman, M. J., and Seinfeld, J. H.: Influence of vapor wall loss in laboratory chambers on yields of secondary organic aerosol, Proc. Natl. Acad. Sci. U. S. A., 111, 5802-5807, 10.1073/pnas.1404727111, 2014.

Zhang, X., Schwantes, R. H., McVay, R. C., Lignell, H., Coggon, M. M., Flagan, R. C., and Seinfeld, J. H.: Vapor wall deposition in Teflon chambers, Atmospheric Chemistry and Physics, 15, 4197-4214, 10.5194/acp-15-4197-2015, 2015a.

Zhang, X., McVay, R. C., Huang, D. D., Dalleska, N. F., Aumont, B., Flagan, R. C., and Seinfeld, J. H.: Formation and evolution of molecular products in alpha-pinene secondary organic aerosol, Proc. Natl. Acad. Sci. U. S. A., 112, 14168-14173, 10.1073/pnas.1517742112, 2015b.

Table 1: Experimental conditions and results for the α-pinene ozonolysis experiments

Experiment	Initial Seed Surface Area ($\mu m^2\ cm^{-3}$)	Initial [α-pinene][a] ($\mu g\ m^{-3}$)	ΔM_o[b] M_o[b] ($\mu g\ m^{-3}$)	SOA Mass Yield[c] (%)
100 ppb O_3 nucleation	0	290.2±23.2	62.0±1.2[d]	22.6±1.9
100 ppb O_3 low AS	1130	280.5±22.4	63.0±0.8[d]	23.3±1.9
100 ppb O_3 high AS	2700	238.7±19.1	50.6±1.6[d]	23.3±1.9
500 ppb O_3 nucleation	0	274.4±21.9	87.3±0.3[e]	31.8±2.5
500 ppb O_3 low AS	1300	264.9±21.2	75.7±0.6[e]	28.6±2.3
500 ppb O_3 high AS	2720	236.1±18.9	66.3±1.9[e]	28.1±2.4

[a]Concentration of α-pinene injected into the chamber. All the α-pinene reacted in the 500 ppb O_3 experiments, but not the 100 ppb O_3 experiments.

[b]Uncertainties in the peak SOA mass concentration ($\Delta M_o M_o$) are calculated from one standard deviation of the aerosol volume as measured by the scanning mobility particle sizer.

[c]SOA mass yields at peak SOA growth are reported.

[d]The SOA mass concentration is calculated using the density = 1.39 g cm^{-3} obtained from the 100 ppb O_3 nucleation experiment.

[e]The SOA mass concentration is calculated using the density = 1.37 g cm^{-3} obtained from the 500 ppb O_3 nucleation experiment.

Table 2: Coupled vapor-particle dynamics model parameters

Parameter	Definition	Value
α_p	Vapor-particle mass accommodation coefficient	0.1
α_w	Vapor-wall mass accommodation coefficient	10^{-6}
τ_{olig}	Timescale of oligomerization	4 h
C^*	~~Saturation vapor pressures and branching ratios~~ Branching ratios and saturation concentrations of oxidation products	[~~0.57~~0.6 (>10^3), ~~0.35~~ 0.3(10^2), ~~0.04~~ 0.05(10), ~~0.015~~ 0.05(1) and ~~0.025~~ 0(0.1)]
D_i	Gas-phase molecular diffusivity	3×10^{-6} m^2 s^{-1}
A/V	Surface area-to-volume ratio of the chamber	2.5 m^{-1}
C_w	Equivalent organic mass concentration in the wall	10 mg m^{-3}
k_e	Eddy diffusion coefficient	0.03 s^{-1}
M_i	Molecular weight of the diffusing gas-phase molecule i	168, 184, 192, 200 and 216 g $mole^{-1}$
M_{init}	Initially absorbing organic material in seed aerosol	0.01 μg m^{-3}
P	Pressure	1×10^5 Pa
T	Temperature	298 K
ρ_{seed}	Density of inorganic seed	1700 kg m^{-3}
ρ_{org}	Density of organic material on seed particle	1300 kg m^{-3}

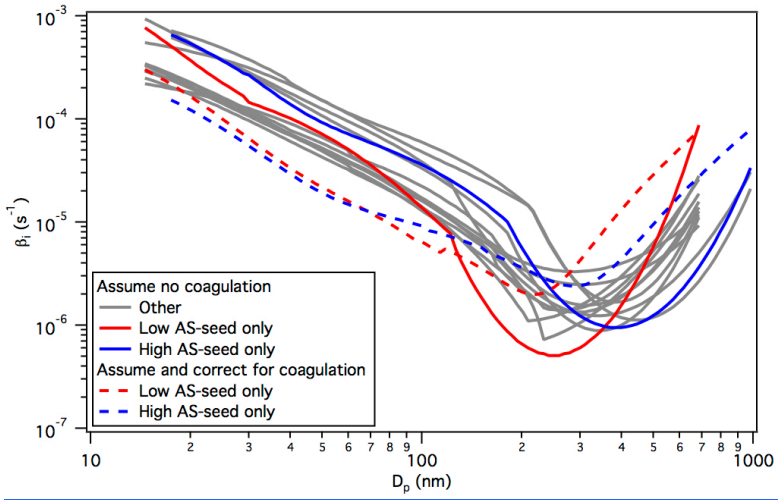

Figure 1: Particle wall deposition coefficients (β_i) measured during the low AS-seed only and high AS-seed only experiments in GTEC. Also shown are the particle wall deposition coefficients (labeled "Other") measured in previous routine monthly AS-seed only experiments in the chamber. These previous routine monthly AS-seed only experiments were performed using either a 0.008 M AS or a 0.1 M AS solution. Coagulation-corrected particle wall deposition coefficients (see Pierce et al. (2008) and main text for details) are also shown, using dashed lines.

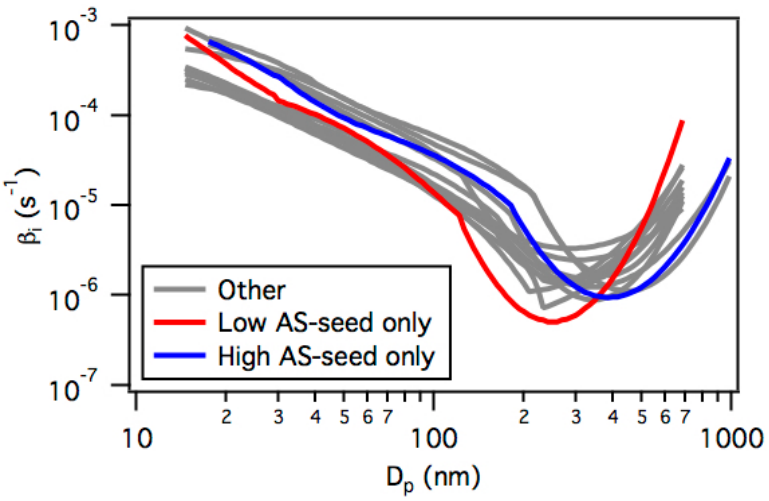

Figure 1: Particle wall deposition coefficients (β_i) measured during the low AS-seed only and high AS-seed only experiments in GTEC. Also shown are the particle wall deposition coefficients (labeled "Other") measured in previous routine monthly AS-seed only experiments in the chamber. These previous routine monthly AS-seed only experiments were performed using either a 0.008 M AS or a 0.1 M AS solution.

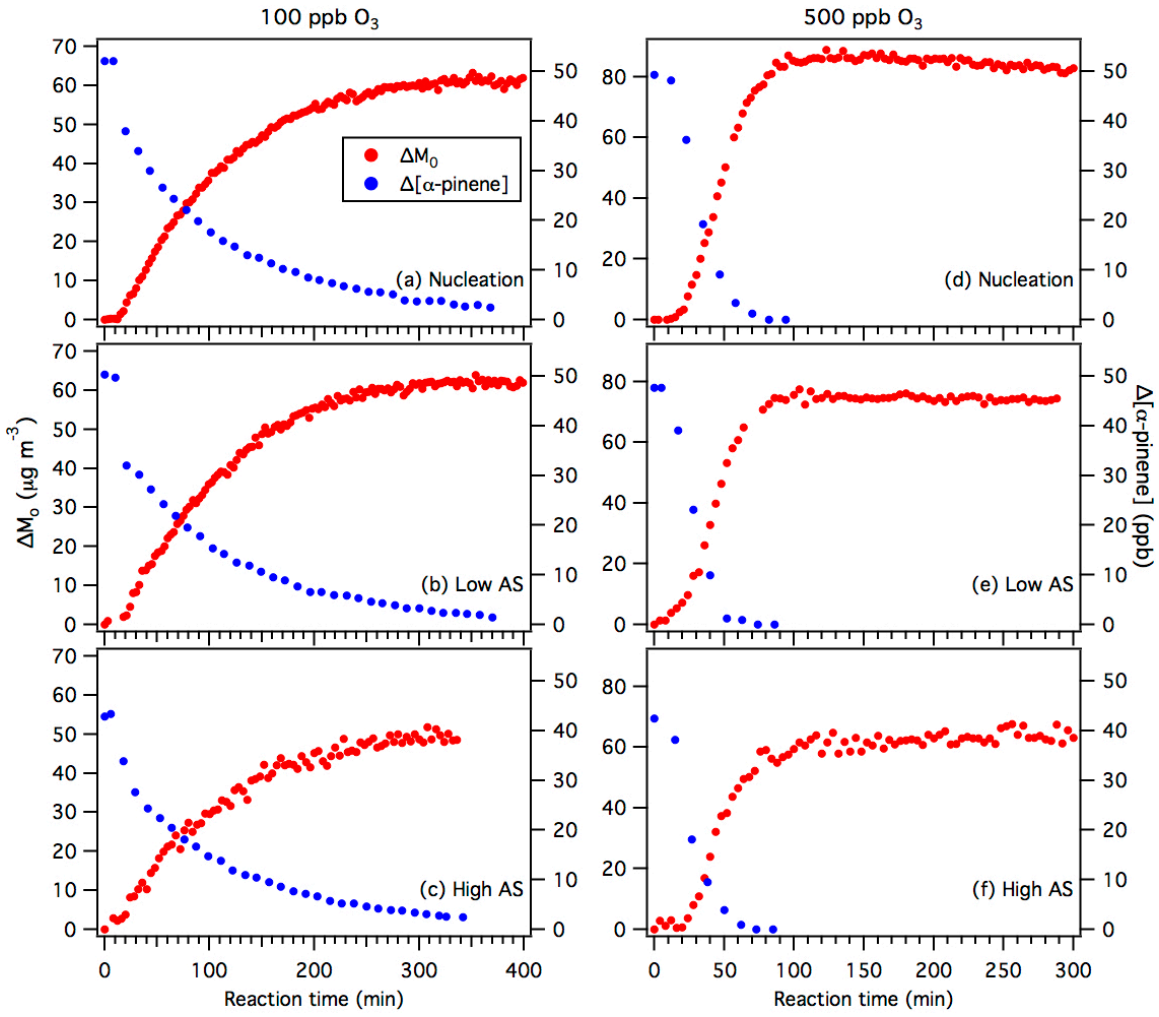

Figure 2: Reaction profiles of the α-pinene ozonolysis experiments. Panels (a), (b) and (c) show results from the nucleation, low AS and high AS 100 ppb O_3 experiments, respectively. Panels (d), (e) and (f) show results from the nucleation, low AS and high AS 500 ppb O_3 experiments, respectively. As explained in the main text, the SOA mass concentrations (ΔM_o) for the nucleation and low AS experiments are obtained using the particle wall deposition rates obtained from the low AS-seed only experiments, while the SOA mass concentrations (ΔM_o) for the high AS-seed experiments are obtained using the particle wall deposition rates obtained from the high AS-seed only experiments.

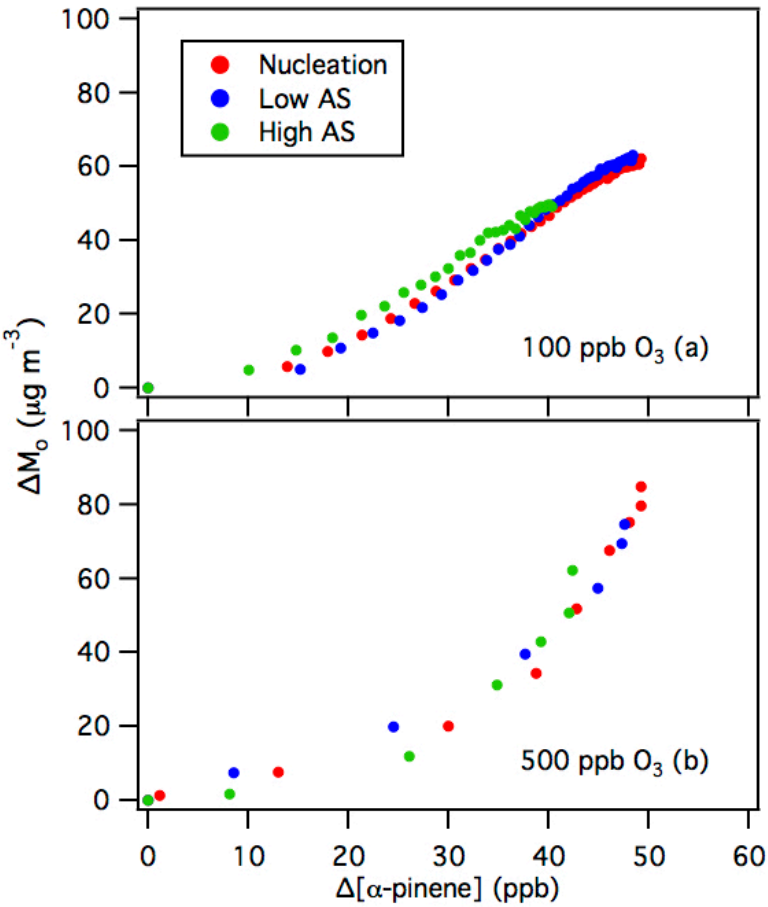

Figure 3: Time-dependent SOA growth curves for α-pinene ozonolysis. Panels (a) and (b) show 10 min-averaged results from the 100 ppb and 500 ppb O_3 experiments, respectively. Only SOA growth data up to the point of SOA peak growth are shown.

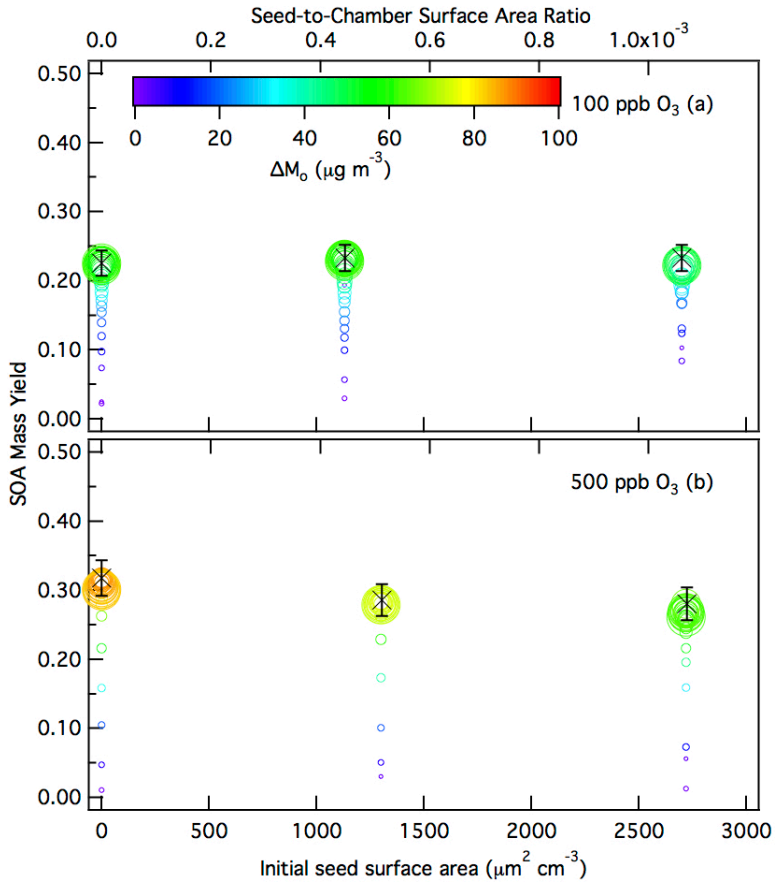

1271

1272 **Figure 4:** 10 min-averaged SOA mass yields over the course of an α-pinene ozonolysis
1273 experiment as a function of initial total AS seed surface area concentration for the (a) 100
1274 ppb O_3 experiments, and (b) 500 ppb O_3 experiments. Symbol color indicates the SOA
1275 mass concentration and symbol size indicates the time after O_3 is injected into the
1276 chamber. The × symbols are the SOA mass yields at peak SOA growth obtained from
1277 the experimental data. The y-axis error bars represent the uncertainty in the SOA mass
1278 yield at peak SOA growth, which originates from the α-pinene injection and the aerosol
1279 volume concentration measured by the SMPS at peak SOA growth (one standard
1280 deviation).

1281

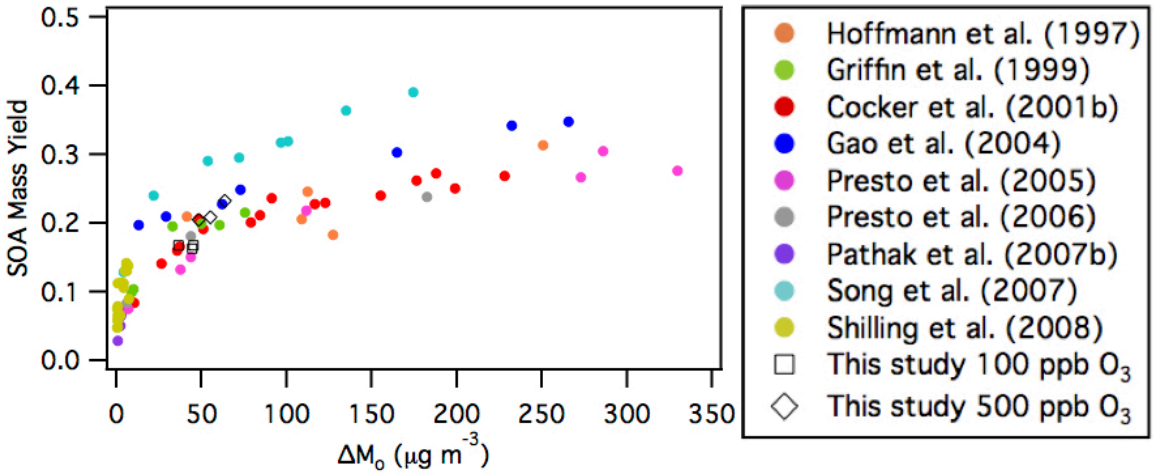

Figure 5: Comparison of SOA mass yields obtained in this study to those of previous dark α-pinene ozonolysis studies (~~Table S2~~Table S3). The SOA mass yields and concentrations of majority of these previous studies (Hoffmann et al., 1997; Griffin et al., 1999; Cocker et al., 2001b; Gao et al., 2004; Presto et al., 2005; Presto et al. 2006; Pathak et al., 2007b; Song et al., 2007) were previously compiled by Shilling et al. (2008). Similar to Shilling et al. (2008), all the data shown here (including those reported in this study) have been adjusted using an organic density of 1.0 g cm^{-3}, and to 298 K using a temperature correction of 1.6 % per K, as recommended by Pathak et al. (2007b) to facilitate easier comparison among the different studies.

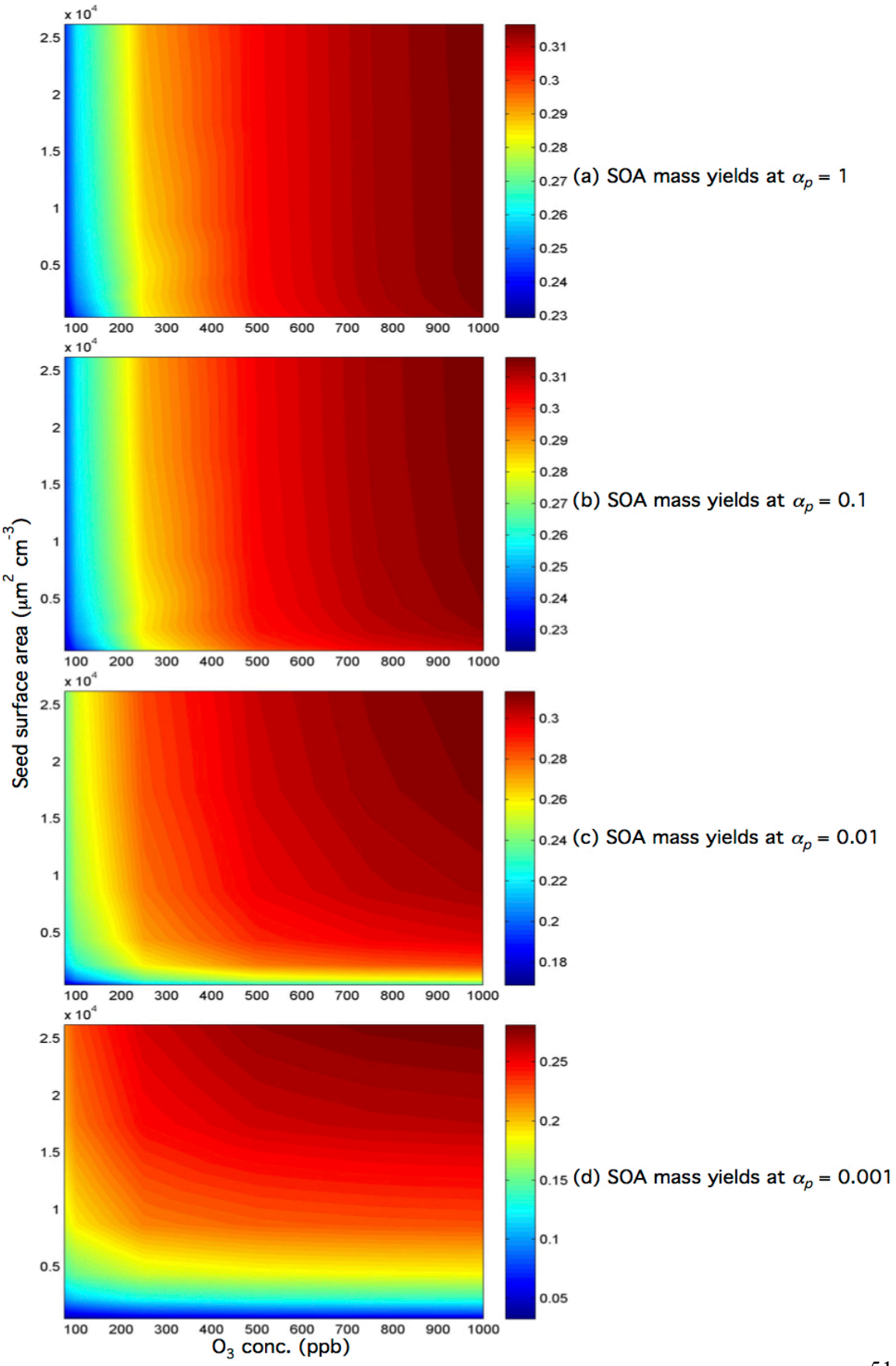
x 10^4
2.5
2
1.5
1
0.5
100 200 300 400 500 600 700 800 900 1000
0.31
0.3
0.29
0.28
0.27
0.26
0.25
0.24
0.23
(a) SOA mass yields at α_p = 1
(b) SOA mass yields at α_p = 0.1
0.22
0.2
0.18
(c) SOA mass yields at α_p = 0.01
0.15
0.1
0.05
(d) SOA mass yields at α_p = 0.001
Seed surface area (μm^2 cm^{-3})
O_3 conc. (ppb)

1293

Figure 6: SOA mass yields at peak SOA growth as a function of both the seed surface area and O_3 concentration for α_p = 1, 0.1, 0.01, and 0.001. The SOA mass yields at peak SOA growth are indicated by colors and contours. Note that the color bars for panels (a), (b) and (c) have different SOA mass yield ranges. Simulations were carried out using the optimal branching ratios, oligomerization rate, and vapor wall deposition rate parameters obtained in this study. The initial α-pinene concentration was set to 50 ppb, and a fixed O_3 concentration was used in place of a linear injection.

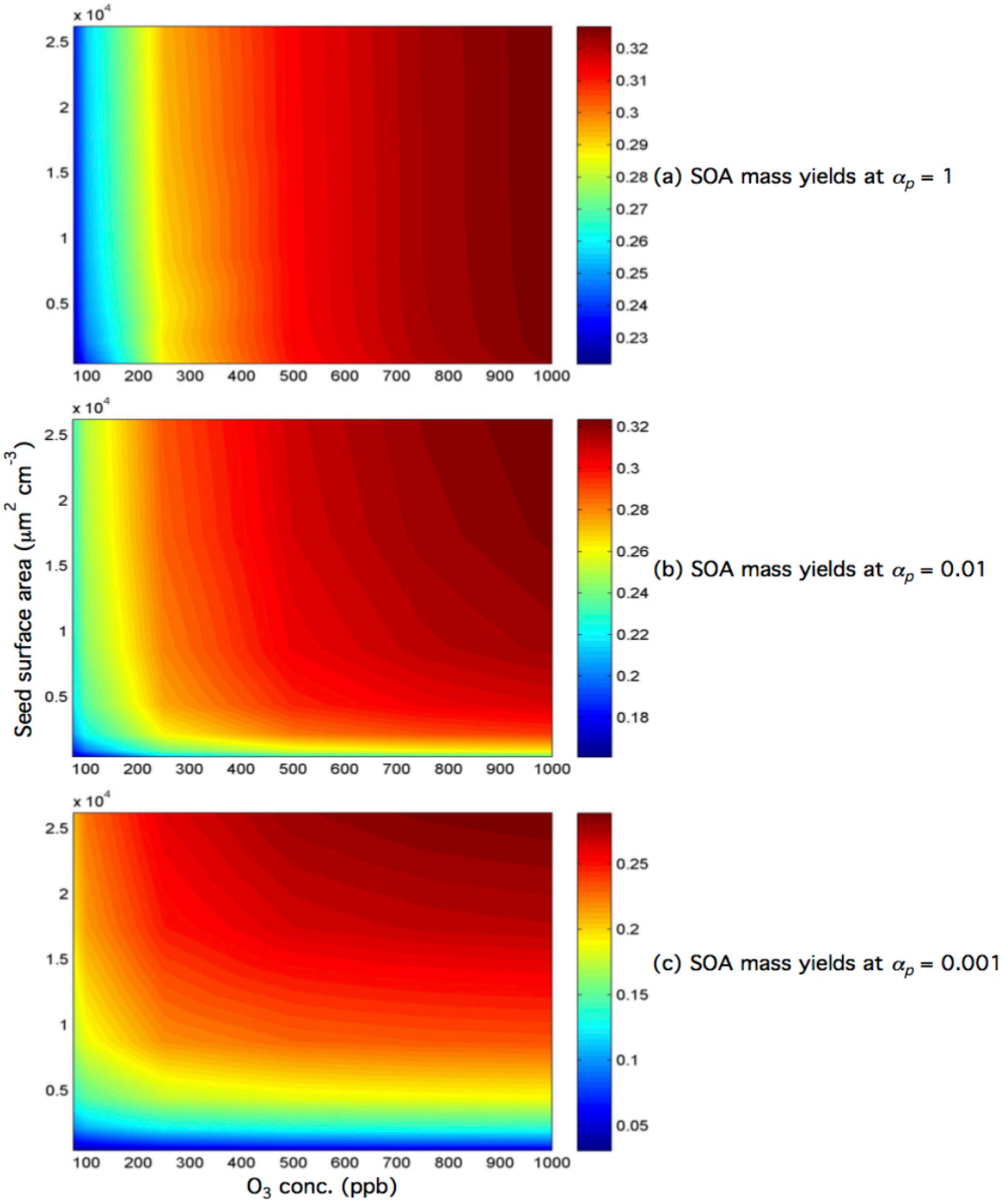

Figure 6: SOA mass yields at peak SOA growth as a function of both the seed surface area and O_3 concentration for α_p = 1, 0.01, and 0.001. The SOA mass yields at peak SOA growth are indicated by colors and contours. Note that the color bars for panels (a), (b) and (c) have different SOA mass yield ranges. Simulations were carried out using the branching ratios, oligomerization rate, and vapor wall deposition rate parameters obtained in this study. The initial α-pinene concentration was set to 50 ppb, and a fixed O_3 concentration was used in place of a linear injection.

Supplementary Information:

Influence of Seed Aerosol Surface Area and Oxidation Rate on Vapor-Wall Deposition and SOA Mass Yields: A case study with α-pinene Ozonolysis

T. Nah,[1] R.C. McVay,[2] X. Zhang,[3,#] C. M. Boyd,[1] J. H. Seinfeld[2,3] and N. L. Ng[1,4*]

[1]*School of Chemical and Biomolecular Engineering, Georgia Institute of Technology, Atlanta, GA, USA*
[2]*Division of Chemistry and Chemical Engineering, California Institute of Technology, Pasadena, CA, USA*
[3]*Division of Engineering and Applied Science, California Institute of Technology, Pasadena, CA, USA*
[4]*School of Earth and Atmospheric Sciences, Georgia Institute of Technology, Atlanta, GA, USA*
[#]*Now at: Center for Aerosol and Cloud Chemistry, Aerodyne Research, Billerica, MA, USA*

** To whom correspondence should be addressed: ng@chbe.gatech.edu*

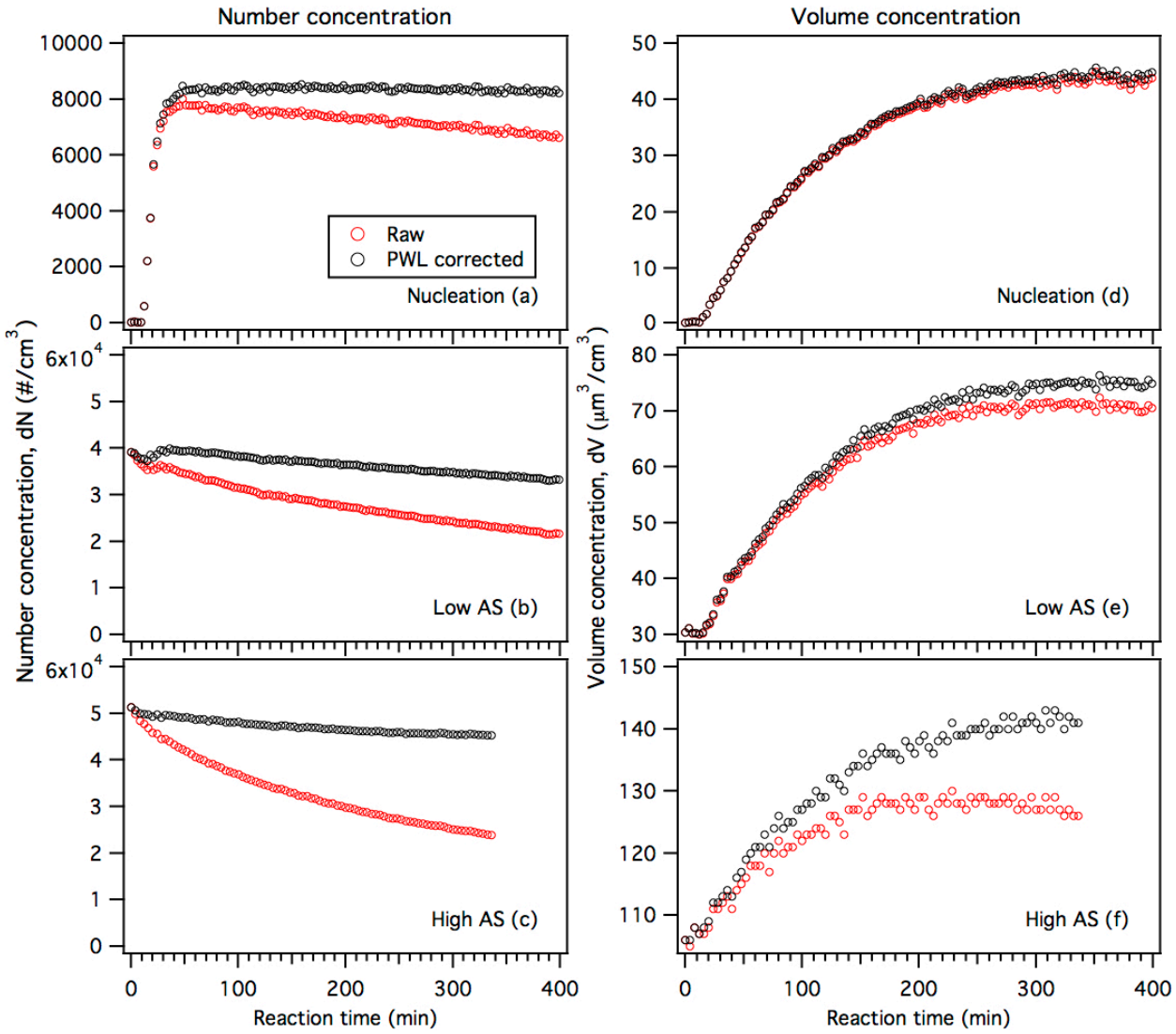

Figure S1: Raw and particle wall loss (PWL) corrected number and volume concentration data for the 100 ppb O_3 experiments. Raw nucleation (panels a and d) and low AS (panels b and e) data are particle wall loss corrected using particle wall loss rates determined from the low AS-seed only experiments. Raw high AS (panels c and f) data are particle wall loss corrected using particle wall loss rates determined from the high AS-seed only experiments.

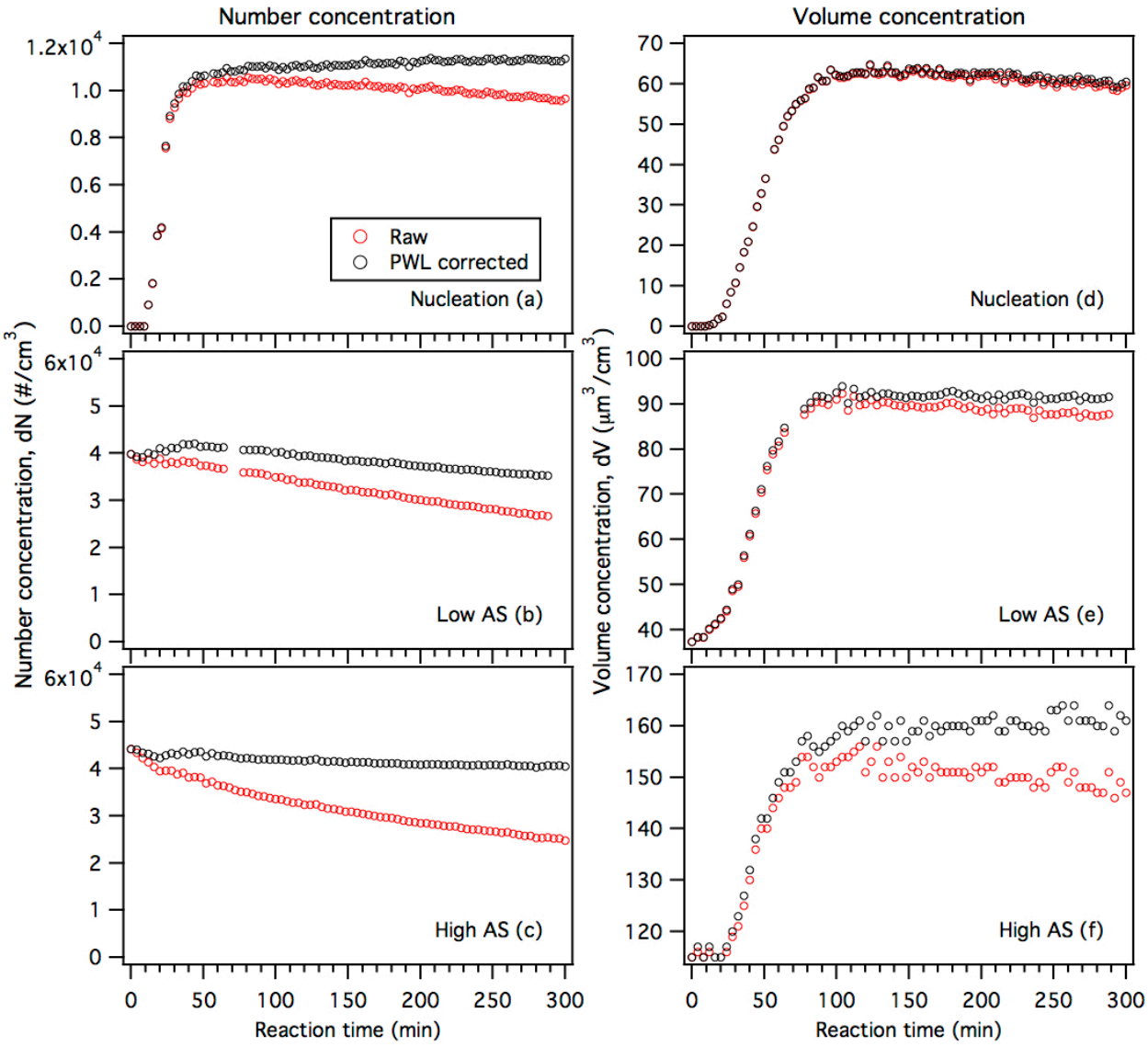

Figure S2: Raw and particle wall loss (PWL) corrected number and volume concentration data for the 500 ppb O_3 experiments. Raw nucleation (panels a and d) and low AS (panels b and e) data are particle wall loss corrected using particle wall loss rates determined from the low AS-seed only experiments. Raw high AS (panels c and f) data are particle wall loss corrected using particle wall loss rates determined from the high AS-seed only experiments.

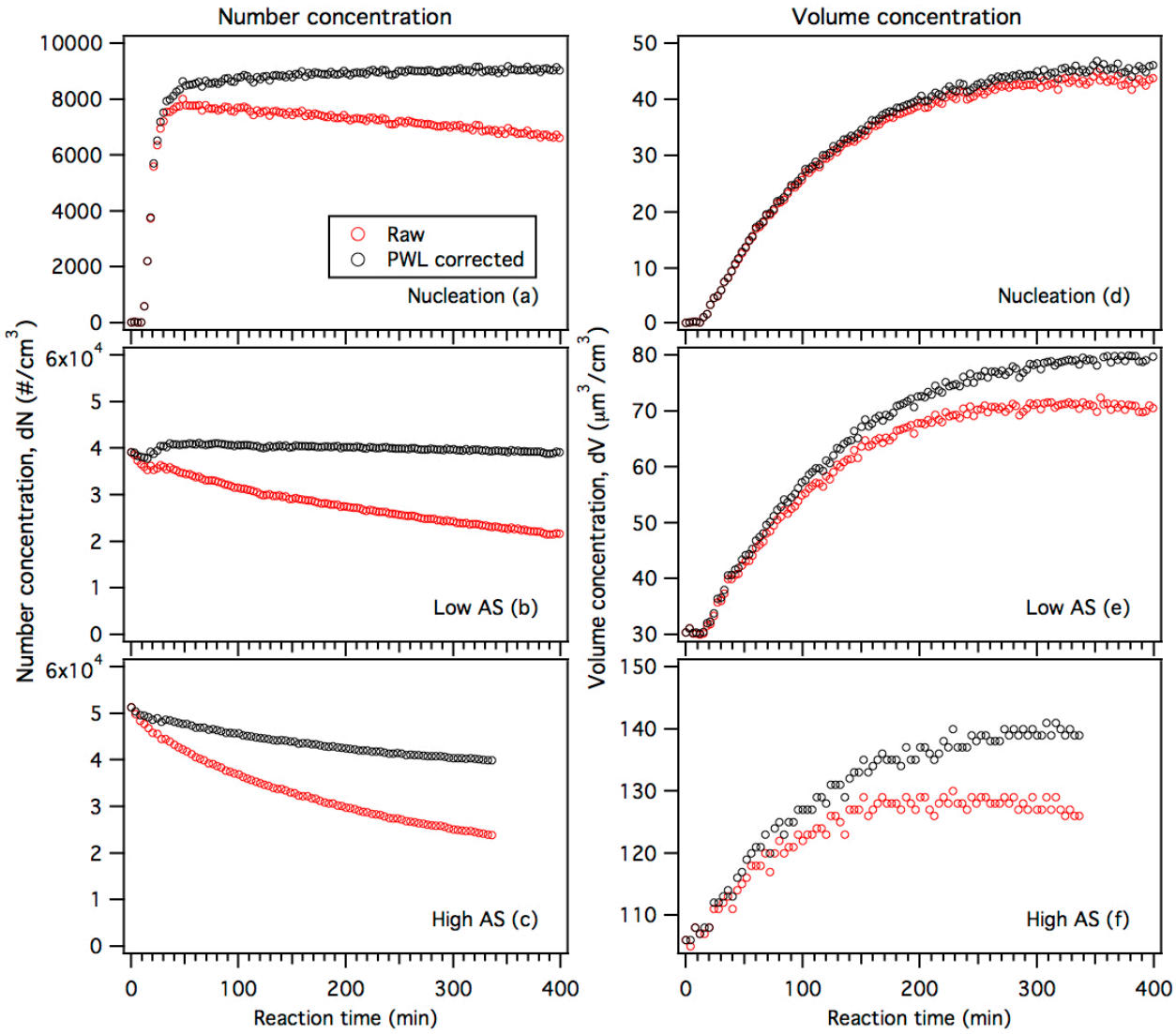

Figure S3: Raw and particle wall loss (PWL) corrected number and volume concentration data for the 100 ppb O_3 experiments. All the raw data are particle wall loss corrected using the average particle wall loss rates (i.e. average of the particle wall loss rates obtained from low AS-seed only and high-AS seed only experiments).

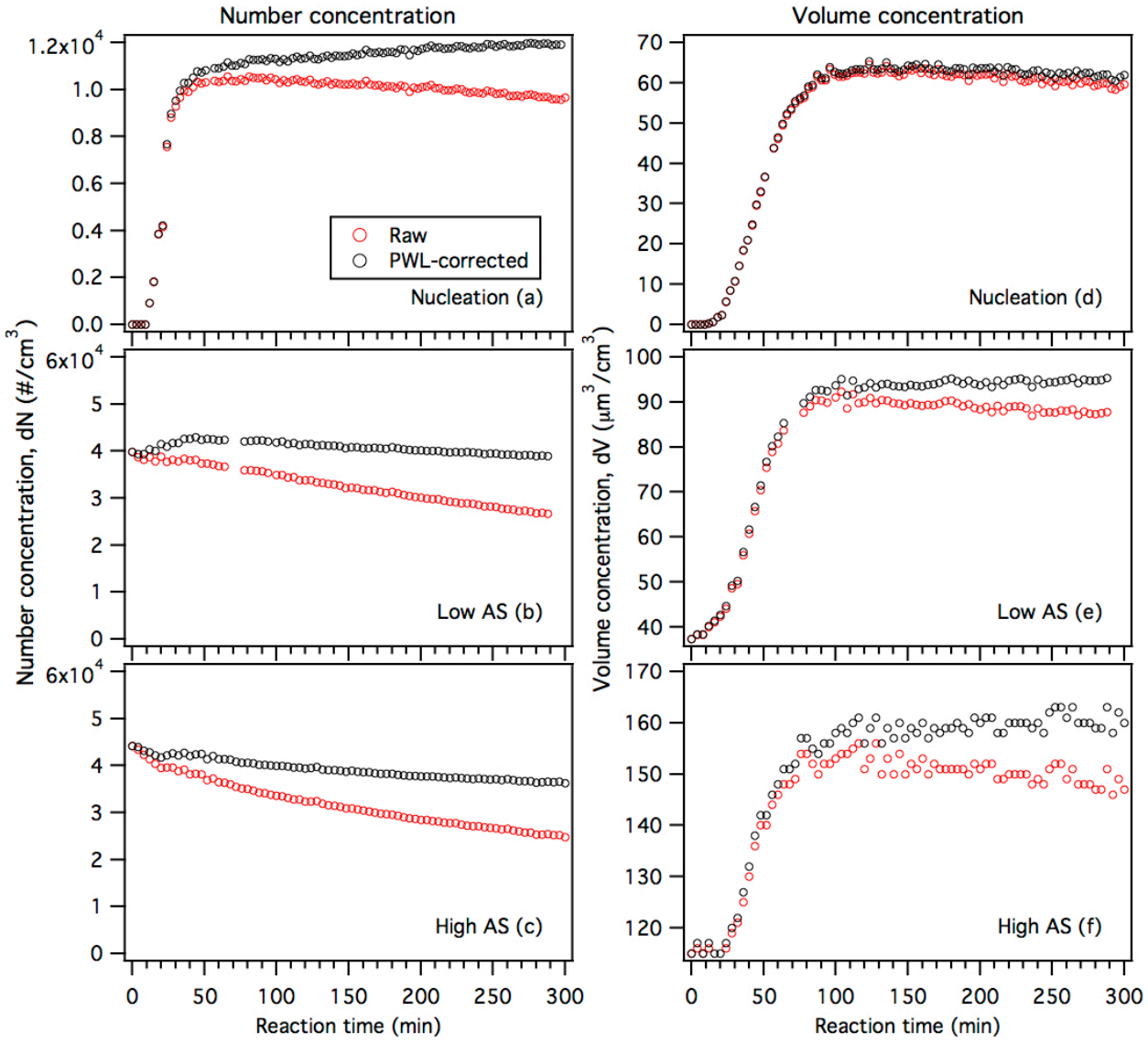

Figure S4: Raw and particle wall loss (PWL) corrected number and volume concentration data for the ~~100~~ 500 ppb O_3 experiments. All the raw data are particle wall loss corrected using the average particle wall loss rates (i.e. average of the particle wall loss rates obtained from low AS-seed only and high-AS seed only experiments).

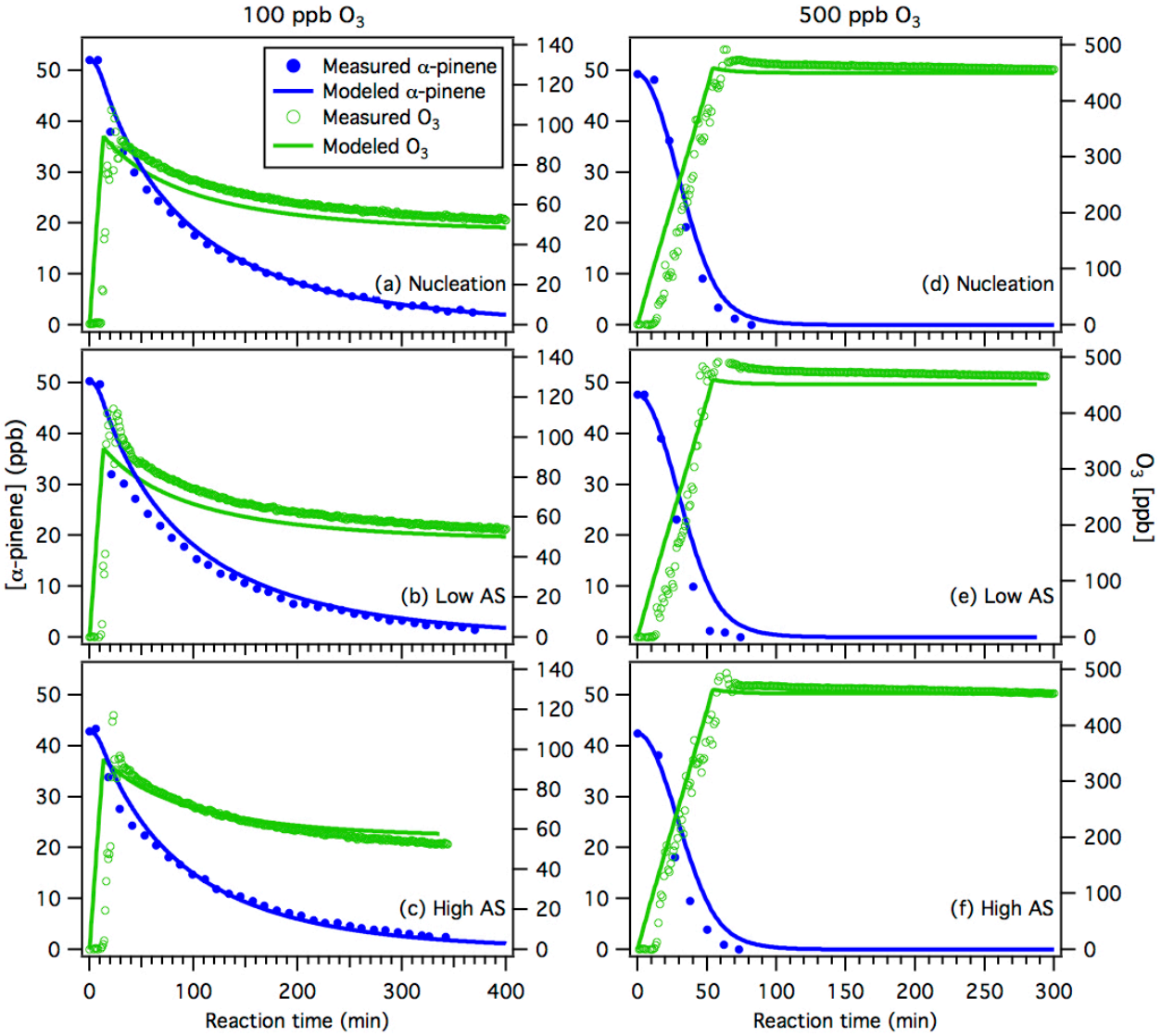

Figure S5: Reaction profiles of the measured and modeled O_3 and α-pinene concentration in the α-pinene ozonolysis experiments. Panels (a), (b) and (c) show results from the nucleation, low AS and high AS 100 ppb O_3 experiments, respectively. Panels (d), (e) and (f) show results from the nucleation, low AS and high AS 500 ppb O_3 experiments, respectively. The blue lines that fit the α-pinene concentration measurements and the green lines that fit the O_3 concentration measurements are model simulation results that come from the coupled vapor-particle dynamics model described in Section 3.

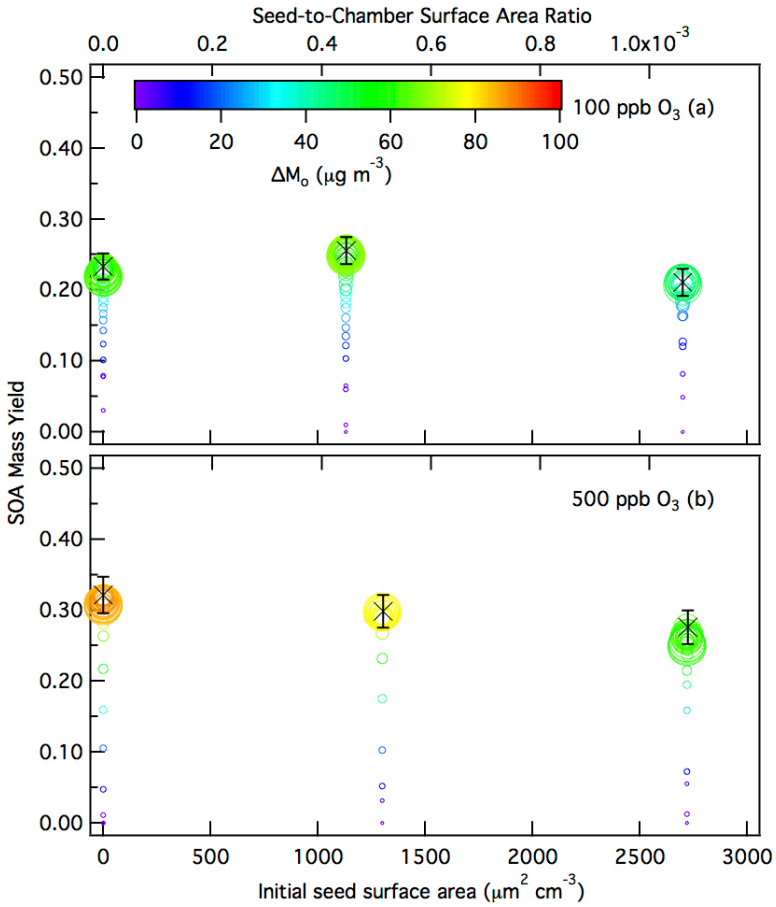

Figure ~~S5~~S6: 10 min-averaged SOA mass yields over the course of an α-pinene ozonolysis experiment as a function of initial total AS seed surface area concentration for the (a) 100 ppb O_3 experiments, and (b) 500 ppb O_3 experiments. Here, all the data have been particle wall loss corrected using the average particle wall loss rates (i.e. average of the particle wall loss rates ~~obtained~~ measured from low AS-seed only and high-AS seed only experiments). Symbol color indicates the SOA mass concentration and symbol size indicates the time after O_3 is injected into the chamber. The × symbols are the SOA mass yields at peak SOA growth. The y-axis error bars represent the uncertainty in the peak SOA mass yield, which originates from the α-pinene injection and the aerosol volume concentration measured by the SMPS at peak SOA growth (one standard deviation). As discussed in the main text, the use of average measured particle wall loss rates for particle wall loss correction does not change the conclusions of this work: 1) SOA mass yields are enhanced at higher O_3 concentrations, and 2) there is a lack of a SOA mass yield dependence on the seed surface area within the range of AS seed surface area concentration used in this study.

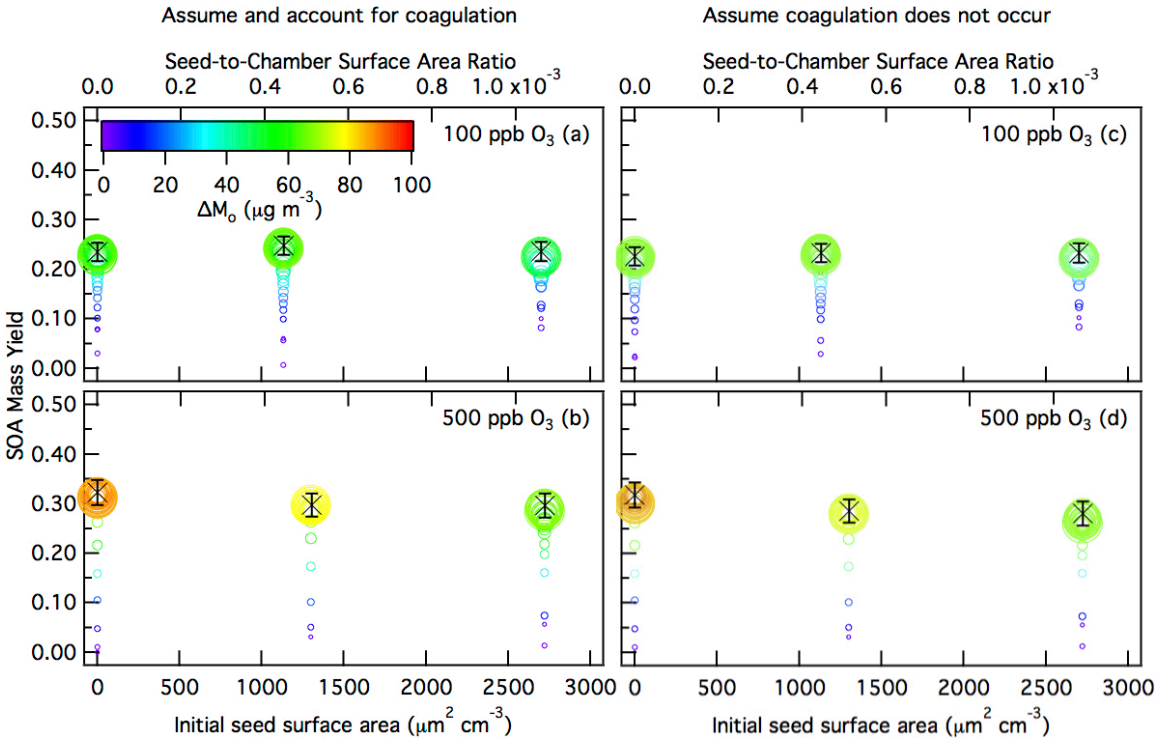

Figure S7: 10 min-averaged SOA mass yields over the course of an α-pinene ozonolysis experiment as a function of initial total AS seed surface area concentration. Panels (a) and (b) show the SOA mass yields obtained using the coagulation-corrected size-dependent particle wall deposition coefficients for the 100 and 500 ppb O_3 experiments, respectively. Panels (c) and (d) show the SOA mass yields obtained using the measured size-dependent particle wall deposition coefficients (that account for coagulation) for the 100 and 500 ppb O_3 experiments, respectively (also shown in Fig. 4 of the main text). Symbol color indicates the SOA mass concentration and symbol size indicates the time after O_3 is injected into the chamber. The ⨯ symbols are the SOA mass yields at peak SOA growth. The y-axis error bars represent the uncertainty in the peak SOA mass yield, which originates from the α-pinene injection and the aerosol volume concentration measured by the SMPS at peak SOA growth (one standard deviation). As discussed in the main text, the use of coagulation-corrected particle wall deposition coefficients for particle wall loss correction does not change the conclusions of this work: 1) SOA mass yields are enhanced at higher O_3 concentrations, and 2) there is a lack of a SOA mass yield dependence on the seed surface area within the range of AS seed surface area concentration used in this study.

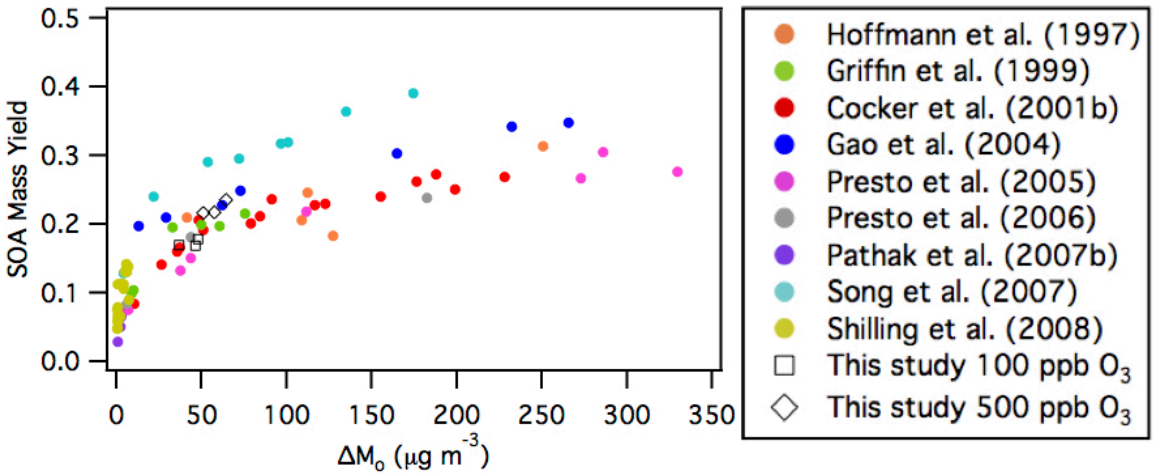

Figure S8: Comparison of SOA mass yields obtained using the coagulation-corrected size-dependent particle wall deposition coefficients to those of previous dark α-pinene ozonolysis studies (Table S2). The SOA mass yields and concentrations of majority of these previous studies (Hoffmann et al., 1997; Griffin et al., 1999; Cocker et al., 2001b; Gao et al., 2004; Presto et al., 2005; Presto et al. 2006; Pathak et al., 2007b; Song et al., 2007) were previously compiled by Shilling et al. (2008). Similar to Shilling et al. (2008), all the data shown here (including those reported in this study) have been adjusted using an organic density of 1.0 g cm^{-3}, and to 298 K using a temperature correction of 1.6 % per K, as recommended by Pathak et al. (2007b) to facilitate easier comparison among the different studies.

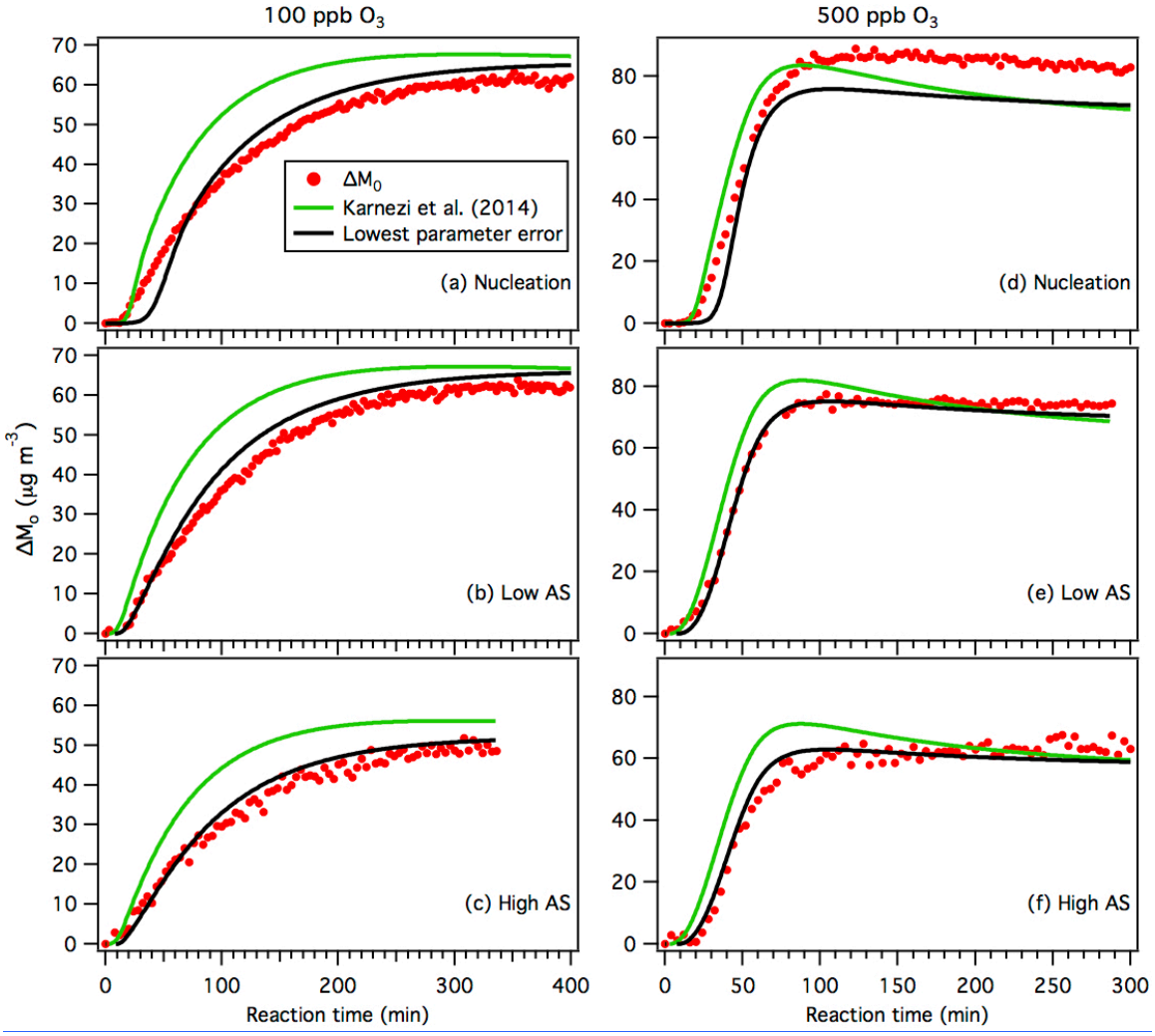

Figure S9: Reaction profiles for measured and modeled SOA concentration, using both the Karnezi et al. (2014) parameters and the lowest-error combination of parameters (see Table S4). Panels (a), (b) and (c) show results from the nucleation, low AS and high AS 100 ppb O_3 experiments, respectively. Panels (d), (e) and (f) show results from the nucleation, low AS and high AS 500 ppb O_3 experiments, respectively.

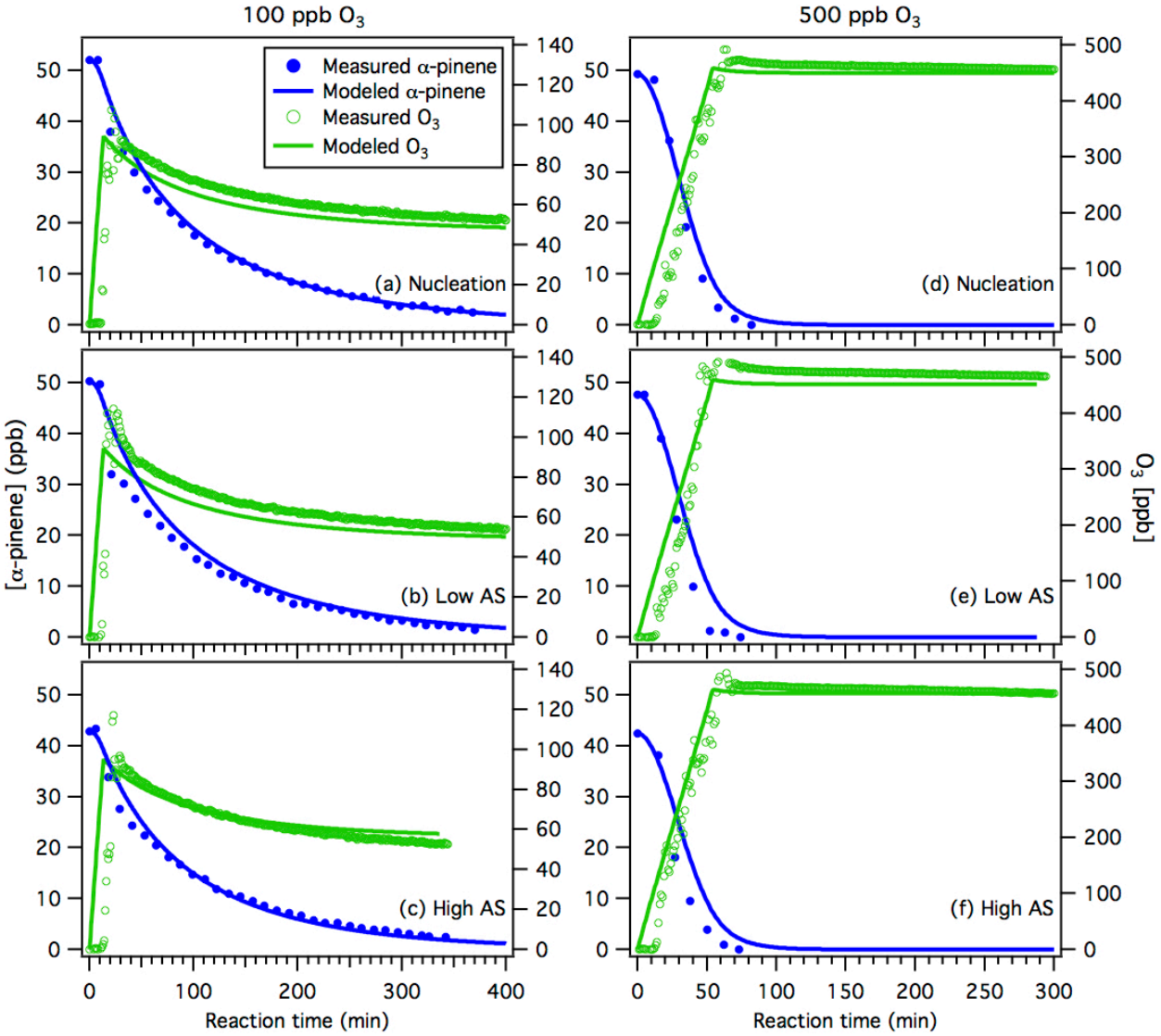

Figure S6: Reaction profiles of the measured and modeled O_3 and α-pinene concentration in the α-pinene ozonolysis experiments. Panels (a), (b) and (c) show results from the nucleation, low AS and high AS 100 ppb O_3 experiments, respectively. Panels (d), (e) and (f) show results from the nucleation, low AS and high AS 500 ppb O_3 experiments, respectively. The blue lines that fit the α-pinene concentration measurements and the green lines that fit the O_3 concentration measurements are model simulation results that come from the coupled vapor-particle dynamics model using the optimal model values: $\alpha_p = 1$, $\alpha_w = 10^{-6}$, $\tau_{olig} = 4$ h, branching ratios = 0.57, 0.35, 0.04, 0.015 and 0.025 for oxidation products with vapor pressures $>10^3$, 10^2, 10, 1 and 0.1 μg m^{-3}, respectively (described in the main text).

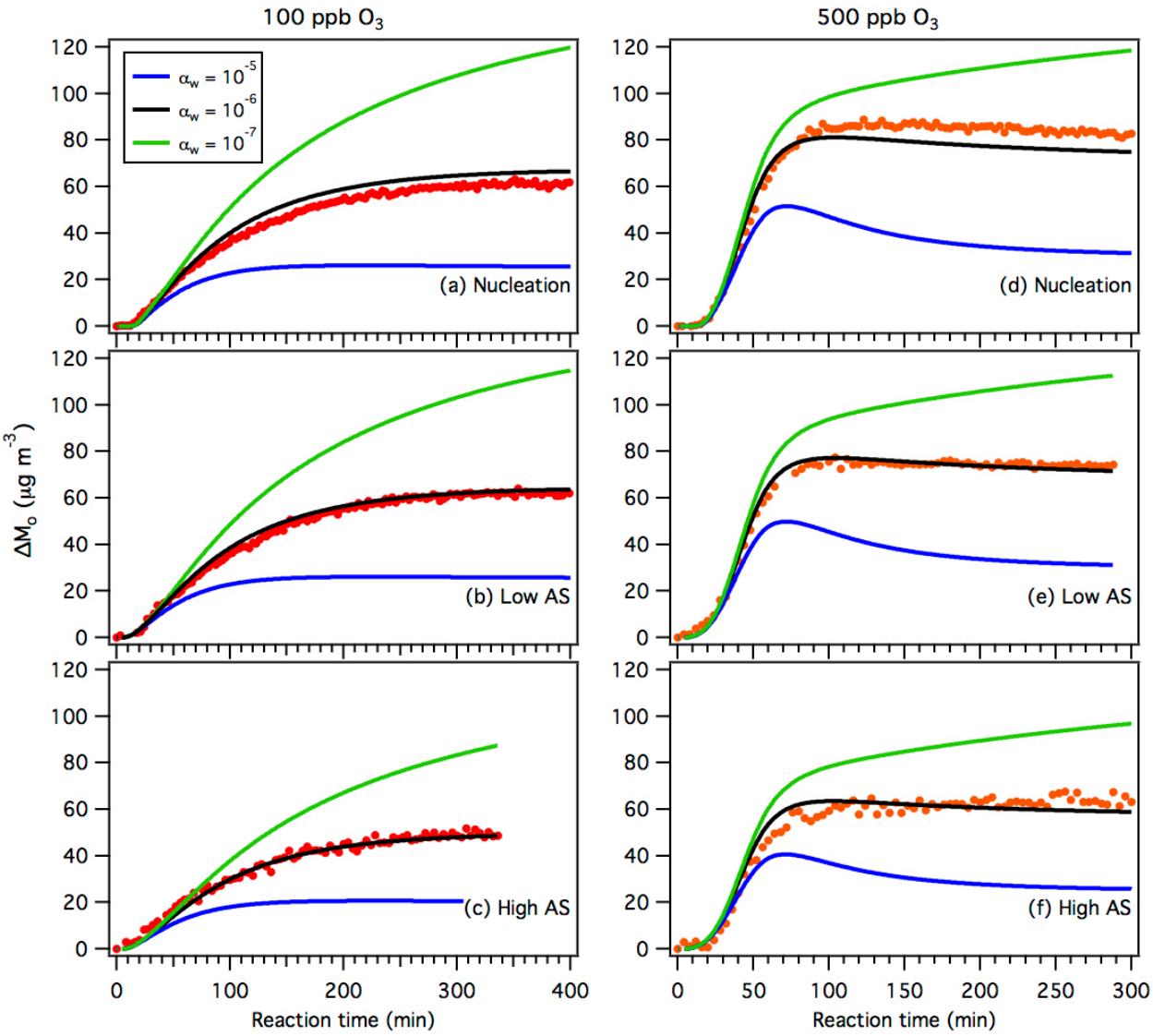

~~Figure S7:~~ ~~Results of sensitivity tests performed for α_w.~~

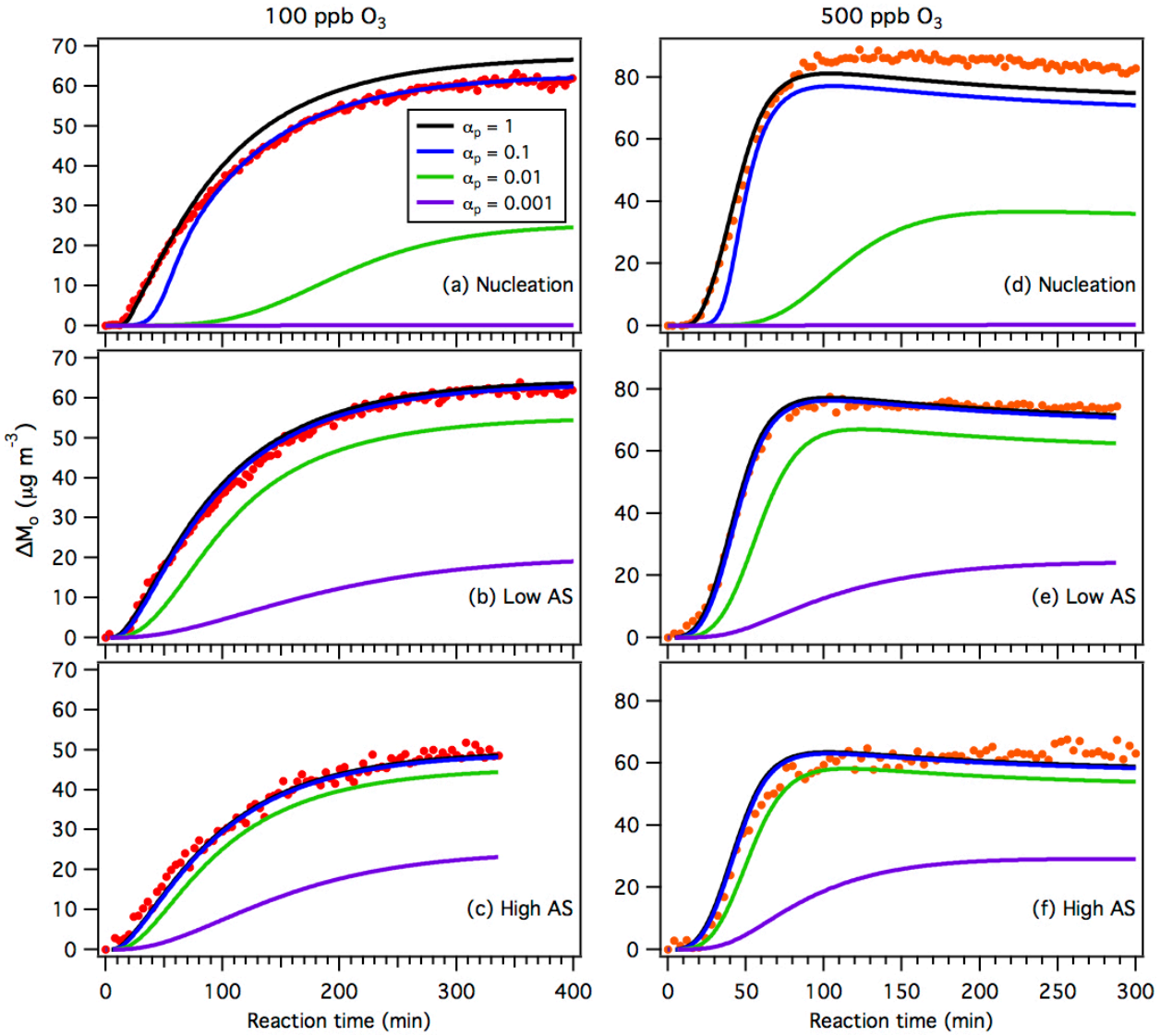

~~Figure S8:~~ ~~Results of sensitivity tests performed for α_p. Note that for all experiments except the two nucleation experiments, $\alpha_p = 1$ and $\alpha_p = 0.1$ give identical results.~~

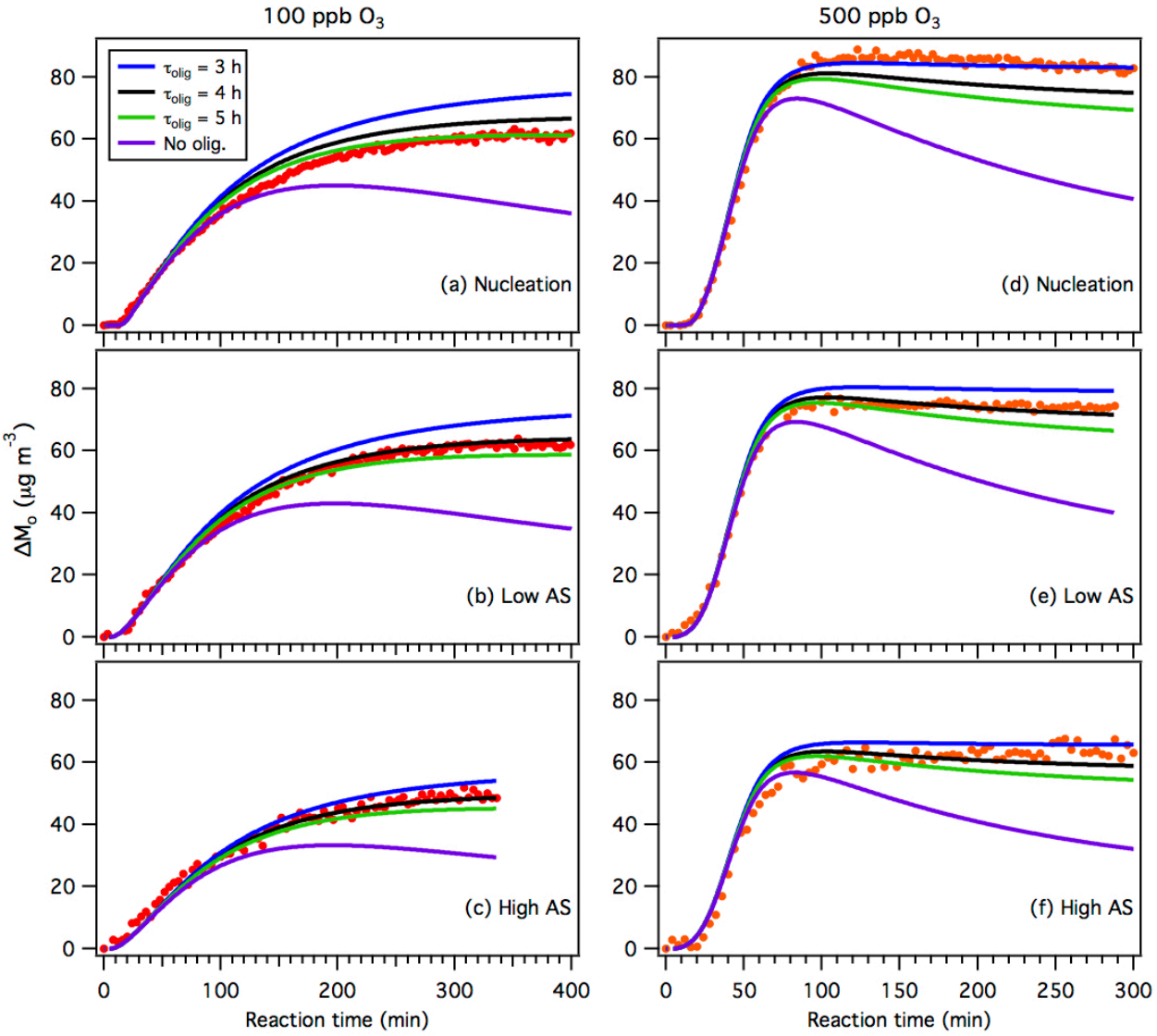

~~Figure S9:~~ ~~Results of sensitivity tests performed for τ_{olig}.~~

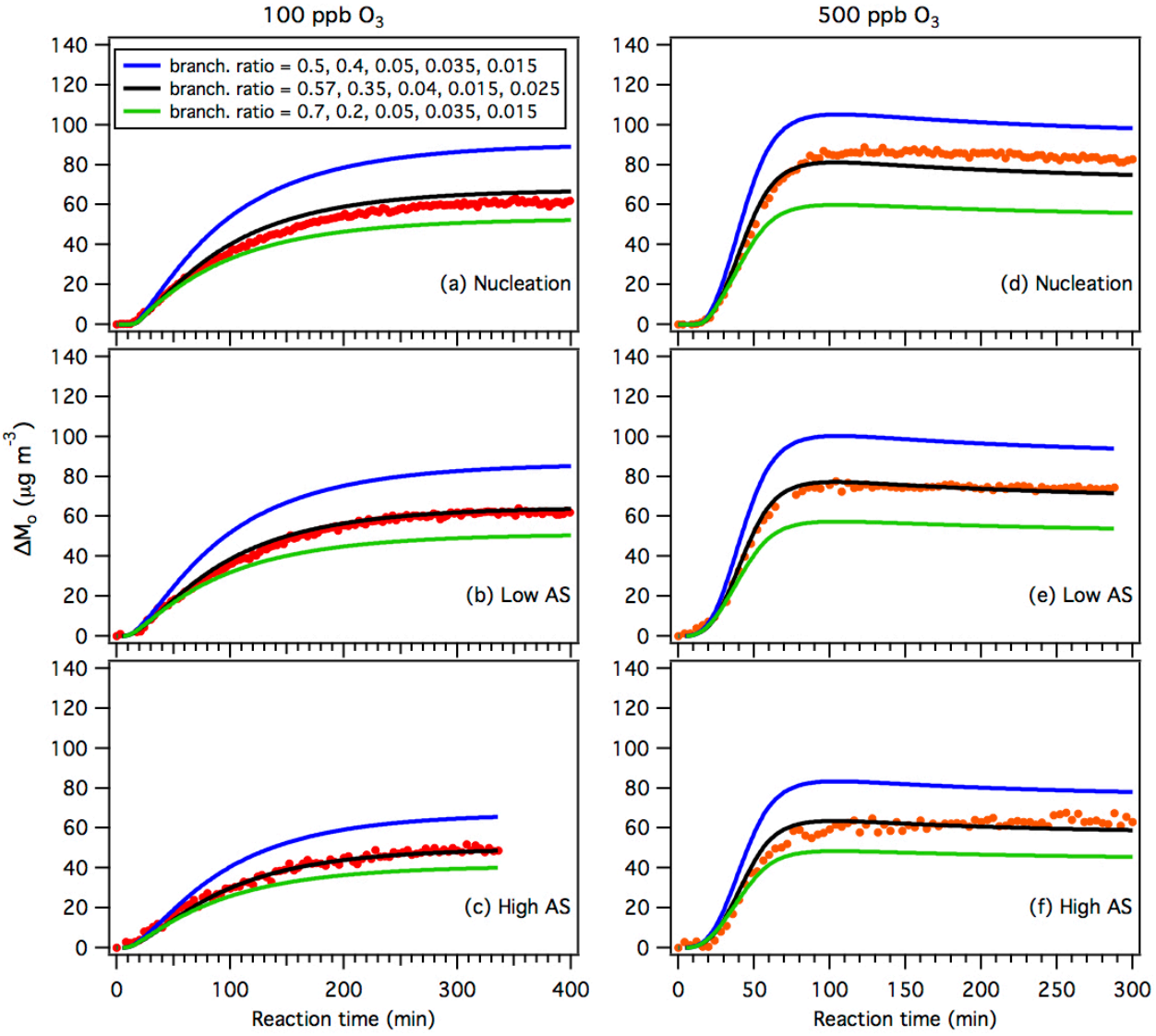

~~Figure S10:~~ ~~Results of sensitivity tests performed for the branching ratios of oxidation products with vapor pressures >10^3, 10^2, 10, 1 and 0.1 µg m^{-3}.~~

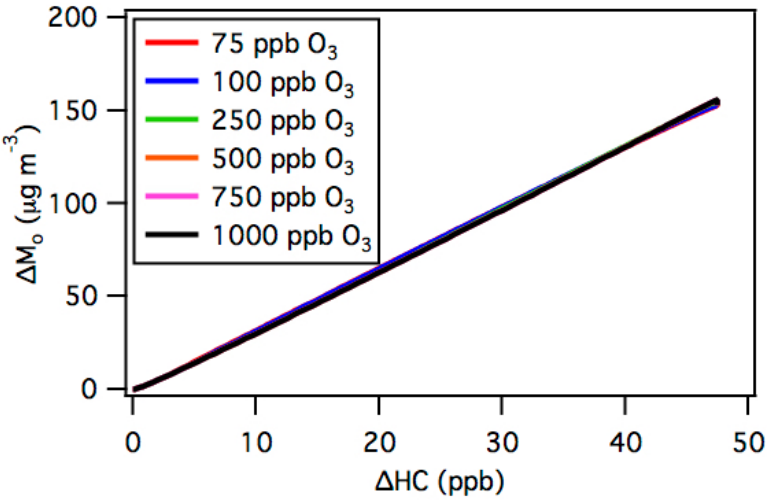

Figure ~~S11~~S10: Results from the coupled vapor-particle dynamics model showing how SOA mass concentration (ΔM_o) changes as a function of reacted α-pinene at different O_3 concentrations, assuming all the α-pinene oxidation products are non-volatile. In these model simulation runs, the initial α-pinene concentration is fixed at 48 ppb, while the O_3 concentration is varied from 75 to 1000 ppb. The O_3 injection rate used in these model simulation runs is 500/54.25 ppb min^{-1}.

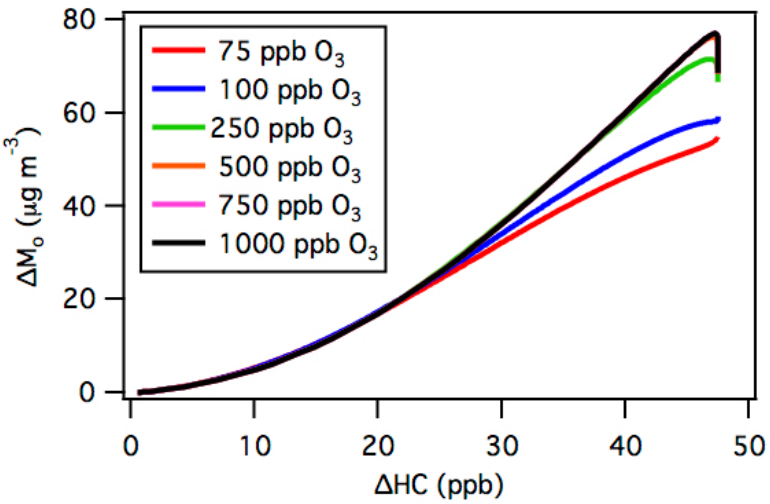

Figure ~~S12~~S11: Predictions from the coupled vapor-particle dynamics model showing time-dependent growth curves for SOA formation from α-pinene ozonolysis at different O_3 concentrations. In these model simulation runs, the initial α-pinene mixing ratio is fixed at 48 ppb, while the O_3 mixing ratio is increased from 75 to 1000 ppb. In the model, the O_3 injection rate is assumed to be fixed at 500/54.25 ppb min^{-1}, and the injection time is increased to achieve the desired O_3 concentration (i.e., 75, 100, 250, 500, 750 or 1000 ppb) in the chamber. The predicted ΔM_o decreased slightly at the end of the experiment at the higher O_3 concentrations (250, 500, 750 and 1000 ppb) due to SOA evaporation. It is important to note that SOA evaporation is predicted at high O_3 concentrations in the coupled vapor-particle dynamics model, but not observed in chamber experiments.

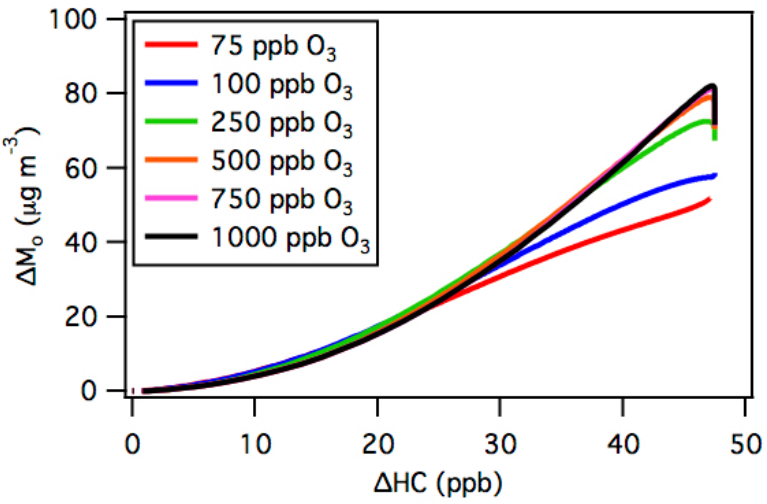

Figure ~~S13~~S12: Results from the coupled vapor-particle dynamics model showing how SOA mass concentration (ΔM_o) changes as a function of reacted α-pinene at different O_3 concentrations. In these model simulation runs, the initial α-pinene concentration is fixed at 48 ppb, while the O_3 concentration is varied from 75 to 1000 ppb. Here, the O_3 injection rate is 5 times faster than~~t~~ the base rate used in the model. The base rate is 500/54.25 ppb min^{-1}, ~~similar to~~ the same rate used to analyze results from the 500 ppb O_3 experiments. As discussed in the main text, the oxidation rate effect persists at a higher O_3 concentration when a faster O_3 injection rate is used. It is important to note that SOA evaporation is predicted at high O_3 concentrations in the coupled vapor-particle dynamics model, but not observed in chamber experiments.

Table S1: Initial and particle wall loss corrected final number concentrations[a]

Experiment	Initial Number Concentration (particle/cm^3)	Final Number Concentration (particle/cm^3)[b]	% Change[c]	Final Number Concentration (particle/cm^3)[d]	% Change[c]
100 ppb O_3 nucleation	23	8222	3.5×10^4	9152	3.9×10^4
100 ppb O_3 low AS	39119	32553	-16.8	38689	-1.1
100 ppb O_3 high AS	51254	45280	-11.7	39889	-22.2
500 ppb O_3 nucleation	1	11303	1.6×10^6	11974	1.7×10^6
500 ppb O_3 low AS	39800	35216	-11.5	38905	-2.2
500 ppb O_3 high AS	44196	40191	-9.1	35189	-20.4

[a]Particle number concentrations (dN)

[b]The data shown here correspond to those shown in Figs. S1 and S2. The nucleation and low AS data have been particle wall loss corrected using particle wall loss rates determined from the low AS-seed only experiments. The high AS data have been particle wall loss corrected using particle wall loss rates determined from the high AS-seed only experiments.

[c]$\%\ \text{Change} = \frac{(\text{Difference between initial and particle wall loss corrected final number concentration})}{\text{Initial number concentration}} \times 100\%$

[d]The data shown here correspond to those shown in Figs. S3 and S4. All the data have been particle wall loss corrected using the average particle wall loss rates (i.e. average of the particle wall loss rates obtained from low AS-seed only and high-AS seed only experiments).

Table S2: Discretization of parameters

Parameter	Discretization
α_p	1, 0.1, 0.01, 0.001
α_w	10^{-7}, 10^{-6}, 10^{-5}
τ_{olig}	4, 6, 8
$>10^3$ branching ratio[a]	0.5, 0.6, 0.7, 0.8, 0.9, 1
10^2 branching ratio[a]	0, 0.1, 0.2, 0.3, 0.4, 0.5
10 branching ratio[a]	0, 0.01, 0.02, 0.03, 0.04, 0.05, 0.1, 0.15, 0.2
1 branching ratio[a]	0, 0.01, 0.02, 0.03, 0.04, 0.05, 0.1, 0.15, 0.2
0.1 branching ratio[a]	0, 0.01, 0.02, 0.03, 0.04, 0.05, 0.1, 0.15, 0.2

[a]Only combinations of parameters summing to one were allowed.

Table ~~S2~~S3: Comparison of experimental conditions used in this work with those of previous dark α-pinene ozonolysis studies. The SOA mass yields and concentrations of these studies are shown Fig. 5~~S6~~.

Study	Temperature (K)	RH (%)	Seed	OH Scavenger	O_3 (ppb)	ΔHC (ppb)
Cocker et al. (2001)[a]	301.2-302.9	<2, 39-49.2	None, $(NH_4)_2SO_4$ and NH_4HSO_4	2-butanol	130-600	22.6-212.3
Gao et al. (2004)[b]	293	55	$MgSO_4$	cyclohexane	24-270	12-135
Griffin et al. (1999)	303.3-309.9	5	$(NH_4)_2SO_4$	2-butanol	67-260	16.7-65
Hoffmann et al. (1997)	289.3-322.1	N.A.	$(NH_4)_2SO_4$	None	210-327	38-154.1
Pathak et al. (2007b)	288-313	< 10	None, $(NH_4)_2SO_4$	2-butanol	750-3100	3.7-8.5
Presto et al. (2005)[c]	295	< 10	None	2-butanol	160-605	15-210
Presto et al. (2006)[d]	295	< 10	None	2-butanol	260-350	13.4-135
Shilling et al. (2008)[e]	298	40	$(NH_4)_2SO_4$	1- and 2-butanol	50, 300, 535	0.3-22.8
Song et al. (2007)[f]	300.6-301.7	< 2	None	cyclohexane	46-369	5.9-81.1
This study	298	< 5	$(NH_4)_2SO_4$	cyclohexane	100, 500	42.4-52.1

[a]Data collected using aqueous seed aerosol is excluded from our analysis.
[b]Data collected using acidic seed aerosol is excluded from our analysis.
[c]Only dark experiments in which [α-pinene]/[NO_x] > 15 are used in our analysis.
[d]Only dark α-pinene ozonolysis experiments are used in our analysis.
[e]Data collected in batch mode and continuous-flow mode are used in our analysis.
[f]Data collected using organic seed aerosol is excluded from our analysis.

Table S4: Best-fit parameters, using lowest percentage error and Karnezi et al. (2014) method

Parameter	Lowest percentage error	Karnezi et al. (2014) method
α_p	0.1	0.35
α_w	10^{-6}	3.6×10^{-6}
τ_{olig} (h)	4	6
$>10^3$ branching ratio	0.6	0.66
10^2 branching ratio	0.3	0.16
10 branching ratio	0.05	0.06
1 branching ratio	0.05	0.06
0.1 branching ratio	0	0.06
Percentage error for combination	**21%**	**37%**